Parahydrogen And Synthesis Allow Dramatically Enhanced Nuclear Alignment

Thesis by
Clifford Russell Bowers

In Partial Fulfillment of the Requirements
for the Degree of
Doctor of Philosophy

California Institute of Technology
Pasadena, California

1991
Submitted October 5, 1990

Acknowledgments

It is a pleasure to acknowledge the excellent educational and research opportunities which have been extended to me by my scientific advisor at Caltech, Dan Weitekamp. Dan provided a unique scientific experience of superlative quality.

I commend the staff of the Chemistry Department for the role they played in the research described herein. The experiments of this thesis would have been significantly more difficult without the talents of Tom Dunn, Guy Duremburg and Larry Henling.

The group also deserves mention for their unswerving support, especially Paul Carson and Dave Norris for their assistance in the experiments of Chapters VI and VII.

It is a pleasure to acknowledge the helpful suggestions of the Caltech organometallic chemists H. B. Gray and J. E. Bercaw. Thanks to J. S. Waugh for providing a copy of the ANTIOPE spin dynamics program. The assistance offered by Dave Smith, who was a student of Gray, was very generous.

For their past scientific guidance, allow me to express my appreciation to John Barnwell, Dudley Herschbach, David Page, Ron Christensen and Robert Gosse.

To Bambi and My Family.

Abstract

The PASADENA effect is a method for transient high-sensitivity proton spin-labelling by molecular addition of dihydrogen. When the parahydrogen mole fraction differs from the high-temperature limit of 1/4, this population difference constitutes a form of spin order which can be converted to magnetization observable by NMR. Large NMR signals are observed, if subsequent to the hydrogen addition, the two protons experience magnetic inequivalence and spin-spin coupling and if observation is made before spin-lattice relaxation restores the equilibrium spin order. The analogous effect for D_2 is also possible.

The kinetic mechanisms of the homogeneous hydrogenation catalysts which permit the realization of the PASADENA effect have been the target of the experimental applications. The enhancement of the NMR transitions has facilitated the determination of true molecular rate constants. Ordinarily, the activity of a catalyst is assessed by dividing the observed rate by the total catalyst concentration. However, the question as to whether most of the catalytic rate is due to a tiny fraction of active species or a large fraction with a relatively low molecular rate is not clearly addressed by such an analysis. This ambiguity is entirely avoided in the PASADENA studies, since only active catalyst molecules can contribute to the enhanced signals from which all kinetic inferences are made.

The sensitivity enhancement has also led to the identification of a novel intermediate in the mechanism for the $Rh(DIPHOS)^+$ catalyzed hydrogenation of styrene. The rate of conversion of this species into product and starting material has been studied using two-dimensional NMR. The dramatically improved sensitivity should make it possible to observe key catalytic intermediates which do not

build up in sufficient quantity to allow detection by conventional NMR arising from Curie-Law magnetization.

The study of surface sites which bind pairwise with H_2 is also a potentially fruitful area for future experimental work. The ambient temperature NMR spectroscopy of surfaces is not often feasible due to sensitivity limitations. Simulations have been performed using typical shift and coupling parameters in an effort to characterize the enhanced lineshapes which can be expected.

The inverse of the PASADENA effect has also been proposed, whereby the spin order of a molecule containing hydrogen is probed by measuring the branching ratio to ortho and para dihydrogen. This RAYMOND phenomenon (*r*adiowave *a*pplication *y*ields *m*odulated *o*rtho *n*umber *d*esorbed) has the potential for measuring precursor NMR with extraordinary sensitivity, since it finesses the need for detection of radiowaves.

Contents

Chapter IV: Liquids

Chapter V: Deuterium

Chapter VI: $Rh(PPh_3)_3Cl$ Catalyzed Hydrogenation of Styrene

Chapter VII: 2-D PASADENA
Kinetic Study of Enhanced Intermediates

Chapter VIII: Enhancement of Surface NMR by Para-Hydrogen Addition

Chapter IX: Radiowave Application Yields Modulated Ortho Number Desorbed

Appendix A: Dual Interface Spectrometer Control Object

List of Figures

Chapter I

Introduction

§ I-1. Historical Perspective

The original theoretical prediction that the symmetrization order of dihydrogen could be transformed by chemical reaction and resonant radio frequency pulses into enhanced nuclear magnetic resonance transitions was published in November 1986.[1] The first experimental observation[2] of the effect was performed shortly thereafter with stopped flow bubbling of para enriched H_2 into a standard NMR tube at 4.7 T (200 MHz). The sample consisted of CH_2CHCN as the substrate in *d*-cholorform as the solvent and $Rh(PPh_3)_3Cl$ as the catalyst to facilitate the addition reaction. The simple pulse sequence used is shown below.

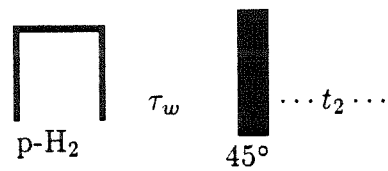

The effect was easily recognized by its distinctive line shape, as seen in Fig. (IV-1), which exactly matched numerical density matrix simulations performed prior to the experiment.

Although the phenomenon known as *p*arahydrogen *a*nd *s*ynthesis *a*llow *d*ramatically *e*nhanced *n*uclear *a*lignment (PASADENA) was first theoretically for-

mulated and experimentally demonstrated only four years ago, the occurrence of this phenomenon actually predates the postulation of its existence. As was realized only after the correct theory was published, several workers had unwittingly performed hydrogenation reactions which were by chance exactly the conditions which lead to PASADENA signals.[3,4]

Eisenberg and coworkers[3] conducted experiments with the intention of using *chemically induced dynamic nuclear polarization*[5,6] (CIDNP) to probe the mechanism for the $Rh_2H_2(CO)_2(DPPM)_2$ catalyzed hydrogenation of $PhC{\equiv}CH$ in C_6D_6. The spectra showed an enhanced *multiplet effect* for the newly added protons. This was contrary to previous data for hydrogenations involving monohydride catalysts, [7] which exhibited *net effect* patterns. In those systems, the observation of the net effect has been explained by the difference in the isotropic g values of the electrons in a metal–organic biradical pair. However, in the hydrogenations involving $Rh_2H_2(CO)_2(DPPM)_2$, the well-known CIDNP rules which summarize the spin physics of electron spin singlet-triplet mixing lead to the conclusion that $\Delta g \approx 0$ and the postulation of an extraordinary metal-centered biradical. However, the true source of the enhancements they observed was the quantum mechanical nature of their H_2 reagent.[8]

The quantum states of molecular H_2 are divisible into two manifolds, orthohydrogen (o-H_2) and parahydrogen (p-H_2), with interconversion between them occurring at a rate far slower than the rate of equilibration within each manifold. Consequently, it is possible in the absence of a catalyst to prepare and store pure p-H_2 or o-H_2 for weeks, so that the two may be considered as different "chemical" reagents. In the work misinterpreted as CIDNP, a common laboratory procedure was employed in the Eisenberg experiments which involves storing the fresh reaction mixture, including dissolved H_2, in liquid nitrogen before beginning the experiment. Under these conditions, the ortho/para states slowly equilibrate at the low temperature, eventually resulting in p-H_2 enrichment to 50% at 77 K. The

spin-state enriched H_2 may then chemically react at ambient temperatures with the substrate after warming the sample, resulting in the increased spin-order of the product which yields the PASADENA effect.

Since the proposal of the PASADENA effect, the spectra resulting from hydrogenation by $Rh_2H_2(CO)_2(DPPM)_2$ have been re-interpreted and shown[8] to be due to p-H_2 induced polarization, prompting additional studies by at least two groups other than our own.[8–13] It is possible that additional misinterpreted hydrogenation studies might be found in the fifteen-year-old CIDNP literature.

§ I-2. Overview

A brief review of the quantum mechanics of systems of identical particles, proton pairs in particular, is presented in Chapter II. The considerations are used in Chapter III to analyze the spin dynamics which lead to the PASADENA signal. The dynamics are explored in greater detail in Chapter IV using the approximations which are valid in the weak coupling limit often applicable to liquid samples. In Chapter V, the signals which are analogous to the PASADENA signals for H_2 are computed for D_2, the nuclei of which constitute a system of two bosons. Having theoretically explored the PASADENA dynamics, our interest then turns toward applications to the elucidation of hydrogenation mechanisms and kinetic studies. The results of this work are described in Chapters VI and VII. Chapter VIII deals with the specific case of an isolated dipolar coupled proton pair bound to a surface. The consequences of a distribution of orientations of the dipolar and chemical shift tensors with the static field are simulated numerically. In the final chapter, a new method of high sensitivity NMR is proposed in which H_2 desorbed from a surface is analyzed for its ortho/para content. The motivation is to transform the sensitivity problem from that of detecting weak rf signals into the more amenable one of establishing the para mole fraction of free H_2. It is shown with a density operator formalism that the para or ortho mole fraction reports directly on the zero-quantum coherence of the precursor and that other spin operators may be

observed indirectly. Spectra are simulated for the case of a surface site at which release of H_2 occurs.

§ I-3. References

1. C. R. Bowers and D. P. Weitekamp, *Phys. Rev. Lett.* **57**, 2645 (1986)
2. C. R. Bowers and D. P. Weitekamp, *J. Am. Chem. Soc.* **109**, 5541 (1987)
3. S. I. Hommeltoft, D. H. Berry and R. Eisenberg, *J. Am. Chem. Soc.* **108**, 5345 (1986)
4. H. Bryndze, "The Monday Effect," Ph.D. thesis, R. G. Bergman, University of California, Berkeley (1980)
5. G. L. Closs, *Adv. Magn. Reson.* **7**, 157 (1974)
6. R. Kaptein, *Adv. Free-Radical Chem.* **5**, 319 (1975)
7. R. L. Sweany and J. Halpern, *J. Am. Chem. Soc.* **99**, 8335 (1977)
8. T. C. Eisenschmid, R. U. Kirss, P. P. Deutsch, S. I. Hommeltoft, R. E. Eisenberg, J. Bargon, R. G. Lawler and A. L. Balch, *J. Am. Chem. Soc.* **109**, 8089 (1987)
9. R. U. Kirss, T. C. Eisenschmid and R. Eisenberg, *J. Am. Chem. Soc.* **110**, 8564 (1988)
10. R. U. Kirss and R. Eisenberg, *J. Orgmet. Ch.* **359**, 22 (1989)
11. T. C. Eisenschmid, J. McDonald and R. Eisenberg, *J. Am. Chem. Soc* **111**, 7267 (1989)
12. R. U. Kirss and R. Eisenberg, *Inorg. Chem.* **28**, 3372 (1989)
13. J. Bargon, J. Kandels and K. Woelk, *Angew. Chem.* **29**, 58 (1990)

Chapter II

Identical Quantum Particles

§ Introduction

A brief review of the quantum mechanics of systems of identical particles, proton pairs in particular, is presented in this chapter. For a detailed exposition on this topic, consult any classic quantum text, such as Merzbacher,[1] Landau and Lifshitz,[2] Baym,[3] or Cohen-Tannoudji, Diu and Laloë.[4]

Simple considerations of the indistinguishability of identical quantum particles lead to the symmetrization of the total wave function. The *spin statistics theorem* dictates the symmetry of the wave function based on whether the value of the spin quantum number is fractional or integral. A direct consequence of this is the correlation of the symmetries of the spin states with other parts of the overall wave function. Two distinct forms of H_2 arise from this "coupling" between rotation and spin.

To investigate the spin dynamics of H_2 which stem from symmetry breaking magnetic interactions, it is convenient to employ density operator methods. This requires finding the nuclear spin eigenstates of H_2, from which it is straightforward to construct the density matrix. From this matrix, the proper density operator can

be obtained.

§ II-1. Quantum Mechanics of Identical Particles

The motion of a system of macroscopic particles can always be fully characterized when the initial position and momenta are known. For a collection of identical quantum mechanical particles, however, the trajectories become clouded when the wave functions overlap. In fact, it is not possible to follow the individual particles without losing track of their identities.

What is meant by "identical particles" is that there are no interactions which can distinguish them. All of the intrinsic properties are exactly the same (i.e., spin, mass, charge, etc.) for all N particles in the system. Since it is impossible to distinguish the individual particles, the $N!$ unique states which associate the particle labels with coordinate and spin variables must all be physically equivalent. Thus, it is the observable of the system which must account for this indistinguishability by being properly "symmetrized" with respect to permutations of the particle indices.

For example, let $\Psi(1,2)$ be an eigenstate of a two particle Hamiltonian $\mathcal{H}$ with energy E. The permutation operator $\mathcal{P}$ interchanges the particle labels such that

$$\mathcal{P}\Psi(1,2) = \Psi(2,1) \tag{1}$$

The two states, $\Psi(1,2)$ and $\Psi(2,1)$ are "exchange degenerate" since $\mathcal{H}$ is necessarily a symmetric operator,

$$\mathcal{H}\mathcal{P}|\Psi\rangle = \mathcal{P}\mathcal{H}|\Psi\rangle = E\mathcal{P}|\Psi\rangle. \tag{2}$$

Thus,

$$[\mathcal{H}, \mathcal{P}] = 0. \tag{3}$$

From a general theorem of linear algebra, it is known that a basis set can be found whose members are simultaneously eigenfunctions of commuting Hermitian operators. This fact will be used to show that the eigenfunctions of a two particle system are either symmetric or antisymmetric functions, depending on the nature

of the particle. Since

$$\mathcal{P}^2\Psi(1,2) = \mathcal{P}\Psi(2,1) = \Psi(1,2) \tag{4}$$

then

$$\mathcal{P}^2 = 1 \tag{5}$$

$$\mathcal{P} = \pm 1 \tag{6}$$

This implies that the eigenfunctions of $\mathcal{H}(1,2)$ are symmetric and antisymmetric functions,

$$\Psi_S(1,2) = \Psi(1,2) + \Psi(2,1) \tag{7}$$

and

$$\Psi_A(1,2) = \Psi(1,2) - \Psi(2,1) \tag{8}$$

Depending on the nature of the identical particles comprising the multiple particle system, the physically realized states are either completely symmetric or completely antisymmetric with respect to permutation. The *symmetrization postulate*[4] of quantum mechanics classifies particles with antisymmetric states as *fermions* and those with symmetric states as *bosons.* From empirical observations, all currently known particles fall into either of these two categories. Particles with integer spin ($I = 0, 1, 2, \ldots$) are bosons and those with half integer spin ($I = 1/2, 3/2, 5/2, \ldots$) are fermions. Atomic and molecular particles are composites of smaller, more elementary particles. Composite particles consisting of any number of bosons and an odd number of fermions are themselves fermions while those with any number of bosons and an even number of fermions are bosons. Thus, the protons and electrons of H_2 behave as fermions, but the hydrogen atom itself is a boson.

The antisymmetry of the wave function for fermions has profound implications to the structure of matter, since electrons are particles of this type. Since for fermions,

$$\Psi(1,2,3,\ldots,n) = -\Psi(2,1,3,\ldots,n), \tag{9}$$

and Ψ vanishes if $1 = 2$. This is the Pauli Exclusion Principle, which states that it is impossible for two fermions to occupy the same state (the two particles cannot simultaneously have the same coordinates and spin). Mathematically, the many fermion wave function may be written as a Slater determinant which can immediately be seen to vanish when any two rows are identical. Otherwise, interchanging the rows produces an overall change in the sign of the determinant.

§ II-2. Nuclear Spin States of Molecular Hydrogen

Molecular hydrogen is the system of initial interest in this dissertation. The description of the overall wave functions for this molecule makes use of the Born–Oppenheimer approximation, which neglects the kinetic energy terms of the nuclei in the total Hamiltonian, making it possible to factor the electronic and nuclear wave functions. Because the nuclei are so much more massive than the electrons, the latter become distributed into eigenstates of the nearly static Coulombic potential of the former.

To summarize the method, the electronic problem is first solved assuming fixed nuclear coordinates, and then the total electronic energy is used as a potential function to describe the slow nuclear motion. Hence, the overall wave function is the product of a nuclear and an electronic factor

$$\Psi_n(r, R) = \Phi_n(R)\phi(r, R) \tag{10}$$

with R and r the collective coordinates of the nuclei and electrons, respectively. The $\Phi_n(R)$ are products of the translational, rotational, vibrational and the nuclear spin function.

$$\Phi_n(R) = \psi_t\psi_r\psi_v\psi_n \tag{11}$$

The protons are a system of two fermions, and the overall wave function must change its sign with their permutation. The translational part is a function of the center of mass only, making it symmetric. The vibrational part must also be symmetric for a homonuclear diatomic. This leaves the overall symmetry determined

by the product of the rotational and nuclear spin state symmetries, with

$$\psi_r \propto e^{im\phi} P_j^{|m|}(\cos\vartheta) \tag{12}$$

The energy of these states is

$$E_r = \hbar^2 \frac{j(j+1)}{2\mathcal{J}} \tag{13}$$

where $\mathcal{J}$ is the moment of inertia of the H_2 molecule. Exchange of the protons corresponds to $\vartheta \mapsto (\pi - \vartheta)$ and $\phi \mapsto \phi + \pi$, which has the effect of reversing the sign of ψ_r for odd j only. Thus, all ψ_r with j even are symmetric and those with odd j are antisymmetric. To preserve the overall antisymmetry with respect to proton exchange, the symmetric nuclear (triplet) spin states must correlate with odd j and the antisymmetric (singlet) state with even j. These two classifications arise as a consequence of the vector addition of the two proton angular momenta. The sum of the angular momenta, $I_1 + I_2 = I = 1$ gives rise to a magnetic multiplicity of $2I + 1 = 3$, a triplet, whereas the difference angular momentum of zero is a singlet. The Clebsch-Gordon coefficients are used to find the eigenstates of the total angular momentum which are linear combinations of the direct product basis states. Hence, the symmetric nuclear spin triplet states of H_2 belong to *orthohydrogen* ($j = 1, 3, \ldots$).

$$|\psi_{n,o}\rangle = \begin{cases} |\beta\beta\rangle, & m_s = -1 \\ \frac{1}{\sqrt{2}}(|\alpha\beta\rangle + |\beta\alpha\rangle), & m_s = 0 \\ |\alpha\alpha\rangle, & m_s = +1 \end{cases} \tag{14}$$

The singlet state is associated with parahydrogen ($j = 0, 2, \ldots$).

$$|\psi_{n,p}\rangle = \frac{1}{\sqrt{2}}(|\alpha\beta\rangle - |\beta\alpha\rangle) \tag{15}$$

Using the expression for the energy of the rotational levels together with their $(2j + 1)$ degeneracy, the nuclear–rotational partition function can be derived:

$$q_{rn} = \sum_{j=0,2,\ldots} (2j+1) e^{-j(j+1)\Theta_r/T} + 3 \sum_{j=1,3,\ldots} (2j+1) e^{-j(j+1)\Theta_r/T} \tag{16}$$

with the rotational temperature

$$\Theta_r = \frac{\hbar^2}{2\mathcal{J}k} \tag{17}$$

($\Theta_r = 85.4°$ K for H_2, $\Theta_r = 42.7°$ K for D_2). The ratio of the number of ortho to parahydrogen molecules is

$$\frac{N_o}{N_p} = \frac{3\sum_{j=1,3,\ldots}(2j+1)e^{-j(j+1)\Theta_r/T}}{\sum_{j=0,2,\ldots}(2j+1)e^{-j(j+1)\Theta_r/T}} \tag{18}$$

For H_2 gas equilibrated at a temperature of 77° K, $N_o/N_p \approx 1.0$

Since the spin isomer interconversion requires a forbidden transition between the ortho and para manifolds, equilibration of the forms in the gas phase is very slow. However, the conversion rate can be drastically increased by subjecting the H_2 to a paramagnetic solid catalyst which breaks the symmetry. Thus, equilibration at reduced temperature in the presence of the catalyst[5,6†] yields a para enriched mixture. Once equilibrated, the gas can be removed from the catalyst, warmed and stored for weeks without significant reconversion. The polarization which is preserved as a direct consequence of the state symmetrization is sometimes referred to as *symmetrization order.*

§ II-3. Nuclear Spin Density Operator for H_2

Rather than pursuing our calculations of nuclear spin dynamics using the spin functions, it is more convenient to describe the ensemble of two proton systems with a density operator. In this section, a general expression will be derived for the density operator of an arbitrary mixture of ortho and parahydrogen (from now on, all references to the density operator will mean the density operator for nuclear spin). To begin, let us form the density matrix in the singlet–triplet basis for an

---

† Apachi Nickel-Silica catalyst, 197-CP, manufactured by Houdry, Division of Air Products Inc., Philadelphia, Pennsylvania. Activated charcoal can also be used,[6] but is not as efficient.

arbitrary ortho/para mixture with mole fraction χ_p parahydrogen.

$$\rho^P = \begin{array}{c} \\ \Psi_{1,-1} \\ \Psi_{1,0} \\ \Psi_{1,1} \\ \Psi_{0,0} \end{array} \begin{array}{c} \begin{array}{cccc} \Psi_{1,-1} & \Psi_{1,0} & \Psi_{1,1} & \Psi_{0,0} \end{array} \\ \begin{pmatrix} \frac{1}{3}(1-\chi_p) & 0 & 0 & 0 \\ 0 & \frac{1}{3}(1-\chi_p) & 0 & 0 \\ 0 & 0 & \frac{1}{3}(1-\chi_p) & 0 \\ 0 & 0 & 0 & \chi_p \end{pmatrix} \end{array} \tag{19}$$

To find the operator form of this matrix, ρ^P is expanded in terms of a diagonal basis set of operators.

$$\rho^P = \frac{1}{4} - d(\mathrm{I}_{z1} + \mathrm{I}_{z2}) - e(3\mathrm{I}_{z1}\mathrm{I}_{z2} - \mathrm{I}_1 \cdot \mathrm{I}_2) - f\mathrm{I}_1 \cdot \mathrm{I}_2 \tag{20}$$

Equating the matrix elements of ρ^P in Eq. (II-20) with the elements of ρ^P in Eq. (II-19), the coefficients d, e and f can be determined.

$$d = e = 0 \qquad \text{and} \qquad f = \frac{1}{3}(4\chi_p - 1) \tag{21}$$

Henceforth, the density operator for H_2 is written

$$\rho^P = \frac{1}{4} - f\mathrm{I}_1 \cdot \mathrm{I}_2 \tag{22}$$

§ II-4. Incorporation of p-H_2 into Disordered Spin Systems

In most cases, p-H_2 will be physically or chemically incorporated into a substrate spin system which is relatively disordered. The system will usually have some Curie-Law paramagnetism which is proportional to Zeeman order ($d \neq 0$), but at ambient temperatures and currently available magnetic fields, this is neglected in the theoretical analysis because it is smaller by at least three orders of magnitude (the exact factor will be calculated in the following chapter in connection with enhancements).

The density operator for the substrate spin system (spins 3 through N) is assumed to be completely disordered;

$$\rho^S = \prod_{i=3,N} (d_i)^{-1} \tag{23}$$

where $d_i = (2I_i + 1)$ is the total number of states of the ith spin of the substrate with spin quantum number I_i. The total density operator ρ^T which results from p-H_2 addition consists of N spins, with the p-H_2 protons labelled 1 and 2. The tensor product operation is employed to combine the states of each individual spin to form the states of the total system. While the substrate may contain many nuclear spins, it is only necessary to include spins which will significantly couple to the p-H_2 protons. The total density operator is constructed from the tensor product of the substrate and p-H_2 density operators.

$$\rho^T = \rho^P \otimes \rho^S \tag{24}$$

This operator is taken as the initial condition for the spin dynamics leading to the PASADENA signal expression, which is calculated in Chapter III.

§ II-5. References

1. E. Merzbacher, Quantum Mechanics, second edition, John Wiley and Sons, New York (1970)
2. L. D. Landau and E. M. Lifshitz, Quantum Mechanics, Volume 3, third edition, Pergamon Press, Oxford (1977)
3. G. Baym, Lectures on Quantum Mechanics, Benjamin/Cummings, Menlo Park, California (1969)
4. C. Cohen-Tannoudji, B. Diu and F. Laloë, Quantum Mechanics, Volume 2, Wiley-Interscience (1977)
5. I. F. Silvera, *Rev. Mod. Phys.* **52**, 393 (1968)
6. A. Farkas, Orthohydrogen, Parahydrogen and Heavy Hydrogen, Cambridge University Press, London (1935)

Chapter III

The PASADENA Effect

§ Introduction

The spin dynamics which lead to the PASADENA effect can be explored using the density operator given in Eq. (II-24). For the present, only the two protons which originated as p-H_2 will be included in the calculation. This will restrict the complexity of the density operators and signal expressions which are derived from the eigenvalues and eigenvectors of a Hamiltonian which contains a dipolar coupling of variable magnitude. This will keep the focus on the essential physics. In §III-2, the affect of the sudden change in the Hamiltonian on the p-H_2 density operator is considered, followed by an analysis of the affect of finite reaction time on the coherences initiated by the change. Finally, the PASADENA signal is computed in the slow reaction rate extreme, along with theoretical enhancement factors.

§ III-1. Eigenstates of the Two Proton System

The density operator resulting from hydrogenation serves as the initial condition for the ensuing spin dynamics. The exact form of this operator can vary substantially depending upon the details of the chemical steps. The most conspicuous of these subtle effects results from a finite hydrogenation rate. To predict the

response of the spin system, it is useful to find the density matrix in the eigenbasis of the product. To accomplish this, a high field, rotating frame Hamiltonian consisting of chemical shifts, dipolar and J couplings for a magnetically isolated proton pair is diagonalized.

$$\mathcal{H}_{int} = \omega_{z1}\mathrm{I}_{z1} + \omega_{z2}\mathrm{I}_{z2} + D[\mathrm{I}_1 \cdot \mathrm{I}_2 - 3\mathrm{I}_{z1}\mathrm{I}_{z2}] + J\mathrm{I}_1 \cdot \mathrm{I}_2 \tag{1}$$

where $D = \frac{\omega_D}{2}(3\cos^2\vartheta - 1)$ and $\omega_D = \gamma^2\hbar/r^3$. The eigenstates are

$$\begin{aligned} |1\rangle &= |\alpha\alpha\rangle \qquad |2\rangle = c_1|\alpha\beta\rangle + c_2|\beta\alpha\rangle \\ |3\rangle &= -c_2|\alpha\beta\rangle + c_1|\beta\alpha\rangle \qquad |4\rangle = |\beta\beta\rangle \end{aligned} \tag{2}$$

where

$$c_1 = \cos\frac{\kappa}{2} \quad \text{and} \quad c_2 = \sin\frac{\kappa}{2} \tag{3}$$

and

$$\tan\kappa = \frac{D+J}{\Delta} \tag{4}$$

The parameters $\bar{\omega}$ and Δ are defined as the average chemical shift and the chemical shift difference.

$$\bar{\omega} = \frac{1}{2}(\omega_1 + \omega_2) \tag{5}$$

$$\Delta = \omega_1 - \omega_2 \tag{6}$$

The dipolar interaction appearing in Eq. (III-1) is the secular part (i.e., $[\mathcal{H}_D, \mathrm{I}_z] = 0$) of the full dipole-dipole Hamiltonian with a symmetric coupling tensor.[1] The strength of the secular dipolar coupling depends on the angle ϑ which subtends the internuclear vector and the applied field direction. The chemical shifts $\omega_{zi}(\vartheta, \phi, \Omega_i)$ depend on the principal components of the shielding tensor and the set of Euler angles $\Omega_i = \{\alpha_i, \beta_i, \gamma_i\}$ relating its principal axis system to that of the dipolar coupling. The orientational dependence of the shifts and dipolar coupling introduces distinct spectral features for solid or surface bound nuclei, as will be explored in

Chapter VIII. At certain orientations, $D \gg \Delta$, and the singlet–triplet states of p-H_2 are recovered. For a liquid sample, the rapid reorientation of the spins reduces these tensorial interactions to their isotropic counterparts, which is zero for the dipolar coupling. In this case, the so called *weak coupling* limit often applies, with $\Delta \gg J$. The eigenstates are then well approximated by the direct product states $|\alpha\alpha\rangle$, $|\alpha\beta\rangle$, $|\beta\alpha\rangle$ and $|\beta\beta\rangle$.

§ III-2. The Sudden Approximation

When parahydrogen is deposited into magnetically inequivalent sites of a substrate, the parameters of the internal Hamiltonian change. If the change occurs instantaneously, then a given initial state Ψ_i will be unable to vary and will remain a state of the system. By instantaneous, it is meant that the time-scale for the change in the Hamiltonian is short compared to the period of the transitions from the initial state to other states.[2] This is a particular example of the *sudden approximation* of quantum mechanics, which is extremely accurate for the present case of p-H_2 addition to a substrate, since the spin Hamiltonian changes during the reaction occur on a picosecond time-scale while the relevant evolution of the spin system takes milliseconds.

Transitions from the initial p-H_2 eigenstates to those of the product occur subsequent to the sudden change in the Hamiltonian. The transition probability from an initial state Ψ_i to a final state Ψ_f is calculated using the general rules of quantum mechanics, i.e.,

$$w_{fi} = |\langle \Psi_f | \Psi_i \rangle|^2 \tag{7}$$

Hence, the transition probabilities from the singlet state of H_2 to the final states $|1\rangle$, $|2\rangle$, $|3\rangle$ and $|4\rangle$ are

$$w_1 = \frac{1}{2}\langle \alpha\alpha | \alpha\beta - \beta\alpha \rangle^2 = 0 \tag{7a}$$

$$w_2 = \frac{1}{2}\langle c_1\alpha\beta + c_2\beta\alpha | \alpha\beta - \beta\alpha \rangle^2 = \frac{1}{2}(1 - \sin\kappa) \tag{7b}$$

$$w_3 = \frac{1}{2}\langle c_3\alpha\beta + c_4\beta\alpha|\alpha\beta - \beta\alpha\rangle^2 = \frac{1}{2}(1+\sin\kappa) \tag{7c}$$

$$w_4 = \frac{1}{2}\langle\beta\beta|\alpha\beta - \beta\alpha\rangle^2 = 0 \tag{7d}$$

These probabilities determine the population distribution of the final states. Notice that the reaction of pure parahydrogen leads to population of only the middle two states, with the branching ratio being dependent upon the coupling strength. Thus, the intensities of the four allowed transitions which may be stimulated from this distribution will not necessarily be of equal intensity.

The correlation of the initial states of p-H_2 with the final product eigenstates for a Hamiltonian with $J \ll \Delta$ is shown in Fig. (III-1). The population is divided equally between the $|\alpha\beta\rangle$ and $|\beta\alpha\rangle$ states under these conditions. It is also clear from this diagram that absorptive and emisive transitions of equal intensity will result from this population distribution.

The manifestations of the sudden change in the Hamiltonian can be summarized by writing the initial density matrix in the general eigenbasis of the product Hamiltonian.

$$\rho^P \mapsto \begin{array}{c} \\ \langle 1| \\ \langle 2| \\ \langle 3| \\ \langle 4| \end{array} \begin{array}{c} \begin{array}{cccc} |1\rangle & |2\rangle & |3\rangle & |4\rangle \end{array} \\ \begin{pmatrix} \frac{1-f}{4} & 0 & 0 & 0 \\ 0 & \frac{1+f}{4} - \frac{f}{2}\sin\kappa & \frac{\cos\kappa}{2} & 0 \\ 0 & \frac{\cos\kappa}{2} & \frac{1+f}{4} + \frac{f}{2}\sin\kappa & 0 \\ 0 & 0 & 0 & \frac{1-f}{4} \end{pmatrix} \end{array} \tag{8}$$

Indeed, the populations represented by the diagonal elements of this matrix reduce to the transition probabilities w_i of Eq. (III-7a-d) if $f = 1$ (pure p-H_2).

The coherences represented by the off-diagonal elements of the matrix of ρ^P are created when the distribution of reaction times is narrow compared to the period of the coherence $|2\rangle\langle 3|$. In the opposite extreme, this zero-quantum coherence is

Fig. (III-1) Correlation diagram for the PASADENA effect. Molecular addition of parahydrogen into magnetically inequivalent sites gives equal population of the two $m_I = 0$ product molecule spin states, but no population of the $m_I = \pm 1$ states.

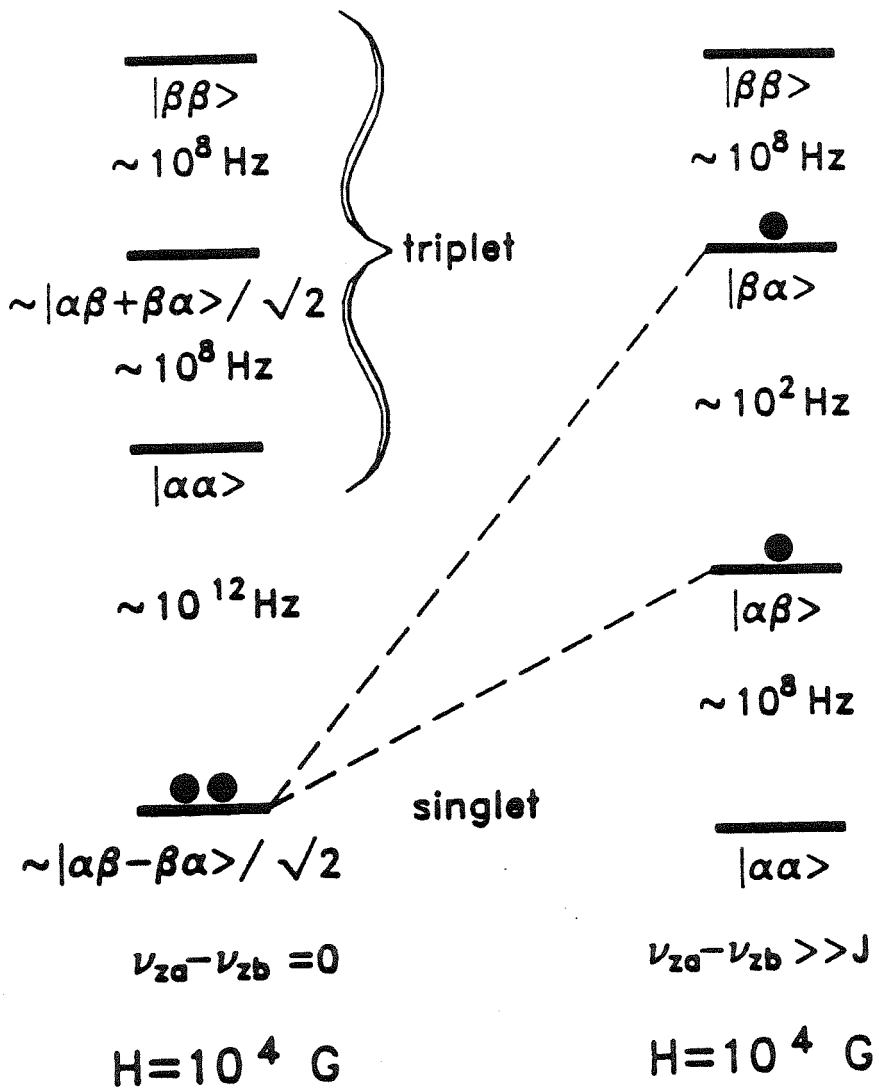

washed out if the distribution over the ensemble is relatively wide. This issue will be pursued in detail in §III-4.

§ III-3. Evolution of the Density Operator

The time dependence of the density operator is found from the Liouville–von Neumann equation.

$$\frac{d}{dt}\rho(t) = -i[\mathcal{H}(t), \rho(t)] \tag{9}$$

The formal solution of this equation is

$$\rho(t) = U(t)\rho(t)U^{\dagger}(t) \tag{10}$$

$$U(t) = T\exp\left\{-i\int_0^t \mathcal{H}(t')dt'\right\} \tag{11}$$

where T is the Dyson time-ordering operator. When $\mathcal{H}$ is time-independent, or if the dynamics can be broken down into periods which are piecewise time-independent, the propagator reduces to a product of factors (which do not necessarily commute).

$$\rho(t_0 + t_1 + t_2) = e^{-i\mathcal{H}_2 t}e^{-i\mathcal{H}_1 t}\rho(t_0)e^{i\mathcal{H}_1 t}e^{i\mathcal{H}_2 t} \tag{12}$$

The time dependence of some expectation value may then be calculated by finding the trace of the product of $\rho(t_0+t_1+t_2)$ with the appropriate observable operator. For example, the complex transverse magnetization is given by

$$M_+ = M_x + iM_y \propto \mathrm{Tr}\{\mathrm{I}_+\rho\} \qquad \text{where} \qquad \mathrm{I}_+ = \sum_i \mathrm{I}_{+i} \tag{13}$$

The observed rotating frame voltage response is proportional to the transverse magnetization. Neglecting the constant factors,

$$S(t) = \mathrm{Tr}\{\mathrm{I}_+ e^{-i\mathcal{H}t}\rho(t=0)e^{i\mathcal{H}t}\} \tag{14a}$$

$$= \sum_{m,n}\langle m|\mathrm{I}_+|n\rangle\langle n|e^{-i\mathcal{H}t}\rho(t=0)e^{i\mathcal{H}t}|m\rangle \tag{14b}$$

$$= \sum_{m,n} \langle m|\mathrm{I}_+|n\rangle\langle n|e^{-iE_n t}\rho(t=0)e^{iE_m t}|m\rangle \tag{14c}$$

$$= \sum_{m,n} \langle m|\mathrm{I}_+|n\rangle\langle n|\rho(t=0)|m\rangle e^{-i\omega_{mn} t} \tag{14d}$$

The allowed single-quantum transition frequencies are

$$\omega_{12} = \bar{\omega} - D + \frac{J}{2} - \frac{1}{2}\sqrt{\Delta^2 + (D+J)^2} \tag{15a}$$

$$\omega_{13} = \bar{\omega} - D + \frac{J}{2} + \frac{1}{2}\sqrt{\Delta^2 + (D+J)^2} \tag{15b}$$

$$\omega_{24} = \bar{\omega} + D - \frac{J}{2} + \frac{1}{2}\sqrt{\Delta^2 + (D+J)^2} \tag{15c}$$

$$\omega_{34} = \bar{\omega} + D - \frac{J}{2} - \frac{1}{2}\sqrt{\Delta^2 + (D+J)^2} \tag{15d}$$

Single-quantum transitions can be stimulated from equilibrium Zeeman order by the application of a resonant radio frequency pulse. During the pulse, the rotating frame Hamiltonian includes a magnetic field vector which lies in the x–y plane. The total Hamiltonian during the pulse is then $\mathcal{H} = \mathcal{H}_{int} + \mathcal{H}_1$, with

$$\mathcal{H}_1 = 2\pi\nu_1(\mathrm{I}_x \cos\Phi + \mathrm{I}_y \sin\Phi) \tag{16}$$

The parameters Φ and ν_1 characterize the phase and the strength (in Hz) of the applied radio frequency field. In the pulsed NMR experiments described in this work, values of $\nu_1 = 40,000$ Hz were typical.

§ III-4. The Time Averaged Density Operator

In theory, the creation of the off-diagonal matrix elements ρ_{23} and ρ_{32} results from the sudden change in the Hamiltonian. The frequency of the $|2\rangle \rightarrow |3\rangle$ transition is

$$\omega_{23} = \sqrt{(J+D)^2 + \Delta^2} \tag{17}$$

Depending on the time-scale of the H_2 addition process, the coherence may be preserved or it may vanish after taking the ensemble average. Consider an ensemble

of substrate molecules, each binding with a single para-H_2 molecule. The states $|2\rangle$ and $|3\rangle$ begin to evolve under the influence of a time independent Hamiltonian.

$$|2(t+t_0)\rangle = e^{-i\mathcal{H}t}|2(t_0)\rangle = e^{-iE_2t}|2(t_0)\rangle \tag{18a}$$

$$|3(t+t_0)\rangle = e^{-iE_3t}|3(t_0)\rangle \tag{18b}$$

The time dependence of the density matrix element is

$$\begin{aligned}\rho_{23}(t+t_0) &= \langle 2|\rho(t+t_0)|3\rangle \\ &= \langle 2|\rho(t_0)|3\rangle e^{-i\omega_{23}t}\end{aligned} \tag{19}$$

Under the experimental conditions of interest, the time of formation is not identical for all molecules of the ensemble, but rather there is a distribution of times $t_0 + \tau_i$ which define the start of the evolution differently for each. Accounting for this variation,

$$\begin{aligned}\langle 2|\rho(t+t_0+\tau_i)|3\rangle &= \langle 2|\rho(t_0+\tau_i)|3\rangle e^{-i\omega_{23}t} \\ &= \frac{\cos\kappa}{2} e^{-i\omega_{23}t} e^{-i\omega_{23}\tau_i}\end{aligned} \tag{20}$$

Taking the ensemble average (over n molecules), the element becomes

$$\langle \rho_{23} \rangle = \overline{\langle 2|\rho(t+t_0)|3\rangle} = \frac{\cos\kappa}{2} e^{-i\omega_{23}t} \sum_i^n e^{-i\omega_{23}\tau_i} \tag{21}$$

As a simple model, let a normalized Gaussian distribution around $\tau = 0$ describe the reaction times.

$$P(\tau) = \frac{e^{-\alpha\tau^2}}{\int_{-\infty}^{+\infty} e^{-\alpha\tau^2} d\tau} \tag{22}$$

The number in the ensemble must be large enough so that the discrete distribution is well approximated by the continuous function $P(\tau)$. The width of the distribution is parameterized by $\tau_{1/2}$, the FWHM of the Gaussian.

$$\tau_{1/2} = \left[\frac{2\ln 2}{\alpha}\right]^{1/2} \tag{23}$$

Thus,

$$\rho_{23} = \frac{\cos\kappa}{2}\exp(-i\omega_{23}t)\quad\frac{\int_{-\infty}^{+\infty} e^{-i\omega_{23}\tau}e^{-\alpha\tau^2}d\tau}{\int_{-\infty}^{+\infty} e^{-\alpha\tau^2}d\tau} \tag{24}$$

$$= \frac{\cos\kappa}{2}\exp(-i\omega_{23}t)\exp\left[\frac{-\omega_{23}^2\tau_{1/2}^2}{8\ln 2}\right] \tag{25}$$

Qualitatively, this formula reveals that the time-scale for the hydrogenation must be on the order of ω_{23}^{-1} in order to preserve the coherence of the initial density matrix. When this is not the case, the density matrix becomes diagonal.

Eq. (III-25) demonstrates that when the hydrogenation rate is sufficiently fast, the full density operator $1/4 - f\mathbf{I}_1 \cdot \mathbf{I}_2$ (for a 2 proton system) is preserved. This scalar operator is not effected by radio–frequency pulses, and no NMR signal results without an evolution period following reaction to the magnetically inequivalent form prior to the rf pulse. These dynamics will be explored for a two spin-1/2 system with arbitrary parameter κ in Chapter IX in connection with the RAYMOND effect. In Chapter IV, the dependence of the signal energy on the delay between the reaction and the acquisition pulse is numerically calculated for several different weakly coupled spin systems.

Typically, the off-diagonal density matrix elements will be averaged away and the rf pulse can immediately convert those populations into single-quantum operators which freely evolve into operators whose trace with I_+ is nonzero. The key requirements for this latter step are magnetic inequivalence of the protons and a dipolar or resolved J coupling between them.

To analytically derive the free induction, it is assumed that the diagonal density operator can be expanded as follows:

$$\langle\rho(0)\rangle = \sum_i \langle i|\left(\frac{1}{4} - f\mathbf{I}_1\cdot\mathbf{I}_2\right)|i\rangle|i\rangle\langle i|$$

$$= \frac{1}{4} - f\ [a(\mathrm{I}_{z1} - \mathrm{I}_{z2}) + b\ \mathrm{I}_1 \cdot \mathrm{I}_2 + c(3\mathrm{I}_{z1}\mathrm{I}_{z2} - \mathrm{I}_1 \cdot \mathrm{I}_2)] \tag{26}$$

with the constants a,b and c to be determined. By setting the off-diagonal elements to zero and equating the diagonal elements with the averaged operator, the initial density operator can be derived.

$$\begin{aligned}\langle\rho(0,\kappa)\rangle = \frac{1}{4} - f\Bigg[&\frac{1}{2}\sin\kappa\cos\kappa(\mathrm{I}_{z1} - \mathrm{I}_{z2}) \\ &+ \frac{1}{3}\cos^2\kappa\ (3\mathrm{I}_{z1}\mathrm{I}_{z2} - \mathrm{I}_1 \cdot \mathrm{I}_2) \\ &+ \left(1 - \frac{2}{3}\cos^2\kappa\right)\mathrm{I}_1 \cdot \mathrm{I}_2\Bigg]\end{aligned} \tag{27}$$

Since $\mathrm{I}_1 \cdot \mathrm{I}_2$ is invariant to rotations, only the first and second terms in the brackets can lead to signal following a single brief pulse.

The pulse sequence consists of a period τ_w during which chemical reaction occurs, followed by a resonant radio frequency pulse with amplitude ν_1 (in Hz) and duration τ_p which rotates I_z by an angle $\theta = 2\pi\nu_1\tau_p$, and then a period of free induction decay during which the signal is detected.

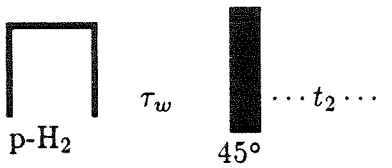

SEQ-III-1

The transformed density operator contains the terms

$$\begin{aligned}\rho_{SQ} = f\Bigg[&\frac{1}{2}\sin\kappa\cos\kappa\sin\theta(\mathrm{I}_{x2} - \mathrm{I}_{x1}) \\ &- \cos^2\kappa\sin\theta\cos\theta(\mathrm{I}_{z1}\mathrm{I}_{x2} + \mathrm{I}_{x1}\mathrm{I}_{z2})\Bigg]\end{aligned} \tag{28}$$

where the subscript SQ indicates that these are the terms which can evolve into signal during free evolution under a secular Hamiltonian satisfying $[\mathcal{H}_{int}, \mathrm{I}_z] = 0$. Having computed the eigenstates and initial density operator, the time dependence

of the detected transverse magnetization can be obtained using the trace expression of Eq. (III-14d). The PASADENA signal is

$$S(t,\kappa) = \frac{f}{4}\cos^2\kappa\sin\theta\Big\{(-\cos\theta+\sin\kappa-\cos\theta\sin\kappa)e^{-i\omega_{12}t} + (-\cos\theta-\sin\kappa+\cos\theta\sin\kappa)e^{-i\omega_{13}t} + (\cos\theta-\sin\kappa+\cos\theta\sin\kappa)e^{-i\omega_{24}t} + (\cos\theta+\sin\kappa-\cos\theta\sin\kappa)e^{-i\omega_{34}t}\Big\} \qquad (29)$$

Notice that the relative amplitudes of the four transitions varies with the coupling strength.

§ III-5. Theoretical Enhancement Factors

To quantify the signal enhancement arising from the PASADENA effect, it is convenient to relate the signal amplitudes with some reference. Two convenient choices are the NMR signals arising from hypothetical samples at zero and 300 K after a 90° pulse.

§ III-5.1. The Conventional NMR Spectrum

The initial condition for the "conventional" NMR spectrum is Zeeman order. The degree of order present is dependent on the temperature and static magnetic field strength. In reality, the spin order is mainly of the Zeeman variety only in the high temperature regime. At milliKelvin temperatures, the actual operator is a linear combination of scalar, dipolar as well as Zeeman order. However, for a 90° pulse, only Zeeman order generates transverse magnetization. For this pulse angle, the initial density operator considered is $b\mathrm{I}_z$. The time domain signal following the pulse evolves from $\sigma(0) = b\mathrm{I}_x$. Substitution of $\sigma(0)$ into the trace relation yields $S(t)$ (relaxation neglected).

$$S(t) = \frac{b}{2}\Big\{(1+\sin\kappa)\left(e^{-i\omega_{12}t}+e^{-i\omega_{24}t}\right) - (1-\sin\kappa)\left(e^{-i\omega_{13}t}+e^{-i\omega_{24}t}\right)\Big\} \qquad (30)$$

The factor b in Eq. (III-30) which scales the Zeeman ordering relates the amplitude of NMR signals for different temperatures and gyromagnetic ratios. In the high temperature approximation, the Curie-Law z-component magnetization is given by

$$b = \frac{\gamma\hbar H_0}{kT(2I+1)^N} \tag{31}$$

At low temperatures (c.a. $T \leq 1$ mK), the population of the levels must be described by a linear combination of scalar, Zeeman and dipolar order.

$$\sigma(0) = \frac{1}{4} + a\mathbf{I}_1 \cdot \mathbf{I}_2 + b\mathbf{I}_z + c(3\mathbf{I}_{z1}\mathbf{I}_{z2} - \mathbf{I}_1 \cdot \mathbf{I}_2) \tag{32}$$

The Curie-Law approximation for b is obviously not applicable at zero Kelvin, but b may be quickly calculated since the equilibrium population distribution is known exactly in this limit. When all the spins are aligned, only the $|\alpha\alpha\rangle$ state is occupied. The matrix element $|\alpha\beta\rangle\langle\alpha\beta|$ is unity and all others are zero. By multiplying $\sigma(0)$ by I_z and taking the trace,

$$\mathrm{Tr}\{\sigma(0, 0^\circ K)\mathrm{I}_z\} = b(0^\circ K)\,\mathrm{Tr}\{\mathrm{I}_z^2\} \tag{33}$$

For two protons

$$b(0^\circ K) \equiv b_0 = \frac{1}{\mathrm{Tr}\{\mathrm{I}_z^2\}} = \frac{1}{2\,\mathrm{Tr}\{\mathrm{I}_{z1}^2\}} = \frac{1}{2} \tag{34}$$

In a magnetic field of $\mathrm{H}_0 = 4.7$ T and T=300° K, $b_0 = 62,753 \cdot b(300^\circ\ \mathrm{K})$. Taking the ratio of the conventional and PASADENA transition amplitudes at ω_{12},

$$\frac{\|S_{para}\|}{\|S(300^\circ)\|} = \frac{\|S_{para}\|}{\|S(0^\circ)\|} \times \frac{\|S(0^\circ)\|}{\|S(300^\circ)\|}$$

$$= \frac{f\cos^2\kappa\sin\theta(\sin\kappa - \cos\theta - \cos\theta\sin\kappa)}{2b(1+\sin\kappa)} \tag{35}$$

This ratio is plotted for $0 \leq \theta \leq \pi/2$ and $0 \leq \kappa \leq \pi$ in Fig. (III-2a) for the $|1\rangle \rightarrow |2\rangle$ or $|2\rangle \rightarrow |4\rangle$ transitions and in Fig. (III-2b) for the $|1\rangle \rightarrow |3\rangle$ or $|3\rangle \rightarrow |4\rangle$ transitions. In the weak coupling limit, the PASADENA signal has a maximum value of $f/2$ for a 45° pulse. In this case, the enhancement is

$$\frac{\|S_{para}\|_{max}}{\|S(300^\circ)\|_{max}} = 31,376 \cdot f \tag{36}$$

Fig. (III-2a) Contour plot of Eq. (III-35) for the $|1\rangle \rightarrow |2\rangle$ or $|2\rangle \rightarrow |4\rangle$ transitions which shows the θ, κ (pulse angle and coupling strength parameter, respectively) dependence of the enhancement of the PASADENA amplitude relative to the conventional NMR for the same transition. The greatest enhancement is obtained in the weak coupling regime using a 45° pulse.

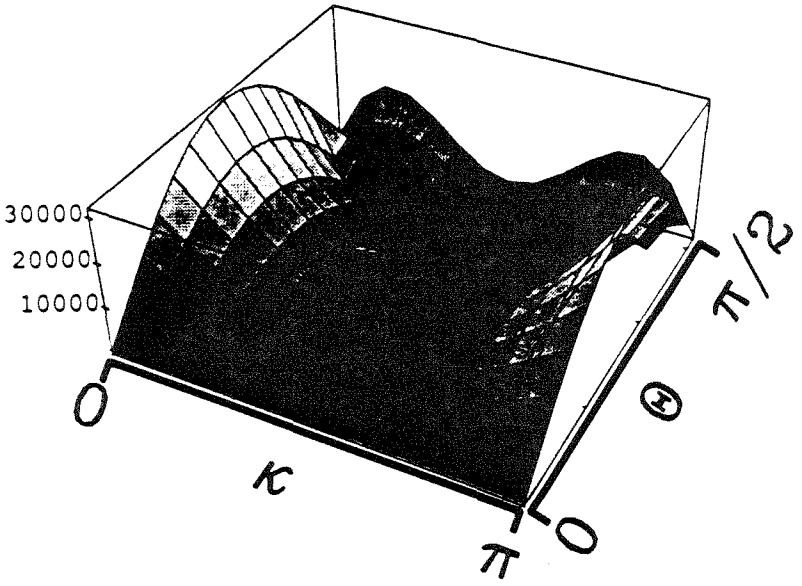

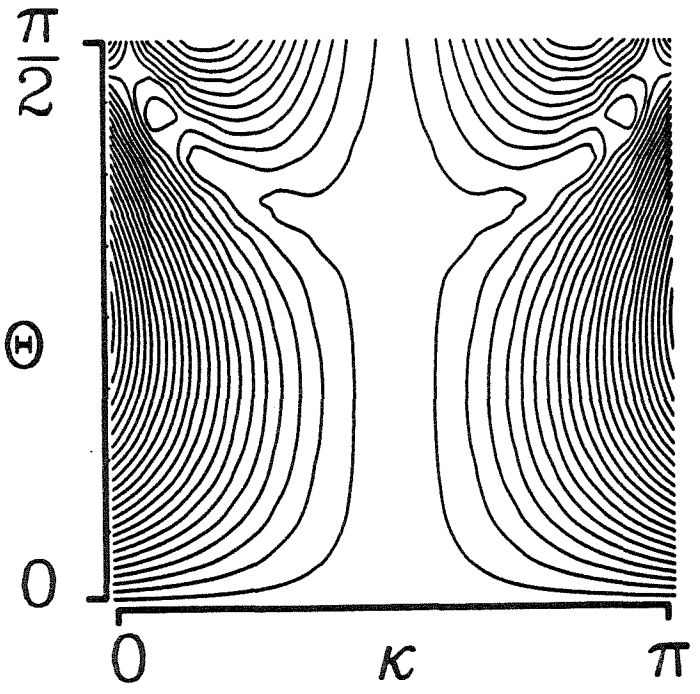

Fig. (III-2b) Contour plot of the analog of Eq. (III-35) for the $|1\rangle \rightarrow |3\rangle$ or $|3\rangle \rightarrow |4\rangle$ transitions.

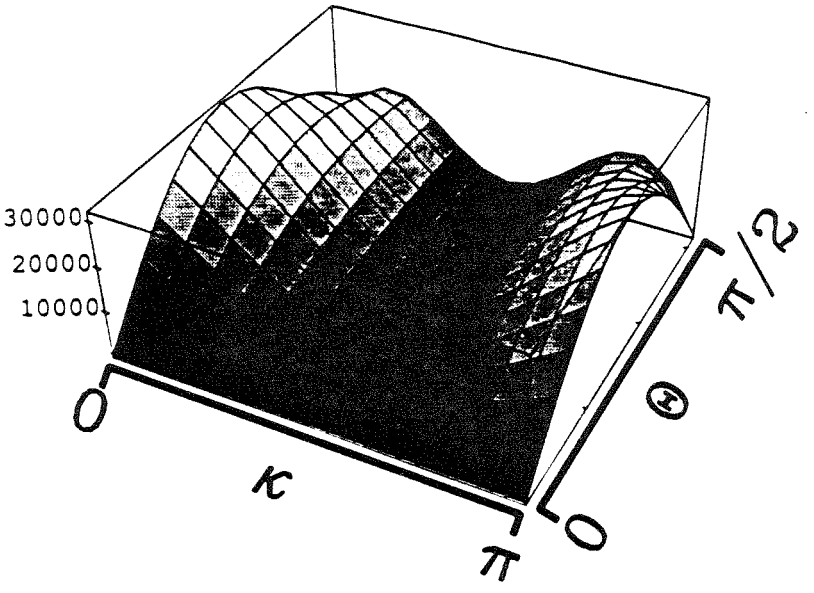

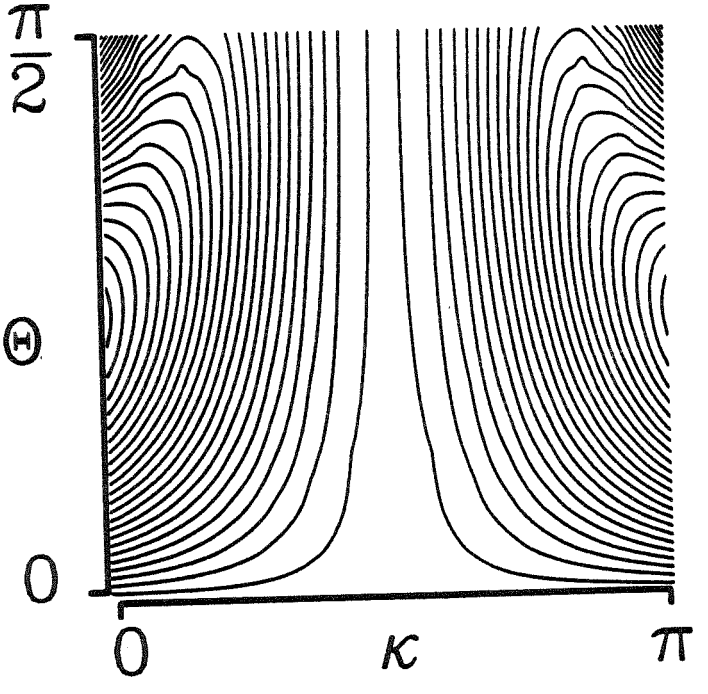

The experimentally observed enhancements will be degraded for several reasons. When the transitions are not resolved, there exists the possibility for destructive interference. This type of cancellation is an important factor governing the inhomogeneous lineshape arising from disoriented samples, in which the dipolar coupling takes a range of values. The above expressions do not account for this "powder broadening," which is dealt with in Chapter VIII. Hence, they only apply to situations for which the principal axis systems of the dipolar coupling and chemical shifts have a fixed orientation with respect to the static field for all sites, or to liquids in which rapid tumbling leads to $D = 0$ and a resolved J coupling.

§ III-6. References

1. M. Mehring, High Resolution NMR in Solids, second edition, Springer-Verlag, Heidelberg (1983)
2. L. D. Landau and E. M. Lifshitz, Quantum Mechanics, Volume 3, third edition, Pergamon Press, Oxford (1977)

Chapter IV

Liquids

§ Introduction

In a nonviscous liquid sample, the electron-nuclear couplings and fast molecular motion reduce tensorial interactions to their isotropic components. For this reason, the dipolar coupling vanishes entirely. The chemical shifts are also averaged to their isotropic values. The liquid state spectra are therefore usually characterized by high-resolution of the individual transitions. The isotropic Hamiltonian assumes the form

$$\mathcal{H}_{int} = \sum_{i<j}^{N} J_{ij}\mathbf{I}_i \cdot \mathbf{I}_j + \sum_{i}^{N} \omega_{zi}\mathrm{I}_{zi} \tag{1}$$

Two spins are said to be weakly coupled when $\Delta \gg J$. In this case, the eigenfunctions are just the direct product functions $|\alpha\alpha\rangle$, $|\alpha\beta\rangle$, $|\beta\alpha\rangle$ and $|\beta\beta\rangle$, since $c_1 = 1$, $c_2 = 0$ in Eq. (III-2). The PASADENA signal expression can be simplified in this limit because the terms in Eq. (III-29) which contain $\sin\kappa$ can be neglected, simplifying both the amplitude and frequency arguments. Neglecting relaxation factors,

$$\lim_{\kappa\to 0} S(t) = \frac{f}{4}\sin\theta\cos\theta\left\{e^{-i\omega_{24}t} + e^{-i\omega_{34}t} - e^{-i\omega_{12}t} - e^{-i\omega_{13}t}\right\} \tag{2}$$

Using $\tan\kappa \ll 1$ and

$$\sqrt{\Delta^2 + J^2} = \sqrt{\Delta^2(1 + \tan^2\kappa)} \approx |\Delta|, \tag{3}$$

Eq. (IV-2) becomes

$$\lim_{\kappa\to 0} S(t) = i\frac{f}{2}\sin\theta\cos\theta\sin\frac{Jt}{2}\left\{e^{-i\omega_1 t} + e^{-i\omega_2 t}\right\} \tag{4}$$

Clearly, a 45° pulse optimizes the signal when $\sin\kappa \ll \cos\theta$. Also notice that the factor of $\sin(Jt/2)$ is mathematically responsible for the A/E multiplet structure observed in the PASADENA effect. For comparison, the conventional free induction decay in the weak coupling limit reduces to

$$\lim_{\kappa\to 0} S(t) = \frac{b}{2}\cos\frac{Jt}{2}\left\{e^{-i\omega_{z1} t} + e^{-i\omega_{z2} t}\right\} \tag{5}$$

which is 90° out of phase with the PASADENA signal at $t = 0$. The dispersive nature of this signal can be rectified in either of two ways; 1) by using an x-phase pulse rather than y-phase or 2) by rotating the phase of the detector by 90°. In the latter, the observed operator becomes

$$e^{-i\pi/2}\mathrm{I}_+ = -i\mathrm{I}_x + \mathrm{I}_y \tag{6}$$

which changes the observed signal as follows:

$$S(t) = \mathrm{Tr}\{e^{i\pi/2}\mathrm{I}_+\rho(t)\} = \frac{f}{2}\sin\theta\cos\theta\sin\frac{Jt}{2}\left\{e^{-i\omega_{z1} t} + e^{-i\omega_{z2} t}\right\} \tag{7}$$

The Fourier transform of Eq. (IV-7) yields the standard PASADENA spectrum. Experimentally, the spectrum can always be phase corrected with software to conform to this standard, regardless of the pulse phase.

§ IV-1. Product Operator Formalism

The weak coupling limit introduces a great simplification for the calculation of spin dynamics in liquids, permitting the simple "product operator formalism" to be employed[1,2]. In this limit, the terms of the internal Hamiltonian commute, permitting the evolution to be carried through one interaction at a time by successive rotations.

When $\Delta \gg J$, the diagonal elements of the internal Hamiltonian become much larger than the off diagonal elements such that the effects of the latter become negligible. This amounts to truncation of the scalar coupling

$$\mathbf{I}_1 \cdot \mathbf{I}_2 \mapsto \mathrm{I}_{z1}\mathrm{I}_{z2} \qquad \text{if} \quad \Delta \gg J \tag{8}$$

The Hamiltonian becomes

$$\mathcal{H}_{int} = \sum_{i<j}^{N} J_{ij}\mathrm{I}_{zi}\mathrm{I}_{zj} + \sum_{i}^{N} \omega_{zi}\mathrm{I}_{zi} \tag{9}$$

This Hamiltonian lends itself to a convenient method for propagation of the density operator. The problem is reduced to one of evaluating the density operator rotations effected by the linear (rf pulses described as Dirac δ functions, chemical shifts) and bilinear (J coupling) terms of the Hamiltonian. This product operator formalism has the advantage of retaining operator quantities and the physical meaning associated with them throughout the calculation. This is of particular importance in designing sophisticated two-dimensional pulse sequences. The rotations can be derived by using a series expansion of the exponentials.

$$\begin{aligned} B' &= e^{-i\chi A} B e^{i\chi A} \\ &= \left(\sum_{n=0}^{\infty} \frac{(-i\chi A)^n}{n!}\right) B \left(\sum_{n=0}^{\infty} \frac{(i\chi A)^n}{n!}\right) \\ &= B - i\chi AB + \frac{i^2\chi^2}{2!}A^2B - \ldots \\ &= B - i\chi[A,B] + \frac{i^2\chi^2}{2!}[A,[A,B]] + \ldots \\ &= \sum_{n=0}^{\infty} \frac{(-i\chi)^n}{n!} C_n \qquad \text{with} \qquad C_0 = B \quad \text{and} \quad C_n = [A, C_{n-1}] \end{aligned} \tag{10}$$

§ IV-1.1. Linear Operators

To derive the transformation formulae for the Cartesian spin operators, let us make the substitution $A = \mathrm{I}_a$, with $a = x, y$ or z; $B = \mathrm{I}_b$, $b = x, y$ or z; $c = x, y$ or z with $a \neq b \neq c$ in Eq. (IV-10). After factoring terms in sine and cosine,

$$\exp(-i\chi\mathrm{I}_a)\mathrm{I}_b \exp(i\chi\mathrm{I}_a) = \mathrm{I}_b \cos\chi + \mathrm{I}_c \sin\chi \tag{11}$$

For example,

$$\exp(-i\mathrm{I}_z\pi/2)\mathrm{I}_x\exp(i\mathrm{I}_z\pi/2) = \mathrm{I}_y \tag{12}$$

Positive angle rotations will consistently be treated as counterclockwise rotations from the viewpoint of looking down the rotation axis toward the origin. For typographical simplicity, such unitary transformations will be represented using an arrow notation, so that Eq. (IV-12) may be written

$$\mathrm{I}_x \xrightarrow{\frac{\pi}{2}\mathrm{I}_z} \mathrm{I}_y. \tag{13}$$

Transformations involving various permutations of x, y and z may be similarly derived using the counterclockwise rotation convention.

§ IV-1.2. Bilinear Operators

For the weak bilinear coupling term between two spins (AX system), substitute $A = \mathrm{I}_{a1}\mathrm{I}_{a2}$ and let $B = \mathrm{I}_{b1}$. This can be viewed as a rotation about the $a1$ axis by an angle of $\chi\mathrm{I}_{a2}$ in spin space. Consequently, it is necessary to evaluate trigonometric functions of a spin operator. Substituting the product $\chi\mathrm{I}_{a2}$ for χ in the series expansion and factoring terms in sine and cosine,

AX system – two spins-1/2

$$\cos(\chi\mathrm{I}_a) = \cos\frac{\chi}{2} \tag{14}$$

$$\sin(\chi\mathrm{I}_a) = 2\mathrm{I}_a\sin\frac{\chi}{2} \tag{15}$$

Thus, using the arrow notation,

$$\mathrm{I}_{b1} \xrightarrow{\chi\mathrm{I}_{a1}\mathrm{I}_{a2}} \mathrm{I}_{b1}\cos\frac{\chi}{2} + 2\mathrm{I}_{c1}\mathrm{I}_{a2}\sin\frac{\chi}{2} \tag{16}$$

Bilinear rotations for AX_2 and AX_3 systems can also be derived.

AX_2 system–3 spins-1/2

$$\cos(\chi I_a) = \cos^2\frac{\chi}{2} - 4I_{a1}I_{a2}\sin^2\frac{\chi}{2} \tag{17}$$

$$\sin(\chi I_a) = I_a \sin\chi \tag{18}$$

with $\quad I_a = I_{a1} + I_{a2}$

AX_3 system–4 spins-1/2

$$\cos(\chi I_a) = \cos^3\frac{\chi}{2} - 4(I_{a1}I_{a2} + I_{a1}I_{a3} + I_{a2}I_{a3})\sin^2\frac{\chi}{2}\cos\frac{\chi}{2} \tag{19}$$

$$\sin(\chi I_a) = 2I_a \sin\frac{\chi}{2}\cos^2\frac{\chi}{2} - 8I_{a1}I_{a2}I_{a3}\sin^3\frac{\chi}{2} \tag{20}$$

with $\quad I_a = I_{a1} + I_{a2} + I_{a3}$

For use in Chapter V in which the PASADENA effect is derived for D_2, the following two formulas are needed.

AX system–2 spins-1

$$\cos(\chi I_a) = 1 - \frac{\chi^2}{2!}I_a^2 + \frac{\chi^4}{4!}I_a^4 + \ldots \tag{21}$$

$$= 1 + I_a^2\left[-\frac{\chi^2}{2!} + \frac{\chi^4}{4!}\ldots\right]$$

$$= 1 + I_a^2(\cos\chi - 1) \tag{22}$$

where the following has been used:

$$I_a^2|1m\rangle = I_a^{2n}|1m\rangle \qquad \text{for} \quad n = 1, 2, 3, \ldots \tag{23}$$

Noting that

$$I_a|1m\rangle = I_a^{2n+1}|1m\rangle \qquad \text{for} \quad n = 0, 1, 2, \ldots \tag{24}$$

then clearly

$$\sin(\chi I_a) = I_a \sin\chi \tag{25}$$

Once the density operator has been propagated through some sequence of rf-pulses and free evolution, expectation values can be calculated as usual by the trace relationship $\langle Q \rangle = \mathrm{Tr}\{\rho Q\}$.

§ IV-2. Creation of Coherence from J–Order

In this section, the response of the averaged, diagonal density operator to an rf pulse and the subsequent free evolution is found when $\Delta \gg J$. Letting $\kappa = 0$ in Eq. (IV-27),

$$\rho_{diag}(0) = \frac{1}{4} - f\mathrm{I}_{z1}\mathrm{I}_{z2} \tag{26}$$

which responds to a θ angle pulse as

$$\begin{aligned} \rho(0) \xrightarrow{\theta \mathrm{I}_y} \frac{1}{4} &- f\cos^2\theta \mathrm{I}_{z1}\mathrm{I}_{z2} - f\sin^2\theta \mathrm{I}_{x1}\mathrm{I}_{x2} \\ &- f\sin\theta\cos\theta(\mathrm{I}_{z1}\mathrm{I}_{x2} + \mathrm{I}_{x1}\mathrm{I}_{z2}) \end{aligned} \tag{27}$$

It is immediately obvious that $\theta = 45°$ maximizes the single-quantum operators. The third term can be rewritten using the identity $\mathrm{I}_x = \frac{1}{2}(\mathrm{I}_+ + \mathrm{I}_-)$, yielding

$$\mathrm{I}_{x1}\mathrm{I}_{x2} = \frac{1}{4}(\mathrm{I}_{+1}\mathrm{I}_{+2} + \mathrm{I}_{-1}\mathrm{I}_{-2} + \mathrm{I}_{-1}\mathrm{I}_{+2} + \mathrm{I}_{+1}\mathrm{I}_{-2}), \tag{28}$$

which is a superposition of zero and double-quantum coherence. Notice that for a 90° pulse, this is the sole term, with single-quantum terms vanishing. This feature will be of central importance in the design of two dimensional pulse sequences for kinetic studies (see Chapter VII). The next step is to calculate the free evolution due to $\mathcal{H}_{int}$. The term $\mathrm{I}_{x1}\mathrm{I}_{x2}$ commutes with the J coupling term and so its time dependence is due to the chemical shifts only. For more than two spins, not all couplings will commute, giving rise to J structure in the $p = 0, 2$ quantum spectra. The overall time evolution is

$$\begin{aligned} \rho(t) = &\frac{1}{4} - f\cos^2\theta \mathrm{I}_{z1}\mathrm{I}_{z2} && \text{populations} \\ &- \frac{f}{4}\left\{\mathrm{I}_{-1}\mathrm{I}_{+2}e^{2i\Delta t} + \mathrm{I}_{+1}\mathrm{I}_{-1}e^{-2i\Delta t}\right\}\sin^2\theta && \text{zero-quantum} \end{aligned}$$

$$
\begin{aligned}
&-\frac{f}{4}\left\{\mathrm{I}_{+1}\mathrm{I}_{+2}e^{2i\bar{\omega}t}+\mathrm{I}_{-1}\mathrm{I}_{-2}e^{-2i\bar{\omega}t}\right\}\sin^2\theta && \text{double-quantum}\\
&-\frac{f}{2}\left\{\cos\omega_{z2}t\left[2\cos\frac{Jt}{2}\mathrm{I}_{z1}\mathrm{I}_{x2}-\sin\frac{Jt}{2}\mathrm{I}_{y2}\right]\right. && \text{single-quantum}\\
&\quad-\sin\omega_{z2}t\left[2\cos\frac{Jt}{2}\mathrm{I}_{z1}\mathrm{I}_{y2}-\sin\frac{Jt}{2}\mathrm{I}_{x2}\right]\\
&\quad-\cos\omega_{z1}t\left[2\cos\frac{Jt}{2}\mathrm{I}_{x1}\mathrm{I}_{z2}-\sin\frac{Jt}{2}\mathrm{I}_{y1}\right]\\
&\quad\left.-\sin\omega_{z1}t\left[2\cos\frac{Jt}{2}\mathrm{I}_{y1}\mathrm{I}_{z2}-\sin\frac{Jt}{2}\mathrm{I}_{x1}\right]\right\}\sin\theta\cos\theta && (29)
\end{aligned}
$$

These terms will be frequently referred to in various contexts.

Taking the trace of the single-quantum terms with I_+ leads to exactly the same result as Eq. (IV-4), which was deduced by introducing the weak coupling, large pulse angle approximation into the signal expression for arbitrary κ.

§ IV-3. PASADENA Spectrum of A_2X_3 Group

The identities derived above can be applied to calculate the proton spectrum of an A_2X_3 group. An example is the CH_2CH_3 of ethylbenzene formed by hydrogenation of styrene. The proton NMR spectrum consists of an aromatic region, shifted down field by 6 ppm, and the methyl and methylene multiplets at approximately 1 and 2 ppm, respectively. The J couplings of the methyl and methylene group nuclei with the aromatic protons are unresolved, so the aromatic region could be treated as an isolated spin system in itself. The coupling between the methyl and methylene protons is 7.5 Hz, small enough compared to their chemical shift difference that the weak coupling approximation may be applied.

The NMR signal of this five-spin A_2X_3 system may be rapidly derived analytically for ordinary NMR and PASADENA using the expansions for the trigonometric functions of spin operators for the AX_2 and AX_3 cases. The initial condition for the conventional NMR is in the high temperature approximation proportional to Zeeman order, $\rho_{eq}(0) = b(\mathrm{I}_{zA}+\mathrm{I}_{zB})$, where the subscripts A and B denote

magnetically equivalent groups of three and two spins respectively.

$$\mathrm{I}_{zA} = \mathrm{I}_{z1} + \mathrm{I}_{z3} + \mathrm{I}_{z5} \qquad \text{and} \qquad \mathrm{I}_{zB} = \mathrm{I}_{z2} + \mathrm{I}_{z4} \tag{30}$$

After creating I_x with a 90°_y rf pulse, inspection of the trigonometric identities of Eq. (IV-19,20) reveals that the only terms with nonzero trace with I_+ are

$$\mathrm{I}_{xa} \cos^2 \frac{Jt}{2} + \mathrm{I}_{xb} \cos^3 \frac{Jt}{2} \tag{31}$$

Following chemical shift evolution and neglecting T_2 relaxation,

$$S_{eq}(t) = 8b \left\{ 3\cos^2 \frac{Jt}{2} e^{i\omega_{az}t} + 2\cos^3 \frac{Jt}{2} e^{i\omega_{zb}t} \right\} \tag{32}$$

The amplitude factor $b(0\ \mathrm{K})$ for the reference signal is

$$b(0) = \frac{5/2}{\mathrm{Tr}\{\mathrm{I}_{zA} + \mathrm{I}_{zB}\}} = \frac{1}{16} \tag{33}$$

The expected spectrum may be deduced by extension of the two-spin theory. The multiplet intensities can be predicted in the weak coupling limit. Instead of the usual paramagnetic multiplet intensity pattern of $\{3/4, 3/2, 3/4\}$ for the methyl triplet at 0 K, for PASADENA, it is $\{1/8, 0, -1/8\}$ for $f = 1$. For the quartet, the patterns are $\{1/4, 3/4, 3/4, 1/4\}$ and $\{1/16, 1/16, -1/16, -1/16\}$ for the conventional and PASADENA signals, respectively, with interference effects partially cancelling the intensity of the inner lines on the latter. The numerically calculated maximum enhancement factor with $\chi_p = 0.5$ for the outer lines of the methyl triplet is

$$\frac{\|S_{para}\|}{\|S_{eq}(300^\circ)\|} = 3.5 \times 10^3 \tag{34}$$

This is approximately an order of magnitude lower than the corresponding number for the AX system because of dilution by unpolarized spins of the reactant.

It turns out that much of the essential spin physics is contained in the two-spin analog of the five-spin propionitrile or ethylbenzene dynamics. This fact will be especially helpful in the design and analysis of pulse sequences in the two-dimensional NMR experiments of Chapter VII, since a reduction in the number of spins in the calculation can dramatically reduce the number of propagated terms. When the exact time dependence of the density operator is required, as is necessary when choosing optimal preparation periods, the additional J coupling structure cannot be disregarded. Numerical density matrix propagations are necessary in these instances.

§ IV-4. Experimental PASADENA Spectrum of Proprionitrile

The first experimental observation of the PASADENA effect involved the hydrogenation of acrylonitrile to propionitrile. This A_2X_3 spin system yields nearly the same spectrum as the ethylbenzene spin subsystem.

The equilibrium acrylonitrile spectrum is shown in Fig. (IV-1a). When H_2 enriched to $\chi_p = 0.5$ is bubbled through the sample for 1.1 s, followed by a 45° pulse (see SEQ-III-1), the ensuing free induction yields the PASADENA spectrum in Fig. (IV-1b). For comparison, a numerical simulation of the PASADENA lineshape appears in Fig. (IV-1d). If sufficient time is allowed to pass, spin lattice relaxation will bring the sample back to thermal equilibrium. After this period, acquisition of the ordinary NMR spectrum with no additional p-H_2 added gives the spectrum of Fig. (IV-1c), in which the enhanced transitions are absent.

§ IV-5. Dynamics of $1/4 - \mathbf{I}_1 \cdot \mathbf{I}_2$

When the rate of chemical reaction is rapid compared to the period of coherence initiated upon incorporation of the H_2 into the substrate, the off diagonal elements of the density matrix represented by the operator $I_{x1}I_{x2} + I_{y1}I_{z2}$ do not vanish. Since $[\mathcal{H}_{int}, \mathbf{I}_1 \cdot \mathbf{I}_2] \neq 0$, the density operator becomes time dependent

Fig. (IV-1) Demonstration that parahydrogen and synthesis allow dramatically enhanced nuclear alignment. Part a. shows the proton NMR spectrum prior to the reaction. The intense lines are due to the acrylonitrile substrate. Part b. was obtained subsequent to the hydrogenation to propionitrile but prior to spin-lattice equilibration. The large antiphase multiplets in response to a 45° pulse are observed only with para-enriched H_2 as reagent. Part c. is the spectrum of the equilibrated sample and shows that the signal of b. was a large transient enhancement. Part d. is a lineshape simulation demonstrating the agreement of the theory with the experiment of part b. The linewidth is 3.5 Hz due to inhomogeneity of the field, which is degraded by the H_2 bubbling.

Fig (IV-1) (Continued)

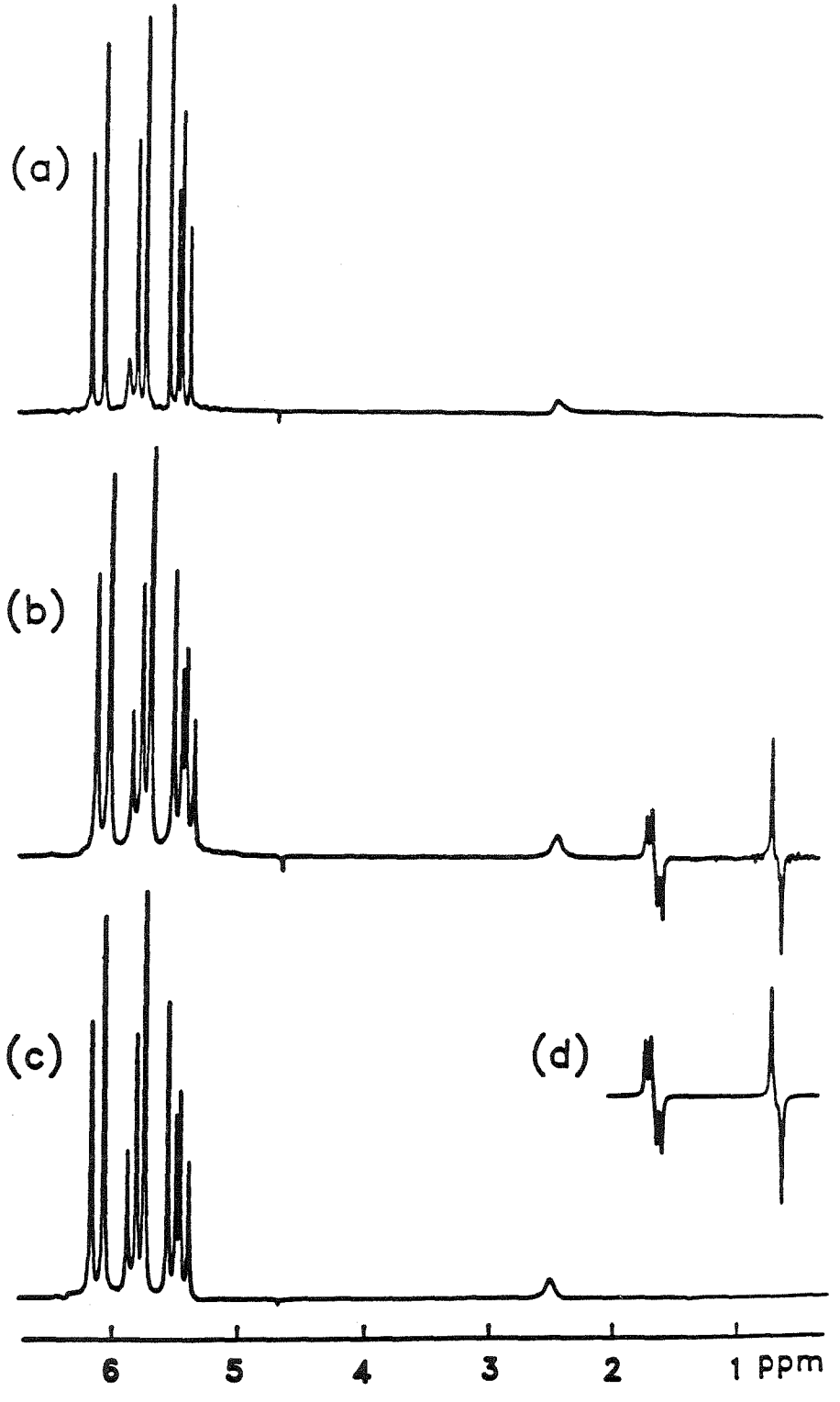

during the period before the rf pulse.

$$\rho(\tau_w) = \frac{1}{4} - \mathrm{I}_{z1}\mathrm{I}_{z2} - (\mathrm{I}_{x1}\mathrm{I}_{x2} + \mathrm{I}_{y1}\mathrm{I}_{y2})\cos(\Delta\tau_w) + (\mathrm{I}_{x1}\mathrm{I}_{y2} - \mathrm{I}_{y1}\mathrm{I}_{x2})\sin(\Delta\tau_w) \tag{35}$$

Application of the θ pulse followed by further free evolution with detection gives the signal during t_2 as

$$\begin{aligned} S(\tau_w,&\theta,t_2) \\ &= -\frac{1}{8}\Big\{(a-ib)[\exp(-i(\omega_{z1} - \tfrac{1}{2}J_{12})t_2) - \exp(-i(\omega_{z1} - \tfrac{1}{2}J_{12})t_2)] \\ &- (a+ib)[\exp(-i(\omega_{z2} - \tfrac{1}{2}J_{12})t_2) - \exp(-i(\omega_{z2} - \tfrac{1}{2}J_{12})t_2)]\Big\} \end{aligned} \tag{36}$$

where

$$a = 2\sin\theta\sin(\Delta\tau_w) \qquad \text{and} \qquad b = \sin(2\theta)[1 - \cos(\Delta\tau_w)] \tag{37}$$

The amplitude of the observed response is a function of τ_w. This is demonstrated by a calculation of the τ_w dependence of the signal energy, which is given by

$$E(\tau_w) \propto \int_0^\infty |S(\tau_w,\theta,t_2)|^2 dt_2 \tag{38}$$

Relating this energy to that which would be obtained from the Zeeman order of a fully polarized product molecule with a 90° pulse yields the dimensionless ratio R for the two-spin system.

$$\begin{aligned} R(\tau_w) &= \frac{E(\tau_w)}{E_0} \\ &= \frac{1}{4}\{4\sin^2\theta\sin^2(\Delta\tau_w) + \sin^2(2\theta)[1-\cos(\Delta\tau_w)]^2\} \end{aligned} \tag{39}$$

This function, which agrees well with numerical density matrix simulations, is plotted in Fig. (IV-2a). Because T_2 relaxation is the same in both the PASADENA and the reference signals, $R(\tau_w)$ is independent of this variable if $T_2 \gg 2\pi J_{12}^{-1}$. If the coupling is not resolved, the phenomenon is suppressed.

Fig. (IV-2) Dependence of the signal energy on the delay between the reaction and a 45° rf pulse. The molecules are (parameters in Hz) a. *cis*-1-deuterio-2-bromoethylene ($J_{12}/2\pi = 7.2$, $\nu_{z1} = -132$, $\nu_{z2} = 112$); b. bromoethylene ($J_{12}/2\pi = 7.2$, $J_{13}/2\pi = 15.0$, $J_{23}/2\pi = -1.7$, $\nu_{z1} = 112$, $\nu_{z2} = -132$, $\nu_{z3} = -200$; c. 1-bromo-2-chloroethane ($J_{12}/2\pi = 5.97$, $J_{14}/2\pi = 9.03$, $(J_{13} - J_{24})/2\pi = 0.95$, $\nu_{z1} = -33.33$, $\nu_{z2} = 71.7$). The chemical shifts correspond to a proton Larmor frequency of 500 MHz. The vertical scales are relative to the signal energies that would be seen for perfect paramagnetic ordering subjected to a 90° pulse. The dashed lines indicate the level expected when the ensemble of product molecules is formed incoherently.

Fig. (IV-2) (continued)

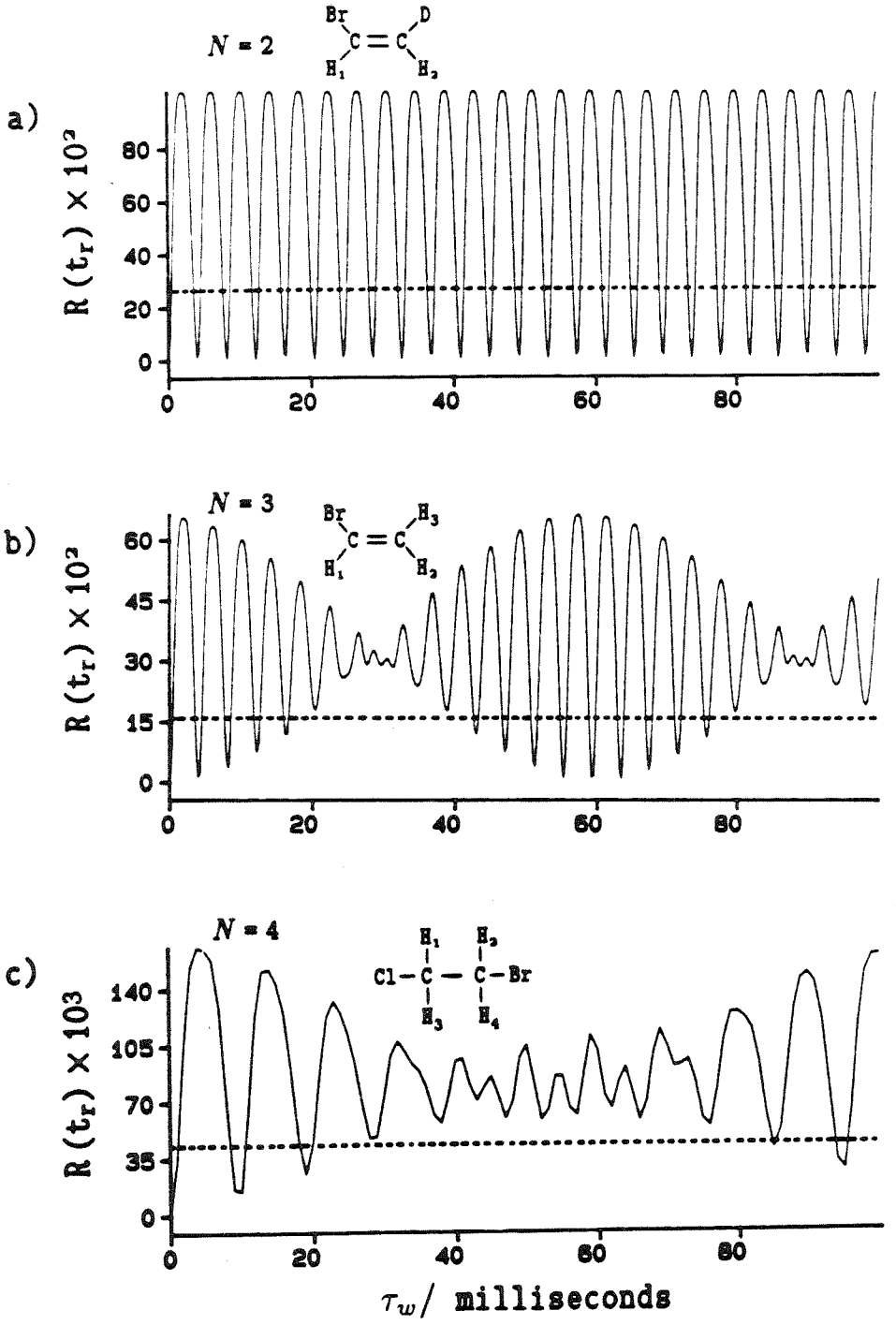

The results of numerical density matrix calculations of the ratio for product molecules with $N = 3$ and $N = 4$ are shown in Fig. (IV-2b,c). Notice that in all cases, the chemical shift difference is important in that it breaks the symmetry during τ_w, allowing escape from the para manifold, but in the weak coupling limit, the J coupling sets the time-scale for development of signal.

§ IV-6. Bilinear Cross Polarization

Recall that for the A_2X_3 spin system, the polarization associated with the original protons of p-H_2 was distributed to other magnetically equivalent spins due to the scalar coupling with them. However, a third magnetically inequivalent spin cannot receive polarization through this mechanism since the scalar coupling is truncated by the chemical shift difference. As an example of this, Fig. (IV-3a) shows the simulated magnitude spectrum for the $N = 3$ product bromoethylene when a 45° pulse acts on the averaged initial condition $\rho(\tau_w)$ to elicit the free induction decay. Notice that the transitions involving the third proton which is *cis* to Br are absent.

In most applications it will be desirable to transfer the spin order to other spins to enhance the detectability of a larger number of site-specific resonances. The sequence below serves this purpose.

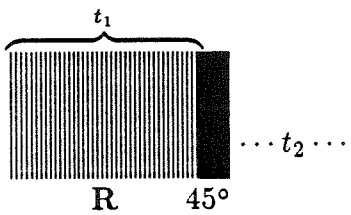

SEQ-IV-1

R may represent a nutation pulse or a multiple pulse train such as a series of π pulses, having the effect of averaging away the chemical shifts.[3–6] The spectrum of Fig. (IV-3b) was obtained by acting on the time averaged initial condition with such a train for a time $t_1 = 131.2$ ms followed by a 45° read pulse and detection during t_2. The intense nonequilibrium magnetization is now shared by the third proton. The dependence of the signal energy of this new multiplet on the cross-polarization

Fig. (IV-3) Bilinear cross polarization on bromoethylene. a. The magnitude of the spectrum (Fourier transform with respect to t_2) without cross polarization ($t_1 = 0$ in Fig. (IV-3c)) b. The corresponding spectrum with $t_1 = 131.2$ ms, at which time the multiplet due to proton 3 (*cis* to Br) has grown to a maximum at the expense of resonances due to the protons from p-H_2 . A Lorentzian broadening of 0.5 Hz FWHM determines the linewidth. c. The signal energy of this multiplet as a function of t_1. The pulse sequence during t_1 consisted of repetitions of a train of 25 contiguous phase-shifted π pulses, each pulse of length 64 μs.

Fig. (IV-3) (continued)

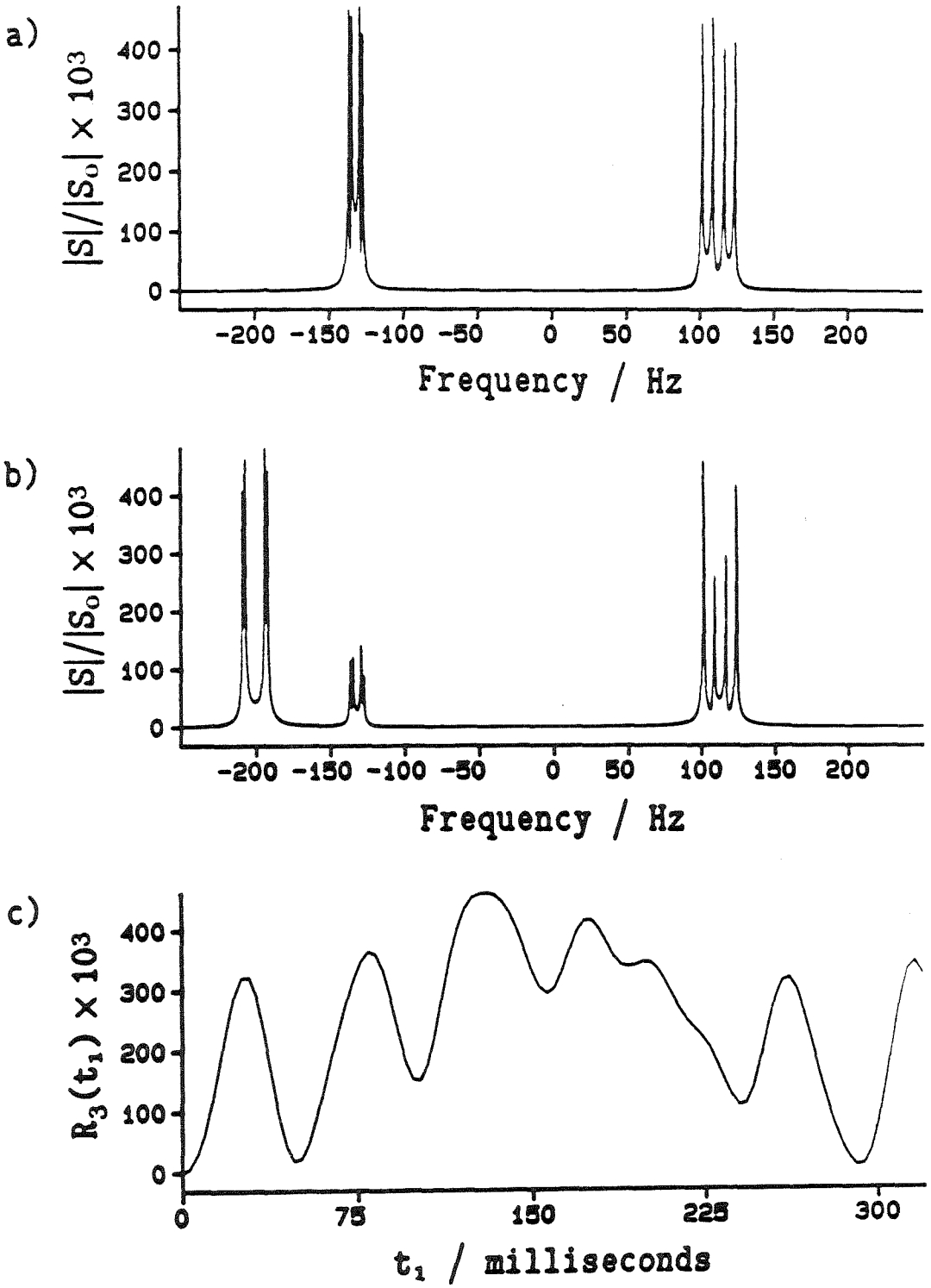

time t_1 is shown in Fig. (IV-3c). The plotted quantity $R_3(t)$ is analogous to the energy ratio introduced in Eq. (IV-39), but with the numerator and denominator referring only to the multiplet of the third proton. The sharing of spin-order occurs prior to any development of magnetization.

§ IV-7. References

1. O. W. Sørenson, G. W. Eich, M. H. Levitt, G. Bodenhausen and R. R. Ernst, *Prog. NMR Spectr.* **16**, 163 (1983)
2. R. R. Ernst, G. Bodenhausen and A. Wokaun, Principles of Nuclear Magnetic Resonance in One and Two Dimensions, Oxford (1987)
3. D. P. Weitekamp, J. R. Garbow and A. Pines, *J. Chem. Phys.* **77**, 2870 (1982)
4. D. P. Weitekamp, J. R. Garbow and A. Pines, *J. Chem. Phys.* **80**, 1372 (1984)
5. L. Braunschweiler and R. R. Ernst, *J. Magn. Reson.* **53**, 521 (1983)
6. J. S. Waugh, *J. Magn. Reson.* **68**, 189 (1986), and references therein.

Chapter V

Deuterium

§ Introduction

The deuterium nucleus is a spin-1 particle and is therefore classified as a boson. The states of molecular deuterium are symmetric, a fact discussed in Chapter II. The symmetry of the electronic eigenfunctions of D_2 are of course the same as H_2, and as with H_2, the product of the rotational and nuclear spin symmetries determines the overall symmetry. Odd j rotational quantum levels go with antisymmetric (para) spin states; even j with symmetric (ortho) spin states.

In this chapter, the PASADENA (para*deuterium* and synthesis allow dramatically enhanced nuclear alignment) signal is computed for an arbitrary mixture of ortho/para D_2. The nuclear spin density operator is derived by equating the matrix elements of the operators in an expansion of a compound irreducible tensor operator of rank zero with the elements of the D_2 density matrix. The time averaged operator required to describe the slow reaction limit is derived from the truncated density operator which is diagonal when written in the eigenbasis of the weak coupling Hamiltonian. The D_2 PASADENA response and its theoretical enhancement

factor are computed under these conditions.

§ V-1. The D_2 Nuclear Spin States

There are $2I_i+1 = 3$ states of a deuterium nuclear spin, which shall be labelled $|\alpha\rangle$, $|0\rangle$ and $|\beta\rangle$. The total number of product states for a two deuteron system is nine; $|m_1 m_2\rangle$ with $-I_i \leq m_i \leq I_i$. These are eigenfunctions of $\mathrm{I}_z = \mathrm{I}_{z1} + \mathrm{I}_{z2}$, but not of $\mathbf{I}^2 = (\mathbf{I}_1 + \mathbf{I}_2)^2$. The Hamiltonian of the isolated D_2 system is invariant to rotations in spin space. It follows that $\mathcal{H}$ must commute with $\mathbf{I}$, and thus $[\mathcal{H}, \mathbf{I}^2] = 0$. This is a manifestation of the conservation of angular momentum in isolated systems, i.e., the total angular momentum of the system is a quantum mechanical constant of the motion.

Hence, to find the spin eigenstates of D_2, it suffices to find the eigenstates of either $\mathcal{H}$ or of $\mathbf{I}^2$. Evidently, what is needed to obtain the eigenstates $|Im\rangle$ is a unitary transformation of the direct product states. Each of the nine orthonormal eigenstates can be written as a linear combination of these.

$$|I_1 I_2 I m\rangle = \sum_{m_1 m_2} C^{I_1 I_2 I}_{m_1 m_2 m} |I_1 I_2 m_1 m_2\rangle \qquad (1)$$

where $I_1 = I_2 = 1$ for deuterium and $m = m_1 + m_2$

The coefficients $C^{I_1 I_2 I}_{m_1 m_2 m}$ are the well-known *Clebsch–Gordon* or *vector-coupling* (VC) coefficients[1–3]. For deuterium, the states $|m_i\rangle$ span the representations $\mathcal{D}^{(1)}$ of R_3, and hence the direct product states $|m_1 m_2\rangle = |m_1\rangle \otimes |m_2\rangle$ span the direct product representation, $\mathcal{D}^{(1)} \otimes \mathcal{D}^{(1)}$. The direct product representation can be expanded as

$$\mathcal{D}^{(1)} \otimes \mathcal{D}^{(1)} = \mathcal{D}^{(2)} + \mathcal{D}^{(1)} + \mathcal{D}^{(0)} \qquad (2)$$

The representations $\mathcal{D}^{(2)}$, $\mathcal{D}^{(1)}$ and $\mathcal{D}^{(0)}$ are five-fold, three-fold and one-fold dimensional, respectively, and thus nine orthonormal states $|Im\rangle$ are required to span the direct product representation. The same conclusion is reached by vector addition of the momenta of the two nuclei. The largest value that the total angular

momentum can have is $I = I_1 + I_2 = 2$ with five Zeeman sublevels and a minimum value of $I = I_1 - I_2 = 0$ with a single Zeeman sublevel.

The proper linear combinations of the states $|Im\rangle$ are determined by calculation of the Clebsch–Gordon coefficients. By multiplying each side of Eq. (V-1) by $\langle I_1 m_1 I_2 m_2|$,

$$C^{I_1 I_2 I}_{m_1 m_2 m} = \langle I_1 m_1 I_2 m_2 | I_1 I_2 I m\rangle \tag{3}$$

Rewriting Eq. (V-1),

$$|I_1 I_2 I m\rangle = \sum_{m_1 m_2} |I_1 I_2 m_1 m_2\rangle \langle I_1 m_1 I_2 m_2 | I_1 I_2 I m\rangle \tag{4}$$

The following rule is helpful when evaluating these coefficients: the coefficient vanishes unless $m = m_1 + m_2$ and unless $I_1 + I_2 \geq I \geq |I_1 - I_2|$, which is merely a consequence of the vector addition rules for angular momentum stated above. An important symmetry property of these coefficients is

$$\langle I_1 m_1 I_2 m_2 | I_1 I_2 I m\rangle = (-1)^{I_2 + m_2} \left(\frac{2I+1}{2I_1+1}\right) \langle I_2 - m_2 I m | I_2 I I_1 m_1\rangle \tag{5}$$

The Clebsch–Gordon coefficients are most conveniently expressed in terms of the Wigner "3-j" symbol[1,2], which is defined in the following relationship:

$$\begin{pmatrix} I_1' & I_2' & I' \\ m_1' & m_2' & m' \end{pmatrix} \equiv (-1)^{I_1' - I_2' - m'} (2I'+1)^{-1/2} C^{I_1' I_2' I'}_{m_1' m_2' - m'} \tag{6}$$

The 3-j symbol has the important symmetry property that odd permutations of the columns multiplies the symbol by $(-1)^{I_1 + I_2 + I}$. Even permutations leave the value of the symbol unchanged. Another general symmetry property of the 3-j symbol is

$$\begin{pmatrix} I_1 & I_2 & I \\ m_1 & m_2 & m \end{pmatrix} = (-1)^{I_1 + I_2 + I} \begin{pmatrix} I_1 & I_2 & I \\ -m_1 & -m_2 & -m \end{pmatrix} \tag{7}$$

These properties will now be used to find a relationship between the Clebsch–Gordon coefficients and the 3-j symbol.

Let us make the following substitutions into the 3-j symbol definition:

$$I_1 = I' \qquad I_2 = I'_1 \qquad I_3 = I'_2 \tag{8a}$$

$$m_1 = -m' \qquad m_2 = -m'_1 \qquad m_3 = m'_2 \tag{8b}$$

A double column permutation yields

$$\begin{pmatrix} I_1 & I_2 & I \\ -m_1 & -m_2 & m \end{pmatrix} = (-1)^{I_2 - I_3 + m}(2I_1 + 1)^{-1/2}\langle I_2 - m_2 I m_3 | I_2 I I_1 m_1 \rangle \tag{9}$$

which yields a formula relating the Clebsch–Gordon coefficients with the 3-j symbol.

$$C^{I_1 I_2 I}_{m_1 m_2 m} = \langle I_1 m_1 I_2 m_2 | I_1 I_2 I m \rangle = (-1)^{I_1 + I_2 + m_2 - m}(2I + 1)^{1/2} \begin{pmatrix} I_1 & I_2 & I \\ m_1 & m_2 & -m \end{pmatrix} \tag{10}$$

Algebraic formulas for a large number of symbols can be found in Edmonds[2]. The symbols relevant to the states of D_2 are

$$\begin{pmatrix} I_1 & I_2 & 0 \\ m_1 & m_2 & 0 \end{pmatrix} = (-1)^{I_1 - m_1}(2I_1 + 1)^{-1/2}\delta_{I_1 I_2}\delta_{m_1 m_2} \tag{11}$$

$$\begin{pmatrix} I & I & 1 \\ m & -m & 0 \end{pmatrix} = (-1)^{I-m}\frac{m}{[(2I+1)(I+1)I]^{1/2}} \tag{12}$$

$$\begin{pmatrix} I & I & 1 \\ m & -m-1 & 1 \end{pmatrix} = (-1)^{I-m}\left[\frac{(I-m)(I+m+1)\cdot 2}{(2I+2)(2I+1)(2I)}\right]^{1/2} \tag{13}$$

$$\begin{pmatrix} I & I & 2 \\ m & -m & 0 \end{pmatrix} = (-1)^{I-m}\frac{2[3m^2 - I(I+1)]}{[(2I+3)(2I+2)(2I+1)(2I)(2I-1)]^{1/2}} \tag{14}$$

$$\begin{pmatrix} I & I & 2 \\ m & -m & 0 \end{pmatrix} = (-1)^{I-m}(1+2m)\left[\frac{6(I+m+1)(I-m)}{(2I+3)(2I+2)(2I+1)(2I)(2I-1)}\right]^{1/2} \tag{15}$$

$$\begin{pmatrix} I & I & 2 \\ m & -m-2 & 2 \end{pmatrix} =$$

$$(-1)^{I-m}\left[\frac{6(I-m-1)(I-m)(I+m+1)(I+m+2)}{(2I+3)(2I+2)(2I+1)(2I)(2I-1)}\right]^{1/2} \tag{16}$$

When all of the coefficients have been calculated, they can be written as a "coupling" matrix relating the $|I_1 m_2 I_2 m_2\rangle$ with the $|I_1 I_2 I m\rangle$ basis states. The columns of this matrix form the eigenvectors of $\mathbf{I}^2$, and hence the eigenstates are

$$\text{ortho-D}_2 \quad \begin{cases} |22\rangle = |\alpha\alpha\rangle \\ |21\rangle = 2^{-1/2}\left(|\alpha 0\rangle + |0\alpha\rangle\right) \\ |20\rangle = 6^{-1/2}\left(|\alpha\beta\rangle + 2|00\rangle + |\beta\alpha\rangle\right) \\ |00\rangle = 3^{-1/2}\left(|\alpha\beta\rangle - |00\rangle + |\beta\alpha\rangle\right) \\ |2\ -1\rangle = 2^{-1/2}\left(|\beta 0\rangle + |0\beta\rangle\right) \\ |2\ -2\rangle = |\beta\beta\rangle \end{cases} \tag{17a-f}$$

$$\text{para-D}_2 \quad \begin{cases} |11\rangle = 2^{-1/2}\left(|0\alpha\rangle - |\alpha 0\rangle\right) \\ |10\rangle = 2^{-1/2}\left(|\beta\alpha\rangle - |\alpha\beta\rangle\right) \\ |1\ -1\rangle = 2^{-1/2}\left(|\beta 0\rangle - |0\beta\rangle\right) \end{cases} \tag{18a-c}$$

Since $[\mathbf{I}^2, \mathcal{H}] = 0$, the above eigenstates also satisfy the Schrödinger equation. Therefore, the coupling matrix A which relates the bases can be used to diagonalize $\mathcal{H}$. Because $\mathcal{H}$ is real and symmetric, the eigenvectors are real and orthonormal and A is therefore orthogonal. The orthogonal transformation of the Hamiltonian is represented as

$$\{\mathcal{H}\}_{Eigen} = A\{\mathcal{H}\}_{prod}A^T, \tag{19}$$

the diagonal elements being the eigenenergies.

§ V-2. The Deuterium Density Matrix

The density matrix for some arbitrary mixture of ortho and paradeuterium is

$$\rho = \begin{pmatrix} \frac{1-\chi_p}{6} & & & & & & & & \\ & \frac{1-\chi_p}{6} & & & & & & & \\ & & \frac{1-\chi_p}{6} & & & & & & \\ & & & \frac{1-\chi_p}{6} & & & & & \\ & & & & \frac{1-\chi_p}{6} & & & & \\ & & & & & \frac{1-\chi_p}{6} & & & \\ & & & & & & \chi_p & & \\ & & & & & & & \chi_p & \\ & & & & & & & & \chi_p \end{pmatrix} \tag{20}$$

where again χ_p is the mole fraction of molecules in one of the three para states. The operator form is the same in the eigenbasis or direct product basis. While it is most convenient to specify the matrix elements in the eigenbasis, the calculations which follow are more easily done in the direct product basis. The orthogonal transformation is performed using the matrix A.

$$\{\rho\}_{prod} = A^T \rho A \tag{21}$$

§ V-3. The Deuterium Density Operator

As in the case of dihydrogen, it is convenient to represent the density matrix as a linear combination of operators. In the case of dihydrogen, this was $\rho = 1/4 - f\mathbf{I}_1 \cdot \mathbf{I}_2$. This operator is a scalar, i.e., it commutes with **I**. Likewise, the density operator of deuterium must also be of a scalar form. The construction of compound scalar operators is most convenient if irreducible tensor operators are used. The irreducible tensor operator (ITO) of rank k is defined as the set of $2k+1$ operators T^k_q which transform under coordinate rotations according to the relation[1–3]

$$D(\alpha,\beta,\gamma)\mathrm{T}^k_q D^{-1}(\alpha,\beta,\gamma) = \sum_{q'} \mathrm{T}^k_{q'} \mathcal{D}^{(k)}_{q'q}(\alpha,\beta,\gamma) \tag{22}$$

where q' and q can take on $2k+1$ values running from $-k$ to k and the $\mathcal{D}^{(k)}_{q'q}(\alpha,\beta,\gamma)$ are elements of the Wigner rotation matrix. The general expression for a compound irreducible tensor operator is[1]

$$\{\mathrm{T}^{k_1}(1)\otimes\mathrm{T}^{k_2}(2)\}^k_q = \sum_{q_1 q_2}\langle k_1 q_1 k_2 q_2|k_1 k_2 k q\rangle \mathrm{T}^{k_1}_{q_1}(1)\mathrm{T}^{k_2}_{q_2}(2) \tag{23}$$

The compound irreducible tensor operator for D_2 spans the representation $\mathcal{D}^{(1)}\otimes\mathcal{D}^{(1)} = \mathcal{D}^{(2)}+\mathcal{D}^{(1)}+\mathcal{D}^{(0)}$. For the particular case of a zero rank compound tensor, let $k=q=0$, which specifies the scalar. In terms of the 3-j symbol,

$$\{\mathrm{T}^{k_1}(1)\otimes\mathrm{T}^{k_2}(2)\}^0_0 = \sum_{q_1 q_2}(-1)^{k_1-k_2}\begin{pmatrix} k_1 & k_2 & 0\\ q_1 & -q_2 & 0\end{pmatrix}\mathrm{T}^{k_1}_{q_1}(1)\mathrm{T}^{k_2}_{q_2}(2) \tag{24}$$

where

$$\begin{pmatrix} k_1 & k_2 & 0\\ m_1 & -m_2 & 0\end{pmatrix} = (-1)^{k_1-m_1}(2k_1+1)^{-1/2}\delta_{k_1 k_2}\delta_{m_1 m_2} \tag{25}$$

The functional form requires that the rank of the individual tensors be the same. The zero rank resultant becomes

$$\begin{aligned}\{\mathrm{T}^k(1)\otimes\mathrm{T}^k(2)\}^0_0 &= \sum_q(-1)^{k-q}(2k+1)^{-1/2}\mathrm{T}^k_q(1)\mathrm{T}^k_{-q}(2)\\ &= (-1)^k(2k+1)^{-1/2}\mathcal{A}^k \qquad (26)\\ \text{where}\qquad \mathcal{A}^k &= \sum_q(-1)^q\mathrm{T}^k_q(1)\mathrm{T}^k_{-q}(2) \qquad (27)\end{aligned}$$

To find the density operator, it is assumed that it may be represented as a linear combination of scalar, compound ITO's;

$$\begin{aligned}\rho &= c_0\mathcal{A}^0 + c_1\mathcal{A}^1 + c_2\mathcal{A}^2\\ &= c_0\mathrm{T}^0_0(1)\mathrm{T}^0_0(2) + c_1\left[\mathrm{T}^1_0(1)\mathrm{T}^1_0(2) - \mathrm{T}^1_{-1}(1)\mathrm{T}^1_1(2) - \mathrm{T}^1_1(1)\mathrm{T}^1_{-1}(2)\right]\\ &+ c_2\left[\mathrm{T}^2_0(1)\mathrm{T}^2_0(2) - \mathrm{T}^2_{-1}(1)\mathrm{T}^2_1(2) - \mathrm{T}^2_1(1)\mathrm{T}^2_{-1}(2)\right.\\ &\qquad \left. + \mathrm{T}^2_{-2}(1)\mathrm{T}^2_2(2) + \mathrm{T}^2_2(1)\mathrm{T}^2_{-2}(2)\right] \qquad (28)\end{aligned}$$

where c_0, c_1 and c_2 are constants to be determined by equating ρ from Eq. (V-28) with ρ in Eq. (V-20). The tensor operators $T^k_{\pm q}(I)$; $k = 0(1)7$ are listed in Buckmaster.[4] Those used in the current calculation are given explicitly here for the reader's convenience.

$$T^0_0(I) = +1 \tag{29}$$

$$T^1_{\pm 1}(I) = \mp \left(\frac{1}{2}\right)^{1/2} I_\pm \tag{30}$$

$$T^1_0(I) = I_z \tag{31}$$

$$T^2_{\pm 2}(I) = +\frac{1}{2} I^2_\pm \tag{32}$$

$$T^2_{\pm 1}(I) = \mp \frac{1}{2} I_\pm \{2I_z \pm 1\} \tag{33}$$

$$T^2_0(I) = + \left(\frac{1}{6}\right)^{1/2} \{3I^2_z - I(I+1)\} \tag{34}$$

Rewriting ρ using these explicit forms,

$$\begin{aligned} \rho = {} & c_0 + c_1 \mathbf{I}_1 \cdot \mathbf{I}_2 \\ & + c_2 \frac{1}{4} [I^2_{-1} I^2_{+2} + I^2_{+1} I^2_{-2} + 6 I^2_{z1} I^2_{z2} - 4 I^2_{z1} - 4 I^2_{z2} + \frac{8}{3} 1 \\ & \quad + (I_{-1} I_{+2} + I_{+1} I_{-2}) (4 I_{z1} I_{z2} - 1) \\ & \quad + 2 (I_{-1} I_{+2} - I_{+1} I_{-2}) (I_{z1} - I_{z2})] \end{aligned} \tag{35}$$

The next step is to find the matrix representation of ρ so that it may be equated with the ρ of Eq. (V-20). The evaluation of the matrix elements of the angular momentum operators is simplest in the direct product basis, so the matrix of ρ is constructed in this basis. Equating the two different matrix formulations of ρ,

$$c_0 = \frac{1}{9} \qquad c_1 = \frac{f}{2} \qquad c_2 = f \tag{36}$$

where f is related to the mole fraction p-D_2

$$f = \frac{1}{4} \left(\frac{1}{3} - \chi_p\right) \tag{37}$$

Hence,

$$\begin{aligned}\rho = &\frac{1}{9}\mathbf{1} + \frac{f}{2}\mathbf{I}_1 \cdot \mathbf{I}_2 \\ &+ f\frac{1}{4}\left[\mathrm{I}^2_{-1}\mathrm{I}^2_{+2} + \mathrm{I}^2_{+1}\mathrm{I}^2_{-2} + 6\mathrm{I}^2_{z1}\mathrm{I}^2_{z2} - 4\mathrm{I}^2_{z1} - 4\mathrm{I}^2_{z2} + \frac{8}{3}\mathbf{1}\right. \\ &\quad + (\mathrm{I}_{-1}\mathrm{I}_{+2} + \mathrm{I}_{+1}\mathrm{I}_{-2})(4\mathrm{I}_{z1}\mathrm{I}_{z2} - \mathbf{1}) \\ &\quad \left. + 2(\mathrm{I}_{-1}\mathrm{I}_{+2} - \mathrm{I}_{+1}\mathrm{I}_{-2})(\mathrm{I}_{z1} - \mathrm{I}_{z2})\right] \end{aligned} \tag{38}$$

Eq. (V-38) agrees with the result obtained by Pravica.[5] While this expression would appear to require a formidable amount of matrix calculations if written out by hand, it may be obtained quickly and easily using the matrix routines of Wolfram's "Mathematica" computer program.[6] This method is highly recommended by the Author to those confronted with tedious matrix calculations.

§ V-4. The Averaged Initial Condition

The pulse sequence for observation of the D_2 PASADENA is the same as that used for the H_2 effect. The D_2 is introduced into the sample and a period τ_w passes before pulsing. When the D_2 reaction rate is slow compared to the period of the ensuing coherence, the matrix representation of the ensemble averaged density operator is diagonal. The signal arising from this scenario will be calculated. Reconstructing the density operator from the diagonal operator components of Eq. (V-38), the averaged operator (with constants removed) is

$$\begin{aligned}\rho(\tau_w) &= \sum_i \langle i|\rho|i\rangle |i\rangle\langle i| \\ &= \frac{1}{9} + \frac{f}{2}\left[\mathrm{I}_{z1}\mathrm{I}_{z2} + 3\mathrm{I}^2_{z1}\mathrm{I}^2_{z2} - 2\mathrm{I}^2_{z1} - 2\mathrm{I}^2_{z2}\right] \end{aligned} \tag{39}$$

§ V-4.1. The PASADENA Signal

The single-quantum operators generated from the the response of $\rho(\tau_w)$ to a θ pulse are

$$\rho(\tau_w) \xrightarrow{\theta \mathrm{I}_x}$$

$$\frac{-f}{2}\sin\theta\cos\theta\Big\{\mathrm{I}_{y1}\mathrm{I}_{z2}+\mathrm{I}_{z1}\mathrm{I}_{y2} - 2\left[\mathrm{I}_{y1}\mathrm{I}_{z1}+\mathrm{I}_{z1}\mathrm{I}_{y1}+\mathrm{I}_{y2}\mathrm{I}_{z2}+\mathrm{I}_{z2}\mathrm{I}_{y2}\right] - 3\cos^2\theta\left[\mathrm{I}_{y1}\mathrm{I}_{z1}\mathrm{I}_{z2}^2+\mathrm{I}_{z1}\mathrm{I}_{y1}\mathrm{I}_{z2}^2 + \mathrm{I}_{z1}^2\mathrm{I}_{Y2}\mathrm{I}_{z2}+\mathrm{I}_{z1}^2\mathrm{I}_{z2}\mathrm{I}_{y2}\right]\Big\} = \rho(\tau_w,\theta) \tag{40}$$

The signal arises from terms in Eq. (V-40) which evolve under $\mathcal{H}_{int}$ to yield nonzero traces with I_+. The relevant traces are

$$\mathrm{Tr}\{\mathrm{I}_+\mathrm{I}_{x1}\mathrm{I}_{z2}^2\} = \mathrm{Tr}\{\mathrm{I}_+\mathrm{I}_{z1}^2\mathrm{I}_{x2}\} = 4 \tag{41a}$$

$$\mathrm{Tr}\{\mathrm{I}_+\mathrm{I}_{y1}\mathrm{I}_{z2}^2\} = \mathrm{Tr}\{\mathrm{I}_+\mathrm{I}_{z1}^2\mathrm{I}_{y2}\} = 4i \tag{41b}$$

With the help of Eq. (IV-22) and Eq. (IV-23), the observed signal is obtained.

$$S(t) = 2f\sin\theta\cos\theta\sin Jt\left\{e^{-i\omega_1 t}+e^{-i\omega_2 t}\right\} \tag{42}$$

This formula resembles the PASADENA signal for a system of two weakly coupled protons (c.f. Eq. (IV-7)), with the exception that the splitting between the lines is now $2J$. The conventional spectrum of two weakly coupled deuterons exhibits two triplets having the relative intensities $\{1,1,1\}$, while the middle transition is absent in the PASADENA multiplet and the relative intensities are $\{-1,0,1\}$ for para-D_2.

§ V-4.2. Theoretical Enhancement Factor

For D_2,

$$b_0 = \frac{\mathrm{Tr}\{\rho(0)\mathrm{I}_z\}}{\mathrm{Tr}\,\mathrm{I}_z^2} = \frac{2}{12} = \frac{1}{6} \tag{43}$$

Due to the lower gyromagnetic ratio and the greater multiplicity of states of the deuteron, the Curie-Law factor b is reduced relative to the proton by the fraction

$$\frac{b(300°)^{\mathrm{D}_2}}{b(300°)^{\mathrm{H}_2}} \approx \frac{1}{15} \tag{44}$$

which indicates that a greater enhancement factor can be achieved with D_2.

The enhancement must relate the intensity of corresponding transitions. Calculation of the time domain signal yields all intensity factors involved.

$$\rho(0) = b(T)\mathrm{I}_z \xrightarrow{\frac{\pi}{2}\mathrm{I}_y} \xrightarrow{\mathcal{H}_{int}} \rho(t)$$

$$S(t) = \mathrm{Tr}\,\mathrm{I}_+\rho(t) = 2b(1 + 2\cos Jt)\left\{e^{-i\omega_1 t} + e^{-i\omega_2}\right\} \tag{45}$$

At a magnetic field of approximately 4.7 T (200 MHz proton),

$$b(300) = \frac{2\pi \cdot 30 \times 10^6 \cdot 1.05 \times 10^{-34}\mathrm{J \cdot s}}{1.38 \times 10^{-23}\mathrm{J\ K^{-1}} \cdot 300\mathrm{K} \cdot 9} = 5.33 \times 10^{-7} \tag{46}$$

Comparing the outer lines,

$$\frac{S_{para}}{S(300°)} = \frac{|f|}{b(300)}$$

$$\Rightarrow 3.1 \times 10^5 \quad \text{for pure para-}D_2 \tag{47}$$

$$\Rightarrow 1.5 \times 10^5 \quad \text{for pure ortho-}D_2$$

§ V-5. References

1. B. L. Silver, Irreducible Tensor Methods, Academic Press, New York (1976)
2. A. R. Edmonds, Angular Momentum in Quantum Mechanics, Princeton University Press, Princeton (1957)
3. M. E. Rose, Elementary Theory of Angular Momentum, Wiley, New York (1957)
4. H. A. Buckmaster, R. Chatterjee and Y. H. Shing, *Phys. Stat. Sol. (a)* **13**, 9 (1972)
5. M. G. Pravica, unpublished (1988)
6. S. Wolfram, Mathematica, Addison-Wesley, Reading, MA (1988)

Chapter VI

$Rh(PPh_3)_3Cl$ Catalyzed Hydrogenation of Styrene

§ Introduction

The symmetrization order of the spins of p-H_2 can only be transformed into enhanced NMR on the molecule of interest when there exists an efficient hydrogenation reaction. In liquids at ambient temperature and pressure, homogeneous catalysts can be employed. Many different transition metal complexes, particularly those of rhodium and iridium, have been identified which facilitate hydrogenation of unsaturated organics (for example, see Ref. 1 for an extensive listing), including the classic $Rh(PPh_3)_3Cl$ (Wilkinson's Catalyst).This system has been extensively studied, making it a good candidate for initial studies employing the PASADENA effect.

While the focus of the previous chapters has been on the spin-dynamics, the complimentary perspective is to study the chemical dynamics using the PASADENA effect as a sensitive probe. The first demonstration of the effect employed this catalyst in the parahydrogenation of acrylonitrile to form propionitrile, the enhanced spectrum for which was shown in Fig. (IV-1). On a qualitative level, this is evidence for molecular addition. The general strategy for quantitative kinetics is to relate the relative or absolute and measured NMR enhancement to a

model of the stepwise chemical rate constants and spin-lattice relaxation times for each of the species upon which the original p-H_2 molecule has been resident.

The profound advantage of PASADENA kinetic studies over conventional methods such as ordinary NMR is that the molecular rates which are determined with the former are independent of all assumptions regarding the concentration of the active catalytic species. Ordinarily, the molecular rate is obtained by dividing the observed rate by the total catalyst concentration. However, the question as to whether most of the catalytic rate is due to a tiny fraction of active species or a large fraction with a relatively low molecular rate is not clearly addressed by such an analysis. This ambiguity is entirely avoided in the PASADENA studies, since only active catalyst molecules can contribute to the enhanced signals from which all kinetic inferences are made.

§ VI-1. NMR-Kinetics

§ VI-1.1. "In Situ" NMR Hydrogenation

Stopped flow kinetic methods are frequently employed to time resolve the individual steps of a reaction pathway. In the PASADENA stopped-flow experiment, d_6-benzene solutions of $Rh(PPh_3)_3Cl$ and a styrene substrate are contained in NMR tubes which are connected to a reservoir of pressurized p-H_2. The apparatus is illustrated in Fig. (VI-1). The sample is placed in the receiver coil region by inserting the entire hydrogenation assembly into the bore of the magnet. The reaction is initiated by momentarily bubbling the p-H_2 , which is controlled by electronic solenoid valves which are activated by the NMR pulse programmer. This interface allows the bursts of p-H_2 to be synchronized with the NMR pulse sequence (see Appendix A for details).

§ VI-1.2. Equilibrium Prior to Reaction

Unless some process such as bubbling mixes the gas and liquid phases, the

Fig. (VI-1) Schematic of the PASADENA NMR hydrogenation apparatus. H_2 gas flows through pyrex coils packed with Apachi nickel silica catalyst and immersed in liquid nitrogen. Two three-way solenoid valves control the flow of gas into and out of the sealed NMR tube. The sample can be pressurized to 2 atm with H_2 gas enriched to $\chi_p = 0.5$. A needle valve at the output valve is adjusted to permit bubbling under a pressurized state through a submersed capillary.

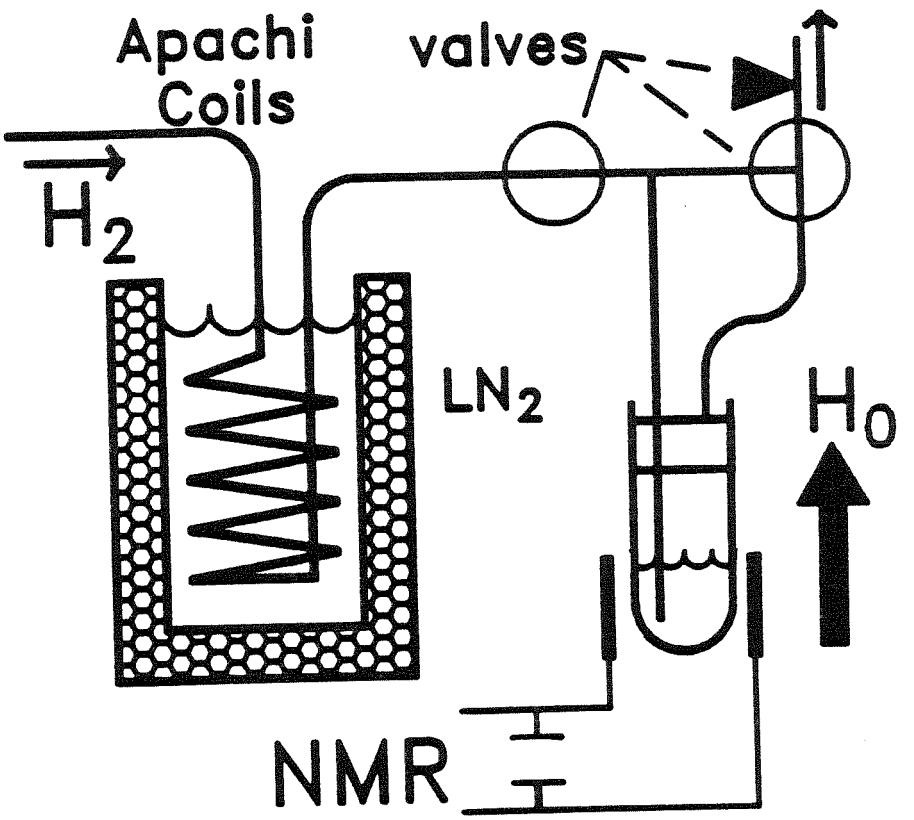

cylindrical geometry of the NMR tube is such that the small ratio of interfacial surface area to liquid volume precludes any significant transport of the H_2 into the benzene. This is evidenced by the lack of any observed product formation when solutions are left sitting for long periods of time in the pressurized apparatus. The initial equilibrium state of the solution may therefore be described by

$$\underset{5.4\text{ mM} \rightarrow 77.1\%}{Rh(PPh_3)_3Cl} \overset{K_1}{\rightleftharpoons} \underset{0.51\text{ mM} \rightarrow 7.2\%}{Rh(PPh_3)_2Cl} \overset{K_9}{\rightleftharpoons} \underset{1.1\text{ mM} \rightarrow 15.7\%}{Rh(PPh_3)_2Cl(>=<)}$$

with $K_1 = 1.4 \times 10^{-4}$ M and $K_9 = 2.43$. The catalyst is largely undissociated. The free PPh_3 concentration is

$$[PPh_3] = [Rh(PPh_3)_2Cl] + [Rh(PPh_3)_2Cl(>=<)] = 1.6 \text{ mM} \qquad (1)$$

§ VI-1.3. Non-Equilibrium

The equilibrium is upset as p-H_2 enters the benzene solution, as it may react directly with any of the three rhodium species. It is known, however, that the triphenlyphosphine and the olefin coordinated complexes react with hydrogen only very slowly. The most productive pathway for hydride formation involves dissociation of PPh_3 or the olefin followed by rapid H_2 addition and then olefin addition. The formation of the "bottleneck" species, $Rh(PPh_3)_2H_2(>=<)Cl$, is limited by the rate of the dissociation step, which is $k_1 = 0.68\ s^{-1}$ for PPh_3.

The other major species initially present, $Rh(PPh_3)_2Cl(>=<)$, reacts only very slowly with H_2. This observation was reported in the original paper by Wilkinson et al.[2] using competitive experiments involving *trans*-stilbene and ethylene, the latter of which has a large equilibrium constant K_9. The lack of any hydrogenation of either olefin is due to all of the rhodium being locked into the form $RhCl(PPh_3)_2(C_2H_4)$, which cannot activate H_2. These studies suggested that the catalytic activity is therefore predominantly due to the so called "hydride route,"

in which H_2 is added prior to olefin coordination, rather than the "unsaturate route". If the $Rh(PPh_3)_2Cl(>=<)$ species is to participate, then the olefin must first dissociate to produce $Rh(PPh_3)_2Cl$, which is extremely reactive with H_2.

At 25° C, the solubility of 1 atm H_2 gas in benzene[3] is 2.5 mM. Initially, there is no p-H_2 present in the benzene. During the bubbling, the gas is transported into the solution at a rate which is some complicated function of the sample geometry, the bubble size, the amount of p-H_2 already present and consequently the rate at which it is being taken up by chemical reaction. The kinetics of $RhCl(PPh_3)_2H_2$ formation has been studied by Halpern[4] using a stopped flow technique, with no substrate present. In that procedure, catalyst solutions were mixed with benzene already saturated with H_2. The disappearance of $Rh(PPh_3)_3Cl$ was reported to obey the following rate law:

$$\frac{-d[Rh(PPh_3)_3Cl]}{dt} = \left[k_1 + \frac{k_2 k_3}{k_{-2}[PPh_3] + k_3[H_2]}\right] \times [H_2][Rh(PPh_3)_3Cl] \quad (2)$$

where $k_1 = 4.81$ mol^{-1} s^{-1}, $k_2 = 0.71$ s^{-1} and $k_{-2}/k_3 = 1.1$. If the condition

$$k_{-2}[PPh_3] \ll k_3[H_2] \quad (3)$$

is satisfied, then Eq. (VI-2) is well approximated by $-d[Rh(PPh_3)_3Cl]/dt \approx k_2[Rh(PPh_3)_3Cl]$. However, this condition cannot physically be fulfilled for $[Rh]_T =$ 7 mM , since $[PPh_3] = 1.6$ mM and the solubility of H_2 is only 2.5 mM ($T = s25°$ C, $p = 1$ atm). If H_2 saturation occurs rapidly within a period τ_a of the initiation of bubbling, then $[PPh_3] \approx [H_2]$ and

$$\frac{-d[Rh(PPh_3)_3Cl]}{dt} \approx \frac{k_2}{2}[Rh(PPh_3)_3Cl] \quad (4)$$

The rate of dissociation becomes $k_F \approx k_2/2 = 0.34$ s^{-1} if $\tau_a \ll 1/k_F$. This assumption will be important in the modelling for the time dependence of the J-order appearing on the product alkane molecules. Its validity will be ascertained by comparing the value $k_F = 0.34$ s^{-1} with the value which optimizes the fit of the model with the experimental data set.

Halpern has also developed a detailed picture (Fig. (VI-2)) for the remainder of the mechanism for the $Rh(PPh_3)_3Cl$ catalyzed hydrogenation of styrene under the conditions of constant H_2 and PPh_3 concentration.[11] The proposed rate law is

$$[k_{cat}]^{-1} = \frac{[Rh]_T}{RATE}$$

$$= \frac{([>=<] + K_5^{-1}[PPh_3])[PPh_3]}{(k_{10}K_8[>=<] + k_6[PPh_3])[>=<]} + \frac{K_1K_9[>=<] + [PPh_3]}{K_1k_4[H_2]} \qquad (5)$$

where the reported values for styrene are: $K_5 = 1.7 \times 10^{-3}$; $k_6 = 0.11\ s^{-1}$; $K_9/k_4 = 5 \times 10^{-4}$ s and $k_{10}K_8 = 1.0 \times 10^{-4}\ s^{-1}$.

For the purpose of assessing the relative importance of each of the terms in Eq. (VI-5), let the PPh_3 concentration take its initial equilibrium value. The actual concentration while H_2 is present will necessarily be smaller. It is evident from Eq. (VI-5) that making this approximation will lead to an *underestimate* of the"true" overall rate. This must be considered when comparing the rates predicted by Eq. (VI-5) with those measured experimentally. In order to produce a numerical value from the second term, it is necessary to assign a value for $[H_2]$. If a saturating level of H_2 is chosen, then

$$\frac{([>=<] + K_5^{-1}[PPh_3])[PPh_3]}{(k_{10}K_8[>=<] + k_6[PPh_3])[>=<]} = 10.56 \text{ s}$$

$$\frac{K_1K_9[>=<] + [PPh_3]}{K_1k_4[H_2]} = 1.13 \text{ s} \qquad (6)$$

This calculation indicates that at sufficiently high H_2 levels, the overall reaction rate is limited by the parallel pathways for decomposition of $Rh(PPh_3)_2H_2(>=<)Cl$ and $Rh(PPh_3)H_2Cl(>=<)_2$and is independent of $[H_2]$.

§ VI-1.4. The Elusive $Rh(PPh_3)_2H_2(>=<)Cl$ Intermediate

The mechanistic description of hydrogenation with $Rh(PPh_3)_3Cl$ places immense importance on the rate determining role of the $Rh(PPh_3)_2H_2(>=<)Cl$ intermediate. Nevertheless, the evidence for its existence is purely circumstantial; there

Fig. (VI-2) Halpern's proposed mechanism for the $Rh(PPh_3)_3Cl$ catalyzed hydrogenation of styrene (adapted from Ref. 11 with permission.)

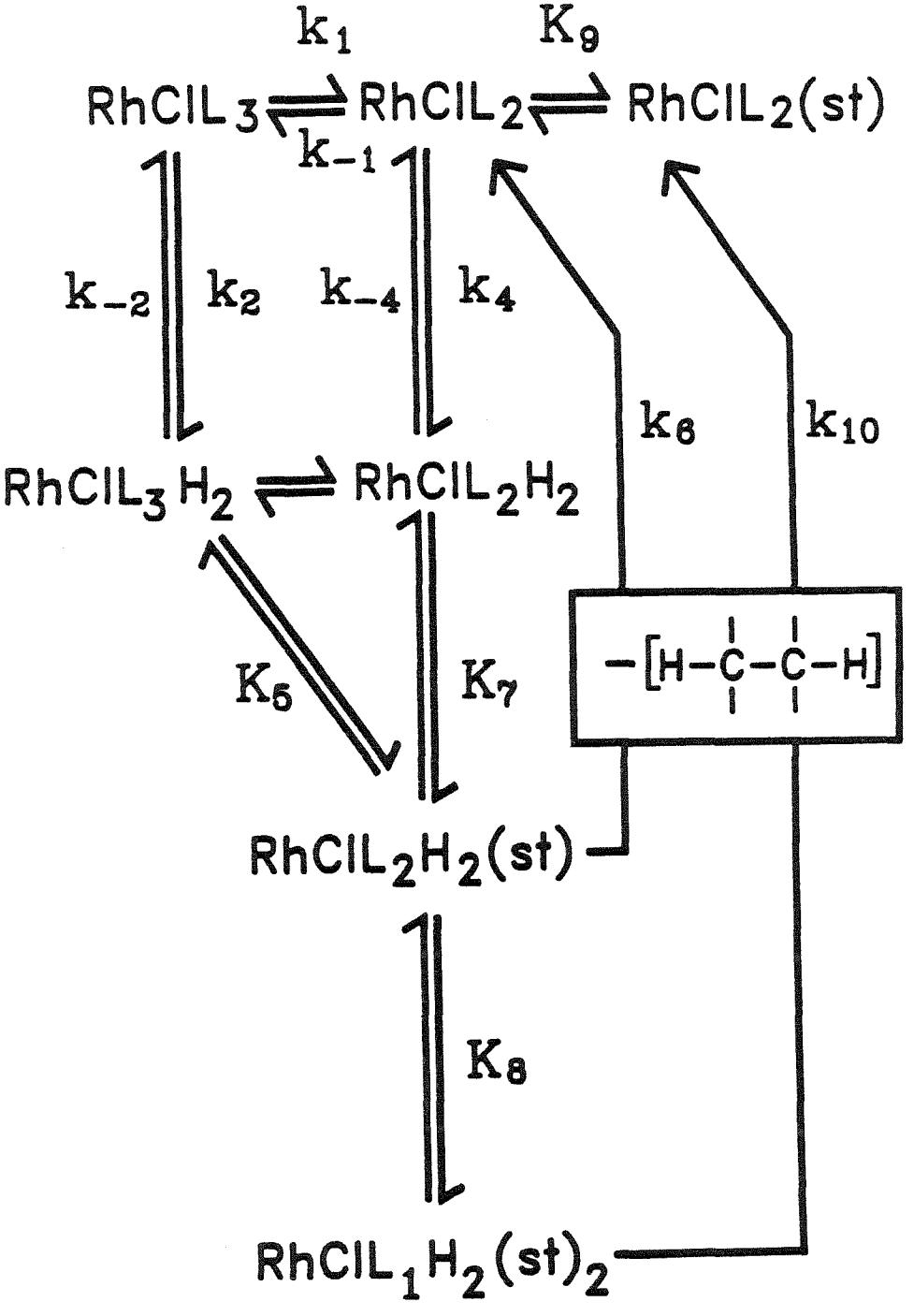

has not been any direct physical observation of this species. Olefin metal-hydride complexes have been widely invoked as requisite intermediates in a variety of other catalytic hydrogenations and related reactions, such as hydroformylation, hydrosilation, olefin isomerization and polymerization.[9] The existence of such intermediates is supported in some cases by spectroscopic characterization, such as for the compound[10] $HRh(P\text{-}i\text{-}Pr_3)(C_2H_4)$. A second piece of evidence is the observation of a deuterium kinetic isotope effect in the $Rh(PPh_3)_3Cl$ catalyzed hydrogenation of cyclohexene in benzene.[5] This indirect evidence is the basis for the assertion that the rate determining step in $Rh(PPh_3)_3Cl$ hydrogenation involves H-atom transfer on the olefin-rhodium dihydride. Halpern and Okamoto also insist (based on unpublished results) on the importance of a second bottleneck species when styrene is the olefin, namely, $Rh(PPh_3)H_2Cl(>=<)_2$. Nonetheless, the key chemical event involving breaking of the Rh-H bond to form an alkyl hydride is the same for both the $Rh(PPh_3)H_2Cl(>=<)_2$ and $Rh(PPh_3)_2H_2(>=<)Cl$ species, as shown in Fig. (VI-2). Future references to $Rh(PPh_3)_2H_2(>=<)Cl$ in the context of its rate determining role will also imply a reference to the $Rh(PPh_3)H_2Cl(>=<)_2$ complex, under conditions when the concentration of the latter is significant.

§ VI-1.5. Estimation of the Overall Rate Constant

The second term in Eq. (VI-5) clearly dominates at low H_2 concentrations, i.e., at less than about 10% saturation. However, as the concentration of H_2 decreases, the overall reaction rate becomes negligibly small. That the rate of formation of $Rh(PPh_3)_2H_2(>=<)Cl$ is independent of H_2 at high H_2 concentrations is a key simplifying assumption of the model developed in §VI-3.2. That the overall reaction rate is limited by the rate of decomposition of $Rh(PPh_3)_2H_2(>=<)Cl$ at moderate H_2 levels is consistent with this assumption.

Disregarding the $[H_2]$ dependent term, the rate of product formation is a linear combination of the rates of decomposition of $Rh(PPh_3)_2H_2(>=<)Cl$ and

$Rh(PPh_3)H_2Cl(>=<)_2$, k_D. Specifically,

$$\frac{\text{RATE}}{[Rh]_T} \approx k_D \equiv \left[\frac{([>=<] + K_5^{-1}[PPh_3])[PPh_3]}{(k_{10}K_8[>=<] + k_6[PPh_3])[>=<]}\right]^{-1}$$

$$= \frac{k_{10}K_8[>=<]^2}{([>=<] + K_5^{-1}[PPh_3])[PPh_3]} + \frac{k_6[>=<]}{([>=<] + K_5^{-1}[PPh_3])[PPh_3]}$$

$$= 0.033 + 0.0613 = 0.095 \text{ s}^{-1} \qquad (7)$$

Regarding the problem of the uncertain and transient nature of the PPh_3 concentration, one possible solution would be to add excessive $[PPh_3]$. However, increasing $[PPh_3]$ also has the undesirable effect of severely reducing the rate. No additional phosphine was added to the reaction mixture in the present experiments, the highest priority being to maximize the amplitude of the PASADENA signals.

§ VI-2. Experimental

The sample solutions used in all of the experiments of this chapter initially contained d_6-benzene solutions of 11.1% by volume of substrate (the corresponding molarities are given in Table (VI-1)) and 7.0×10^{-3} M $Rh(PPh_3)_3Cl$ in a total volume of 0.9 ml. The 5 mm diameter NMR tubes were prepared by cleaning with acetone, chromic acid cleaning solution, acetone, aqua-regia, de-ionized water and then baked dry before use. The reagents were mixed in a vial open to the atmosphere and then transferred to the NMR tube. The tube was inserted into the NMR-hydrogenation apparatus, pressurized under an atmosphere of 50% p-H_2 and then immediately purged for 10 s by bubbling p-H_2 through the solution. The total elapsed time between mixing and purging was kept under 300 s. Solutions which were allowed to stand for 1/2 hour before purging, did not yield any PASADENA enhancement.

In one set of experiments, procedures were followed to carefully purify the reagents. The styrene was degassed with four freeze-pump-thaw cycles, vacuum distilled to remove the stabilizer and stored in a freezer in an N_2 glove-box. The

benzene was degassed and dehydrated. The reagents were combined inside the glove-box. The NMR sample tube was inserted into the hydrogenation apparatus without exposure to the atmosphere. These precautions made no observable difference in terms of the PASADENA enhancement, so they were abandoned.

The stopped-flow PASADENA NMR pulse sequence is shown in SEQ-VI-1.

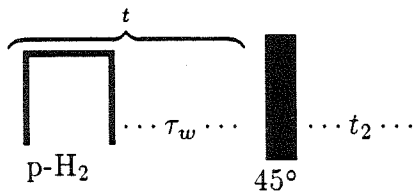

SEQ-VI-1

The p-H_2 burst lasts for 1 s after which a dead time of about 0.25 s is allotted to allow the bubbles to clear, because they severely disrupt the magnetic field homogeneity. This delay sets a limit on the earliest time at which the PASADENA signals can be recorded using the sequence SEQ-VI-1 without severe distortion and destructive interference of the lineshape. A 45° rf-pulse elicits the PASADENA response. For possible future experiments which require earlier observation times, a robust two-dimensional zero-quantum NMR sequence is suggested in Chapter VII.

The J-order on the alkane is sampled at varying time delays between the beginning of the p-H_2 burst and the rf pulse. Samples were spaced closely in time where the enhancement function changed more rapidly. The sequence was repeated three times for the five para-substituted ethylbenzene derivatives. Immediately following these runs, the ordinary NMR spectrum was recorded. In order to measure the overall hydrogenation rate by conventional means, H_2 was then bubbled through the solution for 460 s. The ordinary NMR spectrum was again recorded (after a sufficient delay to allow complete relaxation). The final experiment on the same sample was an ordinary $180° - \tau - 90°$ T_1 sequence. The k_{cat}'s and T_1's measured by conventional means are tabulated below.

Table (VI-1)

Substrate, S	$[S]_0$,M	Rate/$[Rh]_T$,s^{-1}	T_1^p,s
styrene	0.97	0.025	12.1 ± 0.4
p-CH_3O-styrene	0.83	0.088	7.8 ± 0.1
p-Cl-styrene	0.87	0.042	8.3 ± 0.1
p-F-styrene	0.93	0.049	10.8 ± 0.3
p-CH_3-styrene	0.82	–	10.0 ± 0.4

Observe that the rate for styrene is nearly four times lower than the value predicted from Eq. (VI-5). However, the values in Table (VI-1) were obtained by dividing the observed rate of ethylbenzene production by $[Rh]_T$. If the active catalyst concentration were four times lower than $[Rh]_T$, due to carbon monoxide poisoning or irreversible formation of inactive, indeterminate complexes, for example,[6] then the discrepancy would be accounted for. Such complications are automatically avoided in the PASADENA kinetics experiments since only catalytically active molecules contribute to the observed signals from which k_F and k_D are derived.

§ VI-3. Modelling

A conceptually simple model for the time dependance of the PASADENA polarization on the product alkane can be derived on intuitive grounds. The key assumption is that the $Rh(PPh_3)_2H_2(>=<)Cl$ species is formed instantly at $t = 0$. Later, this constraint will be relaxed in order to obtain a more realistic model in which there is a distribution of formation times of the intermediate.

§ VI-3.1. Instantaneous Formation of $Rh(PPh_3)_2H_2(>=<)Cl$

Suppose that once formed, a $Rh(PPh_3)_2H_2(>=<)Cl$ molecule converts to product alkane with a unimolecular rate constant k_D.

$$Rh(PPh_3)_2H_2(>=<)Cl \xrightarrow{k_D} \text{alkane} + Rh(PPh_3)_2Cl$$

The probability that $Rh(PPh_3)_2H_2(>=<)Cl$ survives for at least a time t_A is

$$\frac{[Rh(PPh_3)_2H_2(>=<)Cl](t_A)}{[Rh(PPh_3)_2H_2(>=<)Cl](0)} = e^{-k_D t_A} \tag{8}$$

The probability of decomposition of $Rh(PPh_3)_2H_2(>=<)Cl$ during a time interval $t_A + dt_A$ is

$$\frac{d[Rh(PPh_3)_2H_2(>=<)Cl](t_A)}{[Rh(PPh_3)_2H_2(>=<)Cl](t_A)} = k_D dt_A \tag{9}$$

The product of these two factors gives the distribution of lifetimes, i.e.,

$$P(t_A)dt_A = k_D e^{-k_D t_A} dt_A \tag{10}$$

If all of the $Rh(PPh_3)_2H_2(>=<)Cl$ is formed at $t = 0$ and the observation is made at $t = t_A + t_B$, then the fractional loss L of J-order due to relaxation on either chemical species is clearly

$$\begin{aligned} L(t) &= e^{-t_A/T_{1J}^c} e^{-(t-t_A)/T_{1J}^p} \\ &= e^{-t_A(1/T_{1J}^c + 1/T_{1J}^p)} e^{-t/T_{1J}^p} \end{aligned} \tag{11}$$

Integrating the loss factor over the distribution of lifetimes,

$$\begin{aligned} j_p(t) &= \int_0^t F(t)P(t_A)dt_A \\ &= \frac{-k_D}{R_c + k_D - R_p} e^{-tR_p} \left| e^{-t_A(R_c + k_D - R_p)} \right|_0^t \\ &= \frac{k_D}{R_c + k_D - R_p} e^{-R_p t} \left(1 - e^{-(R_c + k_D - R_p)t}\right) \end{aligned} \tag{12}$$

Only three parameters are necessary for fitting to extract the rate k_D.

§ VI-3.2. Finite Rate of Formation of $Rh(PPh_3)_2H_2(>=<)Cl$

In this treatment, the assumption of instantaneous formation of the intermediate is dropped in favor of a more realistic functional form. The commencement of bubbling of p-H_2 gas through the benzene solutions sets a physically meaningful origin of time for the analysis which follows.

The quantity of fundamental interest is again the time dependence of the J-order, $j_p(t)$, on the product. In terms of the density operator, this is the coefficient of $I_{z1}I_{z2}$. It is derived from the rate of change of J-order on $Rh(PPh_3)_2H_2(>=<)Cl$, $dj_c(t)/dt$, the difference in the rates of formation and reduction of J-order;

$$\frac{dj_c(t)}{dt} = hj_0k_Fe^{-k_F(t-\tau_a)} - j_c(R_c + k_D) \tag{13}$$

where

j_0 ≡amount of J-order present on a dihydride immediately after formation from a molecule of H_2 at a given χ_p

k_F ≡rate of dissociation of PPh_3 from $Rh(PPh_3)_3Cl$

R_c ≡$1/T_{1J}$, rate of decay of J-order on $Rh(PPh_3)_2H_2(>=<)Cl$

k_D ≡rate of reaction of $Rh(PPh_3)_2H_2(>=<)Cl$ into alkane product

The formation function is shifted in time by an amount τ_a with respect to the commencement of bubbling of p-H_2 gas through the benzene solution. To account for a transient H_2 presence, the $Rh(PPh_3)_2H_2(>=<)Cl$ formation function in the model will be truncated when the H_2 concentration becomes rate limiting, coinciding with the point in time at which the formation of $Rh(PPh_3)_2H_2(>=<)Cl$ is essentially complete. The rectangle function $h(t)$ kills the formation prior to τ_a and after τ_b, i.e.,

$$h(t) = \begin{cases} 0, & t < \tau_a; \\ 1, & \tau_a \leq t \leq \tau_b; \\ 0, & t > \tau_b. \end{cases} \tag{14}$$

This somewhat arbitrary shape is satisfactory, since the goal is to make a small correction for the fact that $(\tau_a - \tau_b)^{-1}$ is not very much smaller than the rates to be measured. This choice allows analytical expressions to be derived, while a more complete modelling would require numerical solutions to several coupled rate equations. Roughly, τ_a is the time at which the H_2 concentration becomes high enough for the rate of $Rh(PPh_3)_2H_2(>=<)Cl$ formation to become significant. This will be left as an adjustable parameter in the model since τ_a has not been measured

experimentally. The parameter τ_b is then fixed by experimental information about the total amount of $Rh(PPh_3)_2H_2(>=<)Cl$ which was formed per burst of H_2, i.e., the "turnovers" per burst (see Table (VI-2)). The formation function is truncated at the point in time τ_b when the turnover number T has been reached. Specifically,

$$\tau_b - \tau_a = -\ln(1-T)/k_F \tag{15}$$

In all experiments, $T \ll 1$, so that multiple turnovers by a single catalyst molecule can be neglected in the modelling.

Eq. (VI-13) is solved by taking its Laplace transform and invoking linearity and the differential formula $\mathcal{L}\{j_c'(t)\} = sJ_c(s) - j_c(0)$. Obviously, $j_c(0) = 0$, so that

$$J_c(s) = j_0 k_F e^{k_F \tau_a} \left[\frac{e^{-\tau_a(s+k_F)}}{(s+k_F)(s+R_c+K_D)} - \frac{e^{-\tau_b(s+k_F)}}{(s+k_F)(s+R_c+k_D)} \right] \tag{16}$$

The inverse Laplace transform of the terms in brackets can be simplified by using the convolution property;

$$\mathcal{L}^{-1}\{g_1(s)\cdot g_2(s)\} = \int_0^t f_1(u)\cdot f_2(t-u)du \tag{17}$$

Let

$$g_1(s) = \frac{e^{-as}}{s+b} \qquad g_2(s) = \frac{1}{s+c} \tag{18}$$

Then

$$\mathcal{L}^{-1}\{g1\} = \begin{cases} 0, & \text{if } 0 < u < a; \\ e^{-b(u-a)}, & \text{if } u \geq a \end{cases} \tag{19}$$

$$\mathcal{L}^{-1}\{g_2(s)\} = e^{-cu} \tag{20}$$

The total inverse transform formula is therefore

$$\mathcal{L}^{-1}\left\{\frac{e^{-as}}{(s+b)(s+c)}\right\} = \begin{cases} 0, & t < a; \\ \frac{1}{c-b}\left(e^{b(a-t)} - e^{c(a-t)}\right), & t \geq a \end{cases} \tag{21}$$

Applying Eq. (VI-21) to the terms in square brackets in Eq. (VI-16);

$$j_c(t) = j_0 k_F e^{k_F \tau_a} \left[\frac{h_1(t) e^{-k_F \tau_a}}{R_c + k_D - k_F} \left(e^{k_F(\tau_a - t)} - e^{(R_c + k_D)(\tau_a - t)} \right) \right.$$
$$\left. - \frac{h_2(t) e^{-\tau_b k_F}}{R_c + k_D - k_F} \left(e^{k_F(\tau_b - t)} - e^{(R_c + k_D)(\tau_b - t)} \right) \right] \tag{22}$$

The next step is to write out the rate equation for J-order on the product, which contains a positive contribution from alkane formation from decomposition of $Rh(PPh_3)_2H_2(>=<)Cl$ and a relaxation term,

$$\frac{dj_p(t)}{dt} = j_c(t) k_D - j_p(t) R_p \tag{23}$$

where $R_p = 1/T_{1J}^p$ is the spin-lattice relaxation rate of J-order on the alkane. Inserting Eq. (VI-22) into Eq. (VI-23), taking the Laplace transform and rearranging,

$$J_p(s) = \frac{j_0 k_F k_D e^{k_F \tau_a}}{R_c + k_D - k_F} \left[\frac{e^{-k_F \tau_a} e^{-s\tau_a}}{(s + R_p)(s + k_F)} - \frac{e^{-k_F \tau_b} e^{-s\tau_b}}{(s + R_p)(s + k_F)} \right.$$
$$\left. - \frac{e^{-k_F \tau_a} e^{-s\tau_a}}{(s + R_p)(s + R_c + k_D)} + \frac{e^{-k_F \tau_b} e^{s\tau_b}}{(s + R_p)(s + R_c + k_D)} \right] \tag{24}$$

After performing the inverse transform, the final result is

$$j_p(t) = \frac{j_0 k_F k_D}{(k_D + R_c - k_F)(k_F - R_p)(R_c + k_D - R_p)} \times$$
$$\left\{ (k_D + R_c - R_p) \left(\exp\left[R_p(\tau_a - t) \right] - \exp\left[k_F(\tau_a - t) \right] \right) h_1(t) \right.$$
$$- (k_F - R_p) \left(\exp\left[R_p(\tau_a - t) \right] - \exp\left[(R_c + k_D)(\tau_a - t) \right] \right) h_1(t)$$
$$- (k_D + R_c - R_p) \left((1 - T) \exp\left[R_p(\tau_a - t - \ln[1 - T]/k_F) \right] \right.$$
$$\left. \left. - \exp\left[k_F(\tau_a - t) \right] \right) h_2(t) \right.$$

$$+ (k_F - R_p)(1-T)\Big(\exp\Big[R_p(\tau_a - t - \ln[1-T]/k_F)\Big] - \exp\Big[(k_D + R_c)(\tau_a - t - \ln[1-T]/k_F)\Big]\Big) h_2(t)\Big\} \tag{25}$$

where the Heaviside unit step functions h_1 and h_2 are defined as

$$h_1(t) = \begin{cases} 0, & t < \tau_a; \\ 1, & t \geq \tau_a \end{cases} \qquad h_2(t) = \begin{cases} 0, & t < \tau_b; \\ 1, & t \geq \tau_b \end{cases} \tag{26}$$

If the formation of $Rh(PPh_3)_2H_2(>=<)Cl$ is rapid, Eq. (VI-25) simplifies considerably. Taking the limit of an infinite rate of formation of $Rh(PPh_3)_2H_2(>=<)Cl$ and setting $\tau_a = 0$,

$$\lim_{k_F \to \infty} j_p(t) = \frac{j_0 k_D T}{R_c + k_D - R_p} e^{-R_p t}\left(1 - e^{-(R_c + k_D - R_p)t}\right) \tag{27}$$

where the turnover number now scales j_0, the initial amount of J-order present. Setting $T = 1$, this expression becomes identical to Eq. (VI-12).

§ VI-3.3. Fits

Eq. (VI-25) was parameterized for non-linear least squares fitting by defining the following five parameters:

$$a_1 = \frac{j_0 k_F k_D}{(k_D + R_c - k_F)(k_F - R_p)(R_c + k_D - R_p)}$$
$$a_2 = k_D + R_c \qquad a_3 = k_F$$
$$a_4 = \tau_a \qquad a_5 = R_p \tag{28}$$

The Levenberg-Marquardt method was employed by adapting routines found in Ref. 7. The requisite partial derivatives $\partial a_1/\partial t, \ldots, \partial a_5/\partial t$ were computed using Mathematica and automatically transformed into C-language code for use in the fitting program. The results of the fits are given in Table (VI-2). The model $j_p(t)$ given by Eq. (VI-25) is plotted in enhancement units in Fig. (VI-3a-e) for each of

the substrates in the series along with the corresponding experimental data points derived from the enhanced triplet (the quartet is shown for p-methylethylbenzene). These data are summarized in Fig. (VI-3f), which shows only the model fits for the chemical series.

The Curie-Law contribution to the multiplet lineshape in the experimental spectra must be separated from the PASADENA signal in order to compute the enhancement. For the triplet, this was accomplished in a three-step procedure. First, the spectra were carefully phase corrected based on the purely absorptive TMS and substrate NMR lines. Secondly, the integrals over a small frequency range about the outer lines of the triplet were calculated. These two integrals were then subtracted, thereby removing intensity contributions from the ordinary NMR resulting from the build up of alkane product. The enhancements were then obtained by dividing this difference by the sum of the integrals and dividing by $\sqrt{2}$ to account for the 45° pulse (enhancements are reported relative to the reference spectrum obtained with a 90° pulse).

$$\frac{L-R}{\sqrt{2}(L+R)} \equiv \text{Enhancement}$$

The time dependence of the sum was perfectly linear, indicating that the above procedure was successful in isolating the two signal sources.

Table (VI-2)

Substrate	Turnovers	k_F s^{-1}	k_D s^{-1}	T_{1J}^c s	T_{1J}^p	τ_a s	χ^2
styrene	0.27	0.42	0.16	1.68	8.15	+0.01	1.14
p-CH_3O-styrene	0.28	0.47	0.24	1.26	4.39	-0.06	0.15
p-Cl-styrene	0.22	0.55	0.35	1.31	4.32	+0.01	0.42
p-F-styrene	0.29	0.41	0.18	1.61	5.70	-0.20	0.50
p-CH_3-styrene	0.25	0.34	0.19	1.70	5.16	+0.19	0.42

With the spin relaxation constants removed, the modelling equations for J-order

Fig. (VI-3) Experimental data along with theoretical fits to Eq. (VI-25) in units of the enhancement above the ordinary NMR signal are shown in parts a-e. The variable t is relevant to the pulse sequence SEQ-VI-1, with the twenty experimental data points collected at the times $t = \{1.25, 1.31, 1.37, 1.43, 1.49, 1.55, 1.85, 2.15, 2.45, 2.75, 3.05, 3.35, 3.65, 3.95, 4.65, 5.64, 7.25, 10.25, 15.25, 25.25\}$ s. The sequence was repeated three times for the five para-substituted styrene derivatives and the results averaged.

(VI-3a) Styrene.

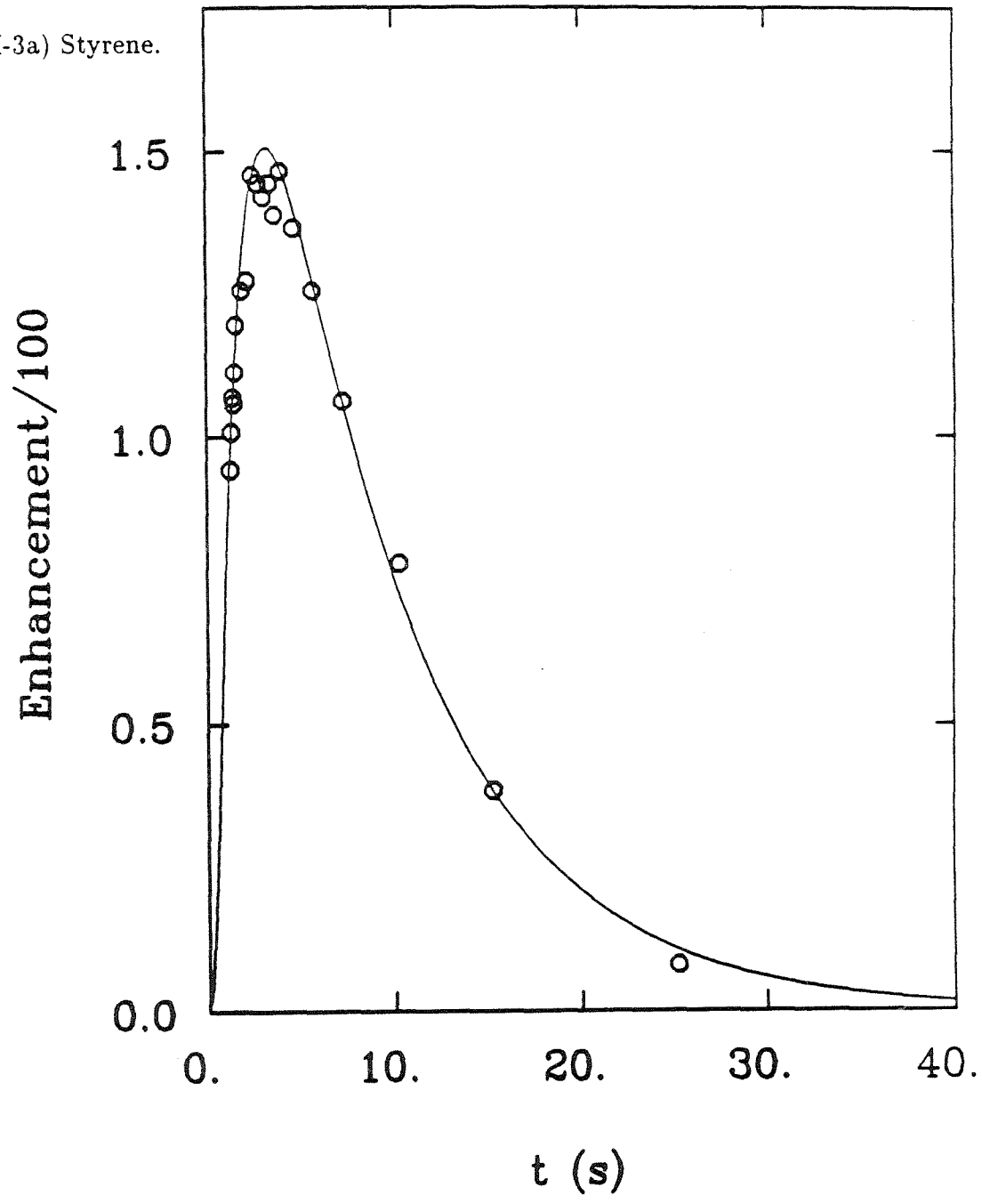

Fig. (VI-3b) p-Methoxystyrene

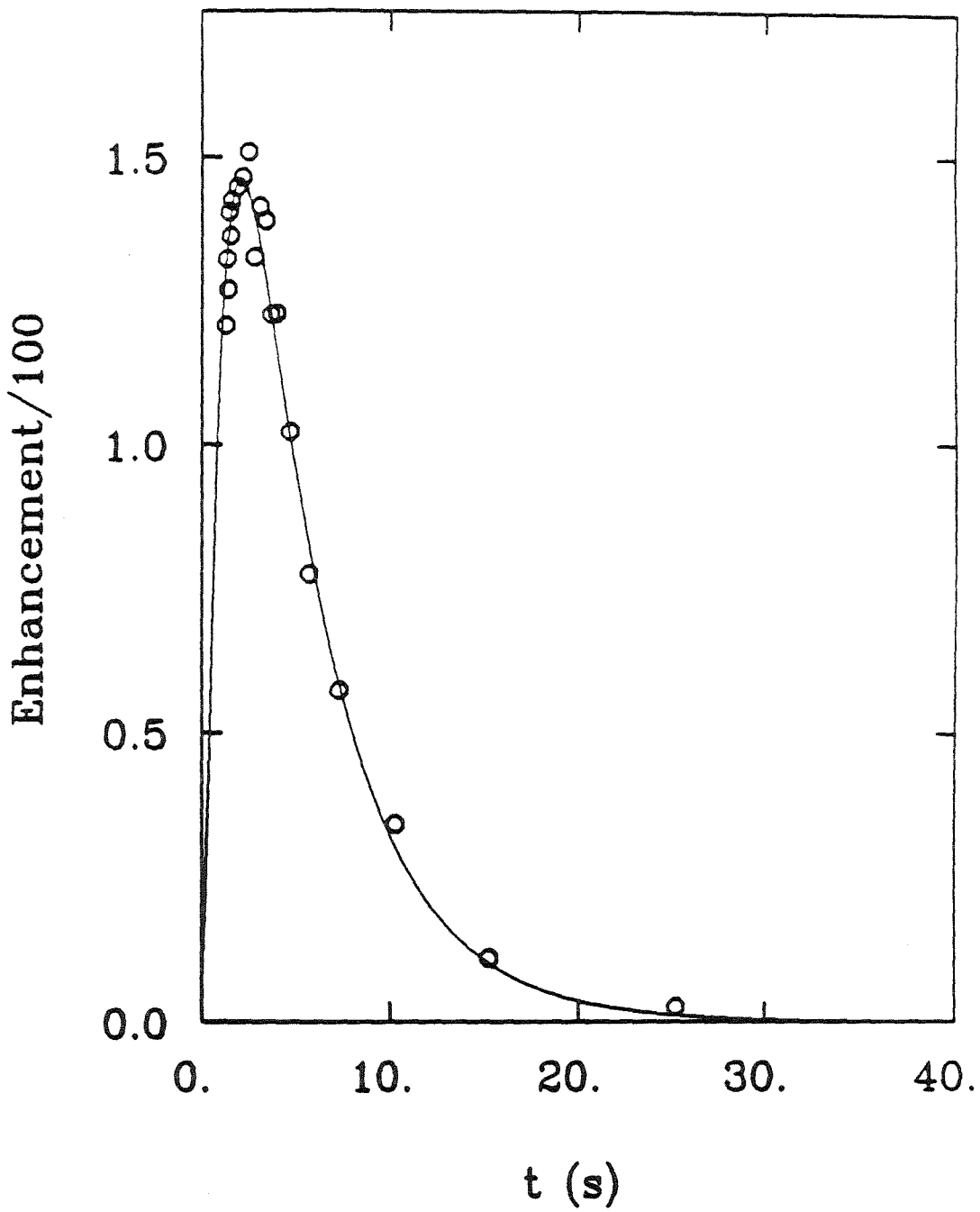

Fig. (VI-3c) p-Chlorostyrene

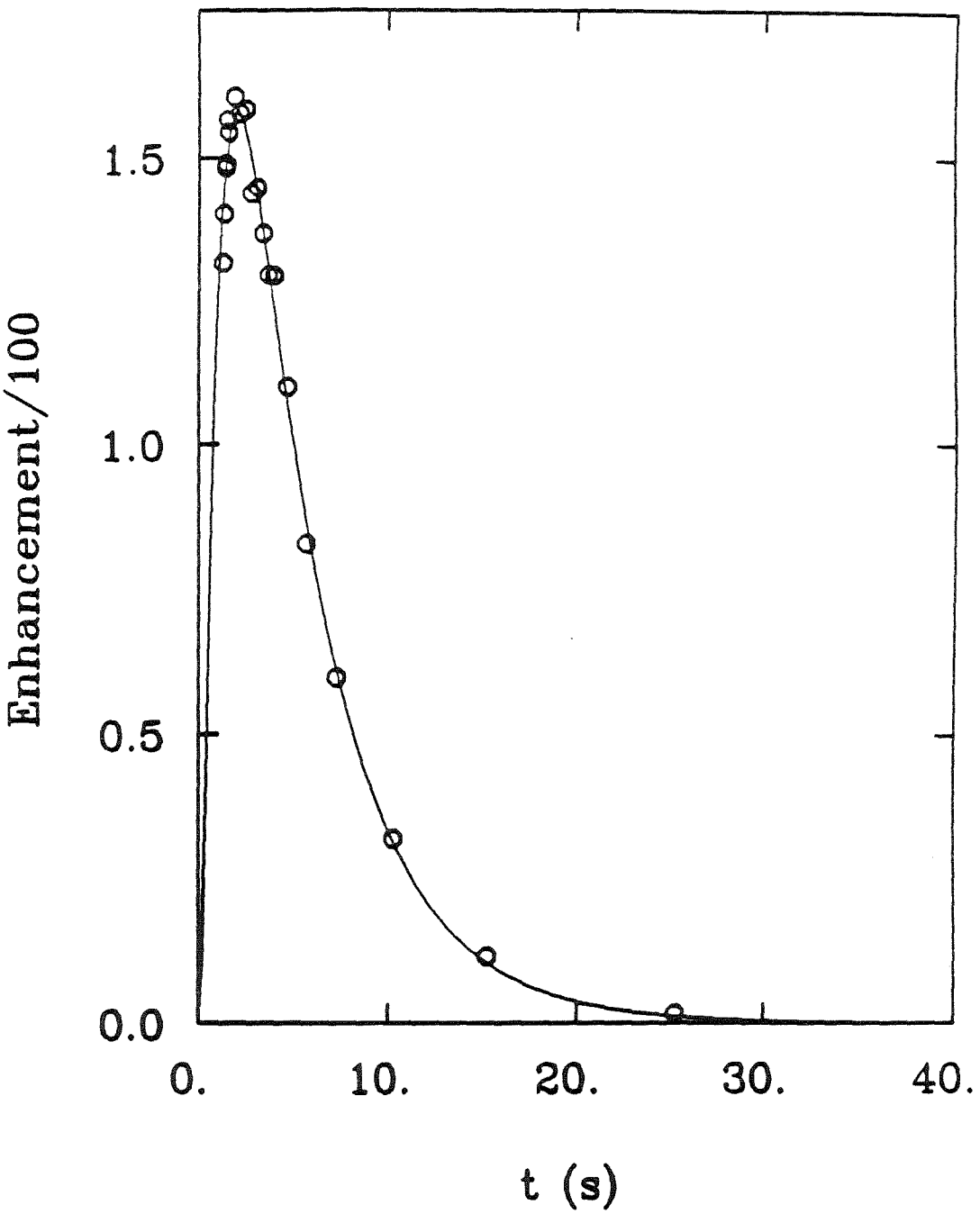

Fig. (VI-3d) p-Fluorostyrene

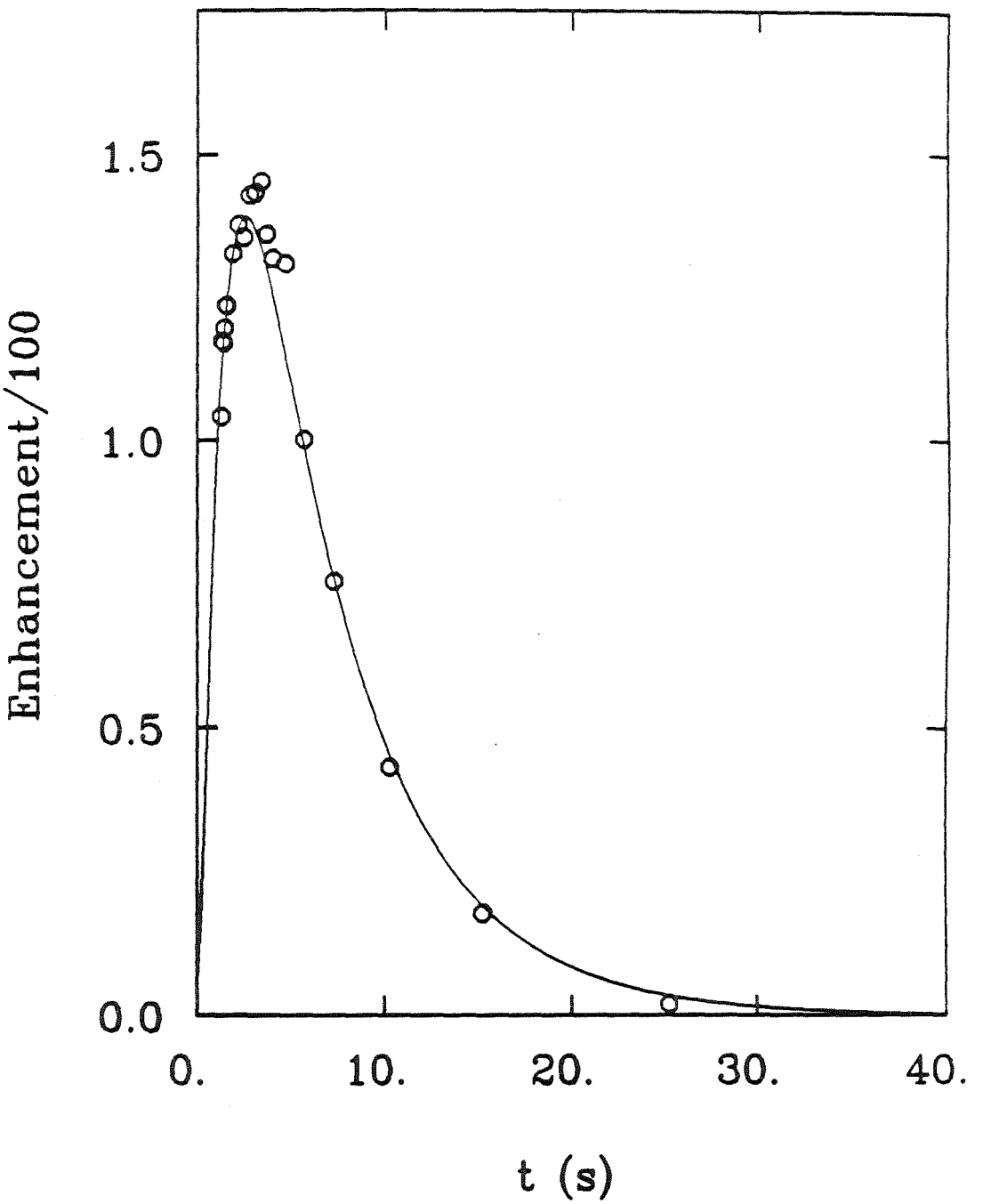

Fig. (VI-3e) p-Methylstyrene (quartet)

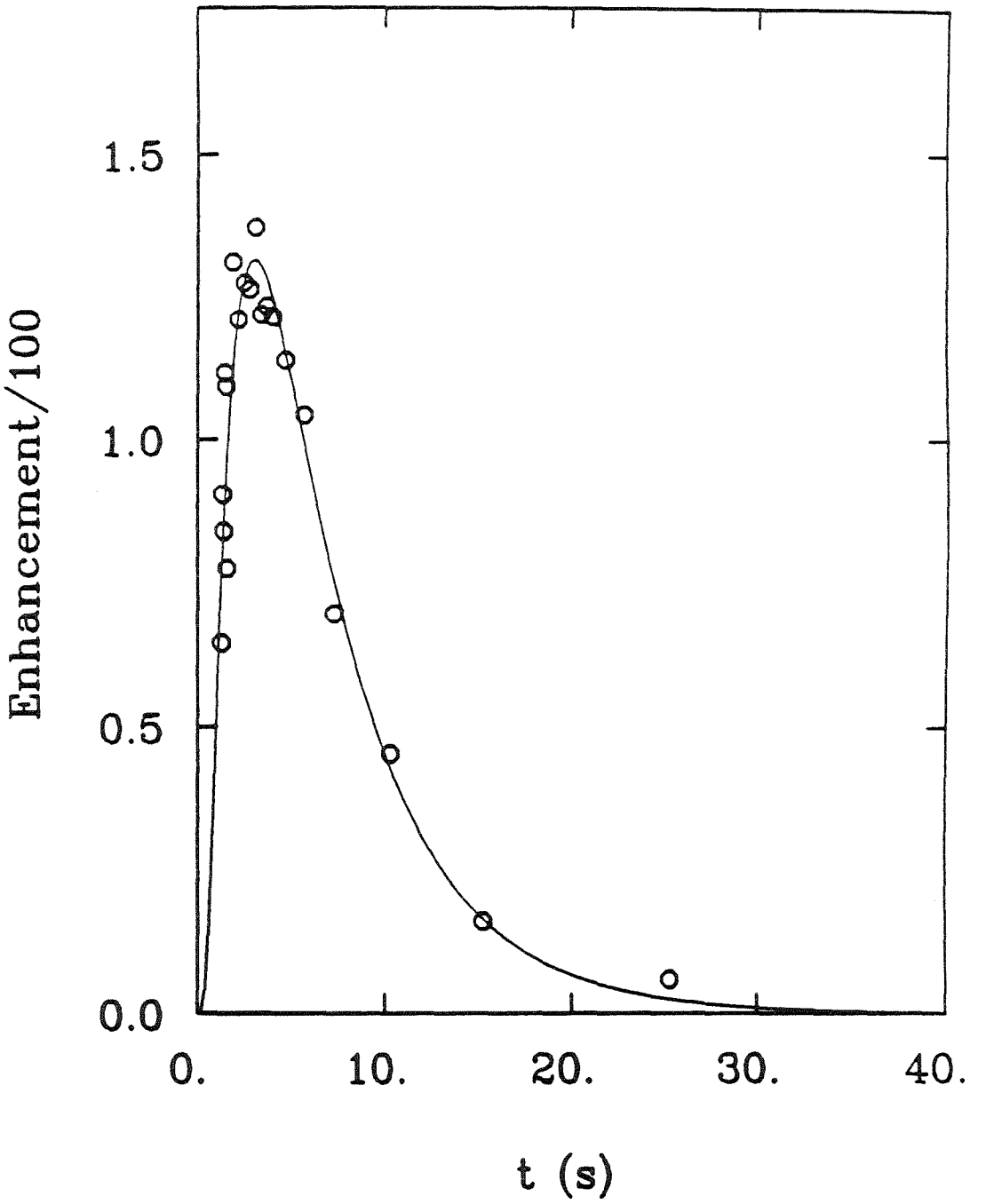

Fig. (VI-3f) Summary of theoretical fits of parts a-e. The maximum enhancements were very similar across the series, which is indicative of the similar rates of $Rh(PPh_3)_3Cl$ catalyzed hydrogenation of these substrates. This is also reflected in the small spread in times of the enhancement maxima.

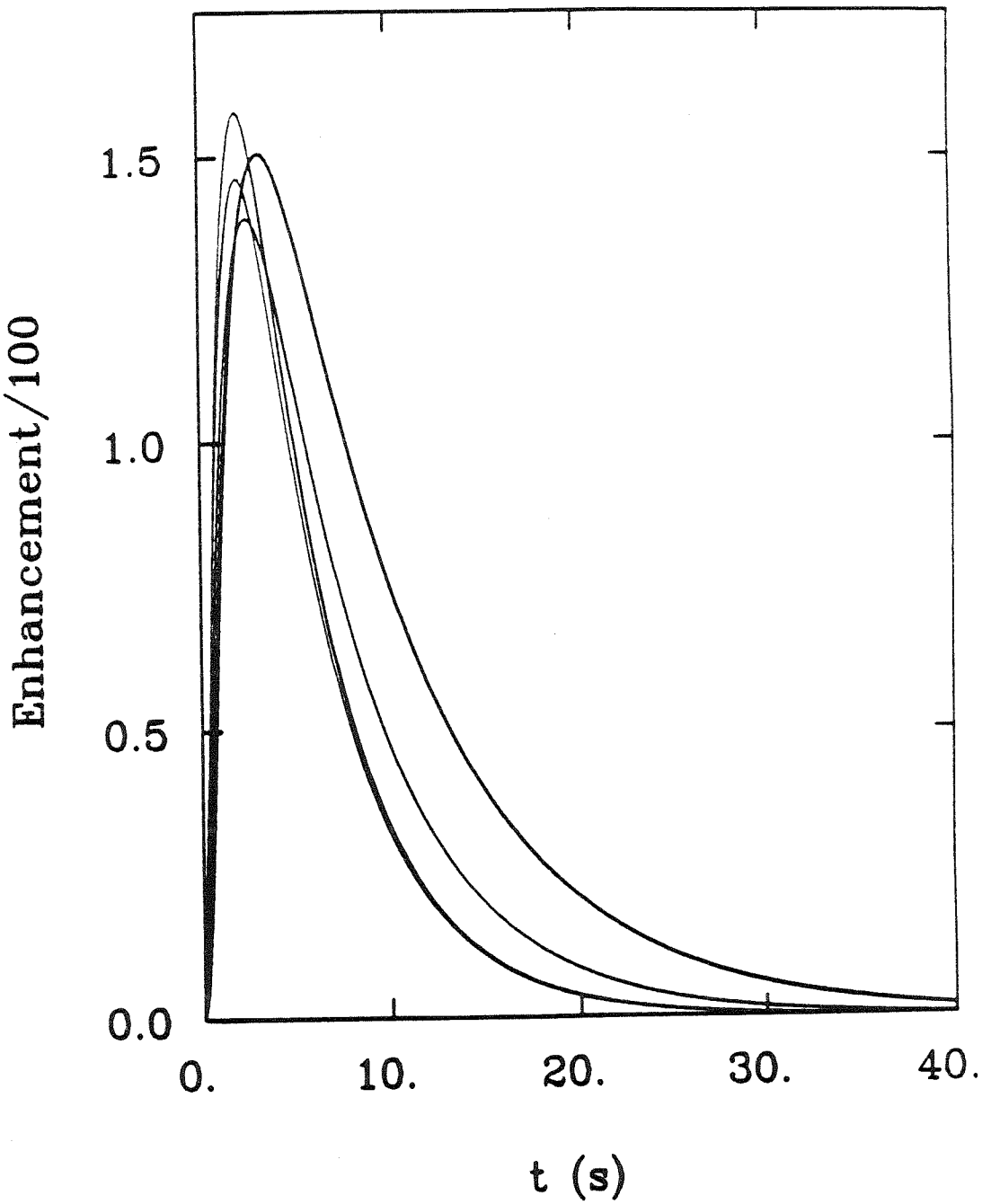

(Eq. (VI-22) and Eq. (VI-25)) reduce to the equations for the concentration of $Rh(PPh_3)_2H_2(>=<)Cl$ and the change in concentration for ethylbenzene, respectively.

$$[Rh(PPh_3)_2H_2(>=<)Cl](t) = [Rh(PPh_3)_3Cl]_0 \cdot k_F \cdot \exp\left[k_F\tau_a\right] \left[\frac{h_1(t)}{k_D - k_F}\left(\exp[-k_Ft] - \exp\left[-k_F\tau_a + k_D(\tau_a - t)\right]\right) - \frac{h_2(t)}{k_D - k_F}\left(\exp[-k_Ft] - \exp\left[-k_F\tau_b + k_D(\tau_b - t)\right]\right)\right] \tag{29}$$

$$\begin{aligned}\Delta[EB](t) = \frac{[Rh(PPh_3)_3Cl]_0}{k_D - k_F}\Big\{ & k_D\Big(1 - \exp\left[k_F(\tau_a - t)\right]\Big)h_1(t) \\ & - k_F\Big(1 - \exp\left[k_D(\tau_a - t)\right]\Big)h_1(t) \\ & - k_D\Big(1 - T - \exp\left[k_F(\tau_a - t)\right]\Big)h_2(t) \\ & + k_F(1-T)\Big(1 - \exp\left[k_D(\tau_a - t - \ln[1-T]/k_F\right]\Big)h_2(t)\Big\}\end{aligned} \tag{30}$$

Eq. (VI-29) and Eq. (VI-30) are plotted for styrene as the substrate in Fig. (VI-4a) using the fitted parameter values of Table (VI-2). The formation of $Rh(PPh_3)_2H_2(>=<)Cl$ is seen to increase rapidly during the H_2 burst (dashed line in Fig. (VI-4a)), which is consistent with the initial kinetic assumptions. The product ethylbenzene asymptotically approaches the turnover number $T = \Delta[EB](\infty)/[Rh_T]$, while the concentration of the bottleneck is transient in nature. The time dependence for the change in concentration of product alkane (Eq. (VI-30)) is plotted in Fig. (VI-4b). The similarity of the reactivities for the substrates in the series is evident. Eq. (VI-29) is plotted for the entire substrate series in Fig. (VI-4c). The ordering of the substrates for $t > 1$ s is consistent with their rates

k_D, i.e., the larger the K_D, the faster the decrease in $[Rh(PPh_3)_2H_2(>=<)Cl]$.

§ VI-4. Discussion

The goodness of the fits were satisfactory, as quantified by the χ^2 entries in Table (VI-2). The catalytic rates are quite similar across this series, which is consistent with the similarity of all of the turnover numbers.

The T_{1J}^c values for the $Rh(PPh_3)_2H_2(>=<)Cl$ species were all comparable, yet showed a certain degree of correlation with the alkane T_{1J}^p's. The alkanes with the bulkiest substituents, p-CH_3O- and p-Cl-ethylbenzene, are likely to have the longest rotational correlation times and hence spectral density nearest to the Larmor frequency. Indeed, these species demonstrated the shortest relaxation times while bound as $Rh(PPh_3)_2H_2(>=<)Cl$ and as free molecules.

The Zeeman T_1^c of $RhCl(PPh_3)_2H_2$ was measured to be 0.28 s. Its spectrum is shown in Fig. (VI-5). Note that the multiplet lineshapes here exhibit the emission/absorption pattern rather than absorption/emission. This underscores a unique aspect of the PASADENA spectra. There is usually no information on the sign of J in the weak coupling lineshape. Measurement of the relative sign of J is only possible in favorable cases. In contrast, the PASADENA lineshape directly reflects the *absolute* sign[12] of J. The destructive interference prevents large enhancements or quantitative analysis. It is unclear whether comparison of this number with T_{1J}^c is meaningful, since they describe the relaxation rates for different types of spin-order and also because they are associated with different chemical species. However, a valid comparison between T_{1J}^p and T_1^p can be made, since discrepancies are associated only with differences in the type of spin-order present. The range of ratios between these relaxation times was $0.52 \rightarrow 0.68$, with the average being $\approx 3/5$. Further theoretical work, i.e., a 5 spin generalization of the Solomon equations, is necessary to quantify the source of this result.

The rate of PPh_3 dissociation from $Rh(PPh_3)_3Cl$, k_F, is insignificantly different from the result predicted by Eq. (VI-4). This is a critical success of the model

Fig. (VI-4a) Plots of the change in concentration time dependence of $Rh(PPh_3)_2H_2(>=<)Cl$ (Eq. (VI-29)) and product (Eq. (VI-30)) for the hydrogenation of styrene to ethylbenzene using the fitted parameters of Table (VI-2). The ethylbenzene concentration asymptotically approaches the turnover number, $T = \Delta[EB](\infty)/[Rh_T]$. The H_2 burst is indicated by the dashed line.

a)

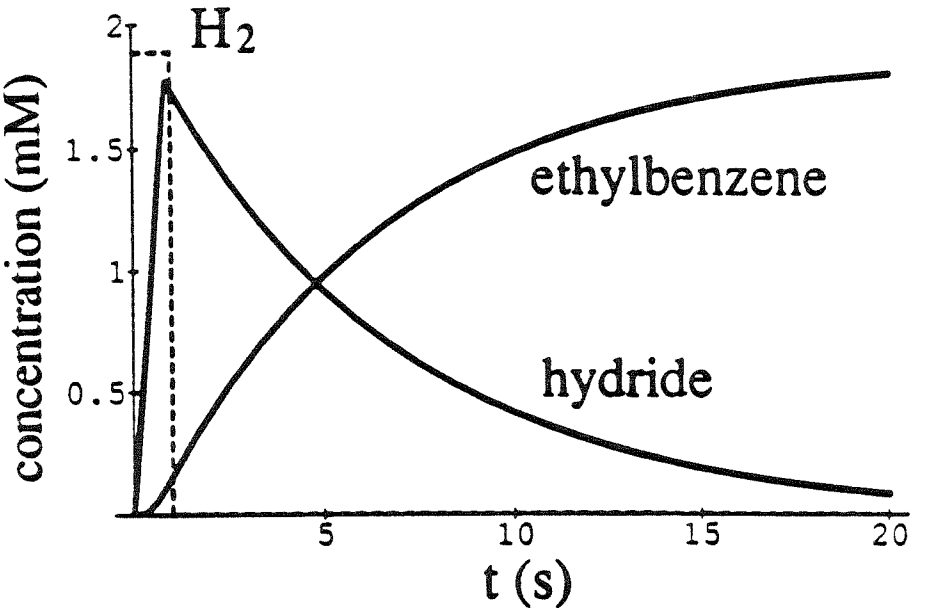

Fig. (VI-4b) The similar reactivities of the para-substituted ethylbenzene derivatives is exhibited by a plot of Eq. (VI-30) using the model fit parameters of Table (VI-2).

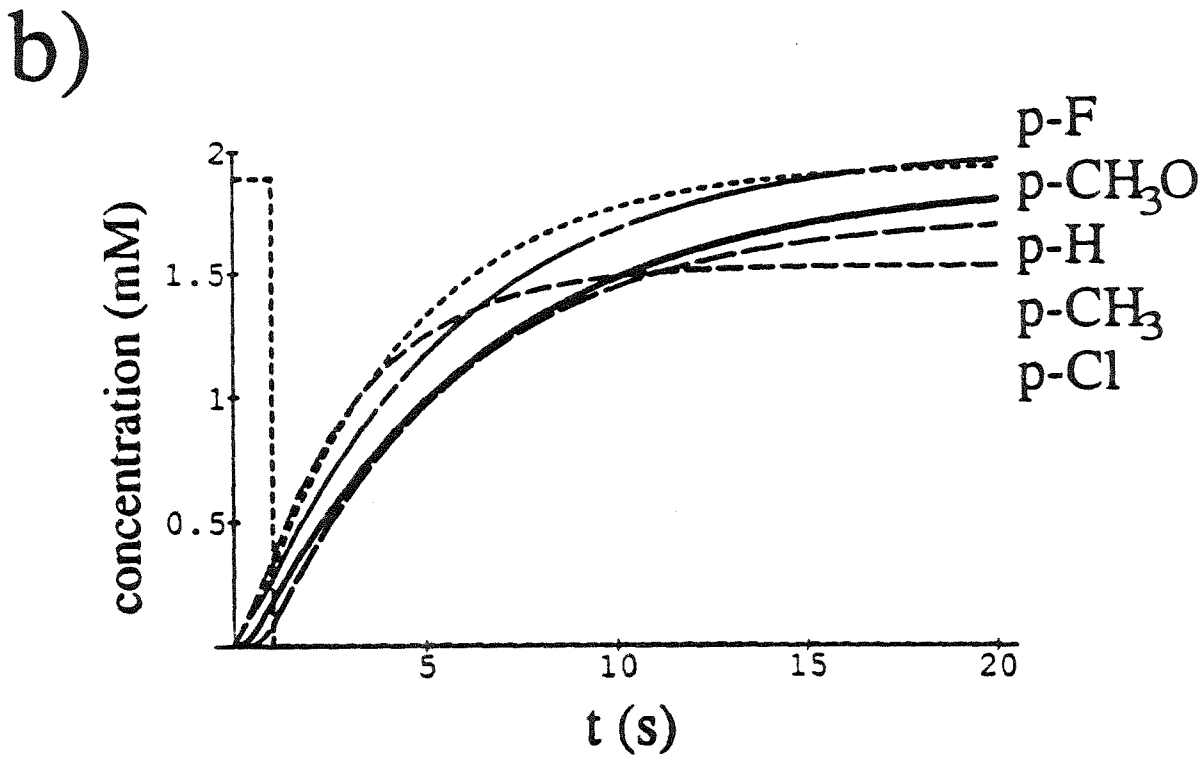

Fig. (VI-4c) Plots of the change in concentration time dependence of $Rh(PPh_3)_2H_2(>=<)Cl$ (Eq. (VI-29)) in the hydrogenation of the substrates listed in Table (VI-2). The dashed line represents the H_2 burst.

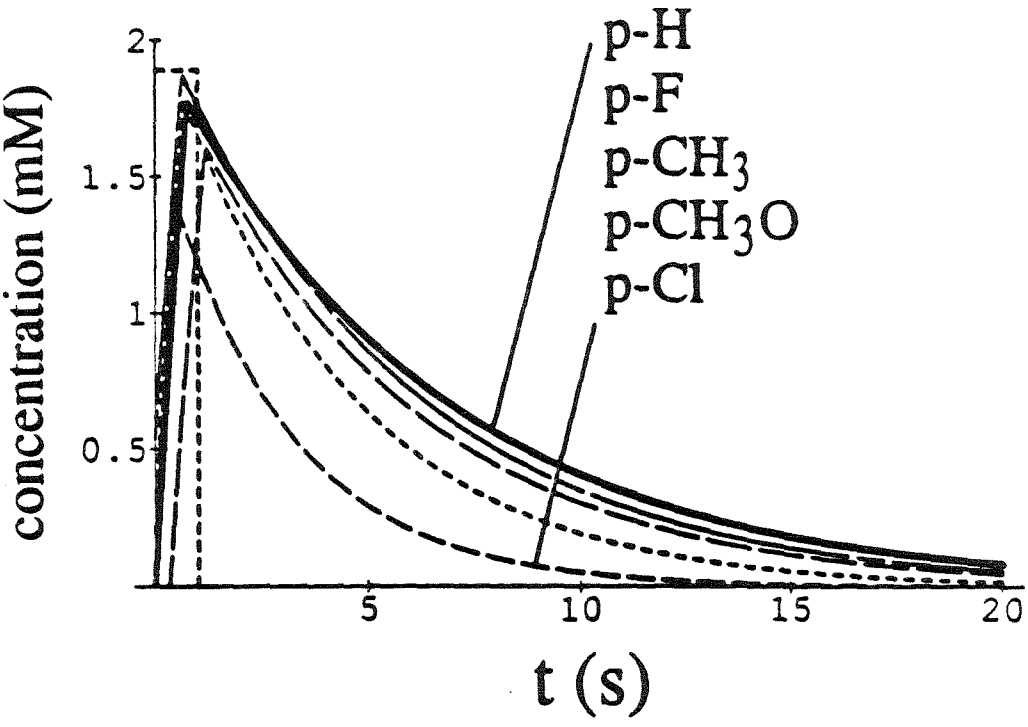

Fig. (VI-5) The enhanced transient NMR spectrum of the hydride region of $RhCl(PPh_3)_2H_2$ (shown below) formed from reaction with parahydrogen in deuteriobenzene. Due to ligand exchange, the only resolved J splitting is for the coupling of the proton at −9.4 ppm to the *trans* ^{31}P.[2,6] The unique information is in the phase of the multiplets which shows that the unresolved scalar coupling between the hydride protons is negative.[12]

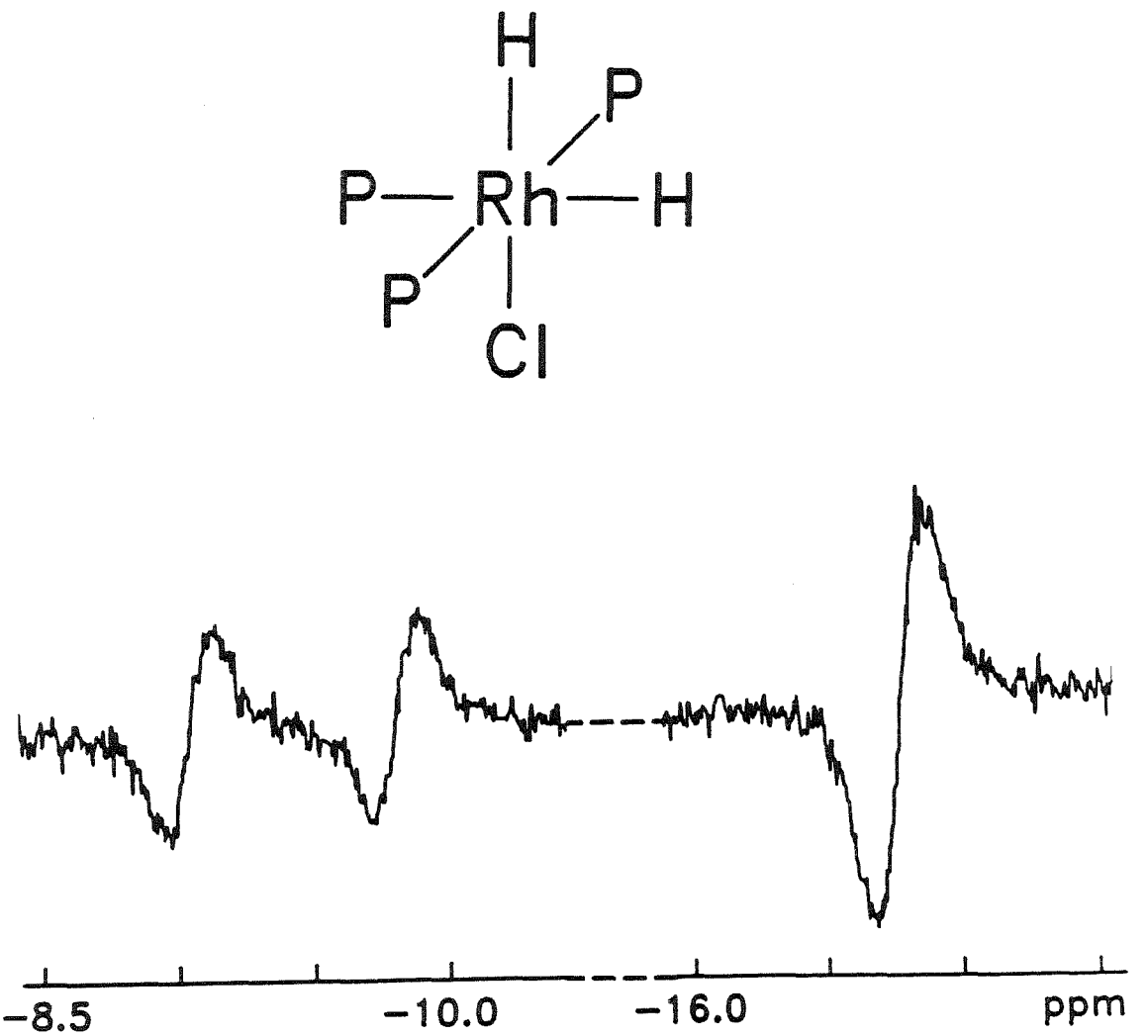

and justifies the assumption that the H_2 concentration is high enough to make k_F independent of $[H_2]$ and that the dissociation of PPh_3 from $Rh(PPh_3)_3Cl$ limits the rate of $Rh(PPh_3)_2H_2(>=<)Cl$ formation. The short τ_a times produced by the fits imply that k_D rapidly reaches its limiting value, ca. within 0.2 s of the front edge of the burst.

The k_D derived from the fit for styrene, the only substrate for which a complete set of literature constants for Eq. (VI-7) is known, [11] is larger by a factor of 1.68 than the value predicted from the rate expression. This is not an unexpected result, considering that the PPh_3 concentration substituted into Eq. (VI-7) is a lower bound on the true value. Consequently, the value of k_D based on this equation was an underestimate.

§ VI-5. Suggestions for Future Study

This chapter has demonstrated, using the $Rh(PPh_3)_3Cl$ system as a prototypical example, how the PASADENA effect can be employed to elucidate the details of a catalytic hydrogenation mechanism. The model which has been constructed appears to be consistent with existing kinetic and mechanistic descriptions. The distinct advantage of the PASADENA kinetic studies over conventional methods such as ordinary NMR is that the former yields rates which are independent of all assumptions regarding the concentration of the active catalyst species. Additional work is necessary, however, to extend these original experiments over a wider range of conditions to provide rigorous tests of the model. In this section, several directions for future efforts are presented.

§ VI-5.1. Reaction Conditions

Recall that Eq. (VI-2) can be simplified if $k_{-2}[PPh_3] \ll k_3[H_2]$. At the high concentrations of rhodium used, it was not possible to satisfy this inequality due to the limiting solubility of H_2. Consequently, the value of k_F was reduced from its limiting value of 0.68 s^{-1} to $\approx$ 0.4 s^{-1}. The upper limit could be reached by

simply reducing $[Rh]_T$. Such a variation in the reaction conditions would serve as a test of the existing model. The response of the fitted k_F and other parameters to systematic variations in the rhodium and phosphine concentrations would also be helpful in assessing the validity of the model.

§ VI-5.2. Two-Dimensional NMR

A major problem with H_2 bubbling as the means for activating the reaction is the severe disruption of the magnetic field homogeneity which can result. This limits the earliest times at which the PASADENA amplitude can be sampled. While this is not a serious problem when $k_F \approx 0.4$, sampling problems could arise for conditions under which a faster rate applies.

To address this issue, the use of zero-quantum coherence is proposed. Zero-quantum coherence is robust against gradients of all sorts, including dynamic ones incurred by bubbles (see Chapter VII). J-order can be transformed into zero-quantum coherence by the application of a 90° pulse, following which the coherence of the weakly coupled spin system evolves at essentially the chemical shift difference. The initial pulse can now be placed arbitrarily close to the burst (or even within the burst!). Only S/N considerations now limit the earliest times which can be sampled. After the bubbles have cleared, a 45° pulse can transform the zero-quantum into observable transverse magnetization. The delay between the two pulses is incremented until a complete two-dimensional zero-quantum spectrum is recorded. The entire process is repeated to collect a complete set of sampling times, each represented by a two-dimensional NMR spectrum.

§ VI-5.3. Flash Photolysis of $RhCl(PPh_3)_2CO$

Ford has recently demonstrated the possibility of sudden formation of the tricoordinate $RhCl(PPh_3)_2$ species by flash-photolyzing $RhCl(PPh_3)_2CO$[8].

$$RhCl(CO)(PPh_3)_2 \xrightarrow{h\nu} RhCl(PPh_3)_2 + CO \qquad (31)$$

Formation of this intermediate is complete within 25 μs of the flash. When H_2 and olefin are present, this species rapidly reacts to form $RhCl(PPh_3)_2H_2$, followed by rapid equilibrium to form $Rh(PPh_3)_2H_2(>=<)Cl$. This chemical shortcut to the creation of the bottleneck species leads to a substantial reduction in the complexity of the analysis. The distribution of formation times would be essentially a delta function.

A significant advantage of the flash-photolysis method is that bubbling is no longer the means of initiating the reaction, thereby removing the limitations imposed by disruption of the magnetic field homogeneity and also the uncertainty in the H_2 concentration. The flash now precisely establishes the origin of time for the subsequent dynamics. The question of the rate of H_2 transport across the liquid gas interface and the difficulties arising from its concentration time dependence also become irrelevant, since the p-H_2 can be pre-dissolved without it adding to the catalyst. The proposed experiment could be performed using the existing apparatus with several modifications; 1) an optical window or fiber-optic access to the sample tube, 2) flat-bottom quartz NMR tubes, 3) additional plumbing to permit cycling of H_2 and CO bubbling through the solution.

§ VI-5.4. Structure of $Rh(PPh_3)_2H_2(>=<)Cl$

One area in which the PASADENA effect could have a major impact on modern conceptions of transition metal chemistry would be the characterization of the elusive $Rh(PPh_3)_2H_2(>=<)Cl$ intermediate. The enhancement afforded by this method makes it particularly well suited for such an application. In combination with flash photolysis to produce temporarily high concentrations of the hydride intermediate, the proton NMR spectrum of this molecule should be obtainable.

§ VI-6. References

1. A. J. Birch and D. H. Wiliamson, *Org. React.* **24**, 1 (1978)
2. J. A. Osborne, F. H. Jardine, J. F. Young and G. Wilkinson, *J. Chem. Soc. (A)*, 1711 (1966)
3. Solubilities of Inorganic and Organic Compounds, H. Stephen and T. Stephen, Editors, Pergamon Press, New York (1963)
4. J. Halpern and C. S. Wong, *J. Chem. Soc., Chem. Commun.*, 629 (1973)
5. J. Halpern, T. Okamato and A. Zakhariev, *J. Mol. Catal.* **2**, 65 (1976)
6. P. Meakin, J. P. Jesson and C. A. Tolman, *J. Am. Chem. Soc.* **95**, 3240 (1972)
7. W. H. Press, B. P. Flannery, S. A. Teukolsky and W. T. Vetterling, Numerical Recipes in C, Cambridge University Press, New York (1988)
8. P. C. Ford, T. L. Netzel, C. T. Spillett and D. B. Pourreau, *Pure and Appl. Chem.* **62** 1091 (1990)
9. G. W. Parshall, Homogeneous Catalysis, Wiley, New York (1980)
10. D. C. Roe, *J. Am. Chem. Soc.* **105**, 7770 (1983)
11. J. Halpern, *Inorg. Chim. Acta.* **50**, 11 (1981)
12. C. R. Bowers and D. P. Weitekamp, *J. Am. Chem. Soc.* **109**, 5541 (1987)

Chapter VII

Two-Dimensional PASADENA

Kinetic Study of Enhanced Intermediates

§ Introduction

The design, execution and interpretation of experiments involving catalytic p-H_2 addition to styrene by rhodium (I) 1,2-bis(diphenylphosphino) ethane, abbreviated Rh(DIPHOS)$^+$, will be the focus of this chapter. This is the prototype for a particular class of rhodium complexes which facilitate hydrogenation of olefinic

substrates with remarkable stereoselectivity.

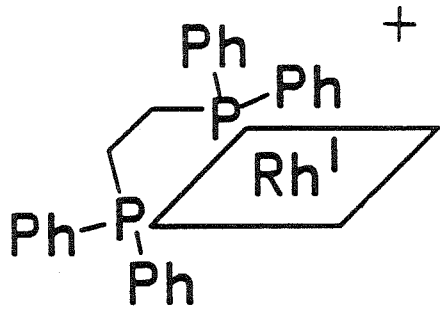

Substantial effort has been extended by a number of investigators[1–8] to elucidate the kinetics and mechanism for this family of complexes, with the larger goal of comprehending the universal factors which regulate the stereoselectivity of catalytic systems in general. Likewise, the scope of the experimental methods and kinetic modelling described herein is not limited to $Rh(DIPHOS)^+$ dynamics alone, but should be generally applicable to a wide range of catalytic hydrogenation systems and their associated mechanisms. The proposed techniques are all discussed in the context of stopped-flow PASADENA, which offers the possibility of observing key intermediates at low concentration through the enhancement of the NMR transitions. However, much of the pulse sequence design, experimental procedure and analytical formulation would be directly applicable or adaptable to the study of NMR-time-scale chemical dynamics for other reactions. The methodology could be extended to dynamic polarization mechanisms other than PASADENA, such as CIDNP, DNP, etc.

§ VII-1. Preparation of Reaction Samples

The catalyst precursor, $[Rh(DIPHOS)(NBD)]^+PF_6^-$ was obtained from Strem[†]

[†] product no. 45-0120, CAS # 60470-22-6, Strem Chemicals, Inc., 7 Mulliken Way, Newburyport, MA 01950

and used as received (NBD≡norbornadiene). In all of the experiments to be described in this chapter, the substrate was styrene (Aldrich) and the solvent was d_6-acetone (Aldrich). Purification and deaeration of the solvent and substrate were found not to improve the amplitude of the observed PASADENA signals, so those procedures were abandoned and the reagents used without further preparation. Reaction solutions contained 1 ml d_6-acetone, 0.015 g $[Rh(DIPHOS)(NBD)]^+PF_6^-$ and 0.1 ml styrene, yielding $[Rh]_T = 0.0185$ M and [styrene]= 1.17 M. The samples were mixed in a vial open to the air and then transferred to the 5 mm NMR tube. The NMR tube was inserted into the NMR hydrogenation apparatus and pressurized, as described in §V-1.

§ VII-2. The Catalyst Precursor

In the presence of H_2, the precursor reacts stoichiometrically with 2 moles of H_2 to form the active catalyst,

$$Rh(DIPHOS)(NBD)^+ + 2H_2 \longrightarrow Rh(DIPHOS)^+ + \text{norbornane}$$

Variation of the counterion present has been shown not to have any effect on the catalytic activity[4]. When styrene is present, it immediately becomes coordinated with an equilibrium constant[4] of $K_2 = 20\ M^{-1}$.

$$Rh(DIPHOS)^+ + >=< \xrightarrow{K_2} Rh(DIPHOS)(>=<)^+$$

At the concentration of styrene used, this reaction proceeds to 96% completion. This is a far greater degree of coordination than that exhibited by the $Rh(PPh_3)_3Cl$ system, a consequence of the greater steric hindrance of the two PPh_3 ligands compared to DIPHOS, and the relative ligand deficiency of $Rh(DIPHOS)^+$ compared to $Rh(PPh_3)_3Cl$.

The currently accepted mechanism[1] for the $Rh(DIPHOS)^+$ catalyzed hydrogenation of styrene including the new step proposed here is shown in Fig. (VII-1). The mechanism was determined for methyl-(Z)-α-acetamidocinnamate (MAC) as

the substrate, but is thought to be similar for other olefinic substrates, such as styrene.[1] The phenyl ring of styrene coordinates to the rhodium, playing the same role as the carbonyl oxygen of MAC.

Following coordination of the olefin to yield **2**, the octahedral complex **3** is formed by H_2 addition in the overall rate determining step. Although this species has not been directly observed, it has been proposed[1] to be a catalytic intermediate, based on indirect evidence and in analogy with a small number of other cases in which this species has been intercepted and characterized spectroscopically.[5,9] The inability to observe **3** is apparently due to the rapid transformation **3**→**4**, which is in contrast to the analogous step in the mechanism for the $Rh(PPh_3)_3Cl$ catalyzed hydrogenation of styrene. In that system, the transformation of the analog of **3** into the analog of **4** is the rate limiting step of the overall reaction. The final step is hydride migration and decomposition to regenerate the initial catalytic form.

§ VII-3. Spectrum of the Intermediate

PASADENA studies using styrene as the substrate reveal that there is yet another intermediate in the $Rh(DIPHOS)^+$ mechanism outlined above. The proposed species, identified as **5** in Fig. (VII-1), is a rhodium-η_6-ethylbenzene complex which has not previously been observed.

When p-H_2 is bubbled through a freshly prepared sample followed by a 45° acquisition pulse, the complicated spectrum of Fig. (VII-2) is obtained. The delay between the end of the burst and the pulse is about 2 s. Dramatic PASADENA enhancements are observed for both norbornene and norbornane. After about 20 s of H_2 bubbling, these signals subside, indicating that all of the norbornadiene has been hydrogenated and that formation of the active catalyst is complete.

As the enhanced signals arising from para-hydrogenation of norbornadiene disappear, a new set of enhanced multiplets begin to dominate the spectrum, as shown in Fig. (VII-3). Strikingly, four distinct multiplets are present; two PASADENA quartets and two triplets having the relative intensity patterns (1,1,-1,-1) and (2,0,-

Fig. (VII-1) Catalytic mechanism for the Rh(DIPHOS)$^+$ catalyzed hydrogenation of styrene. The "bound" species represents a newly identified species in this mechanism. NMR studies are described in this chapter to measure the rate k_6 of the final *slow* step indicated below in which the alkane product is released, freeing the catalyst molecule.

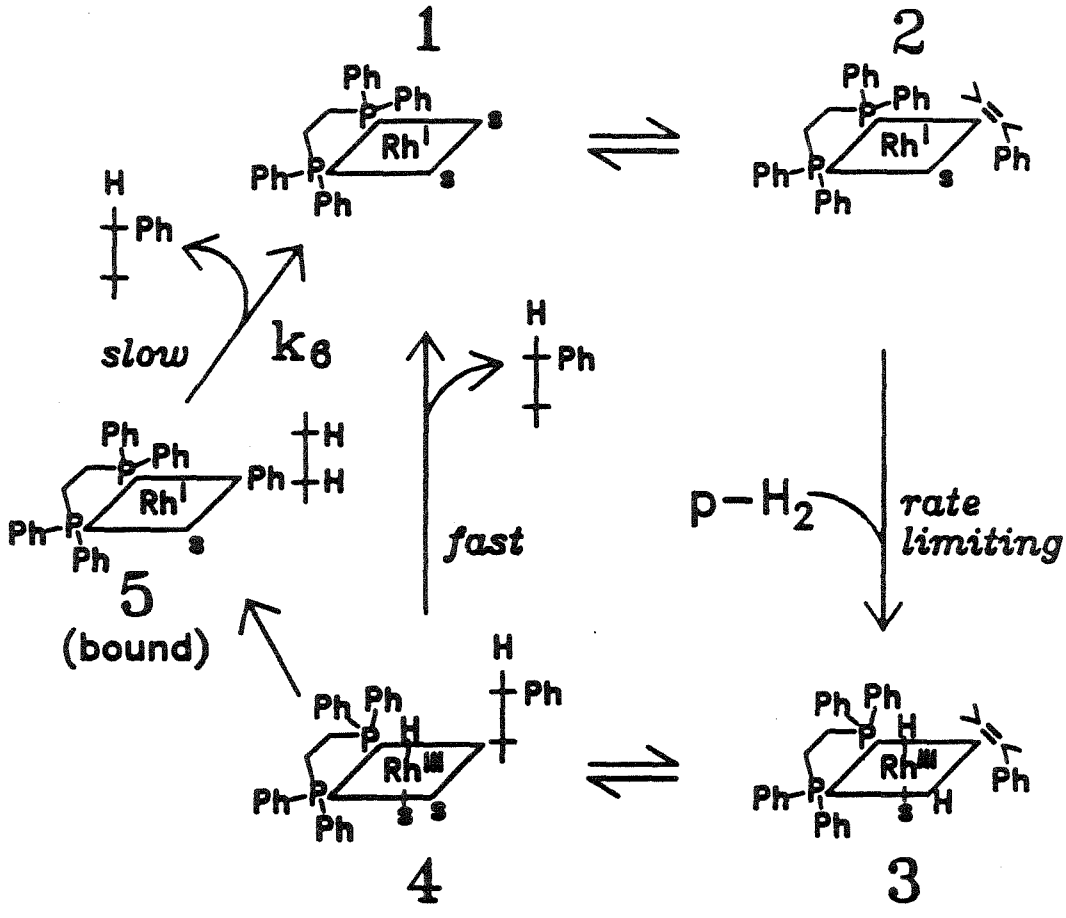

Fig. (VII-2) PASADENA spectrum which results from bubbling para enriched H_2 with $\chi_p = 0.5$ through an acetone solution of $[Rh(DIPHOS)(NBD)]^+PF_6^-$ for 1 s. Enhancements due to both norbornene and nobornane are observed.

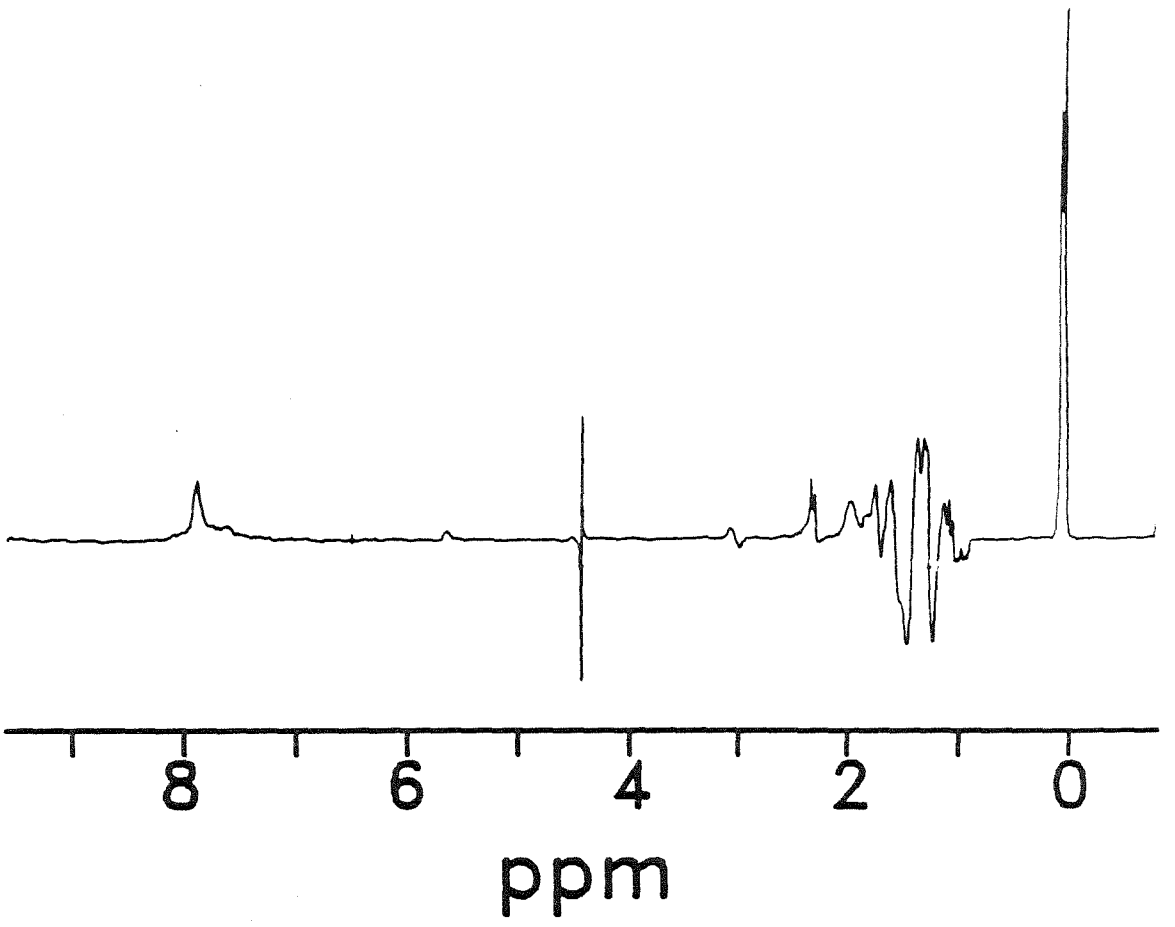

2). If the spectrum is again recorded after a delay which is long enough to permit thorough spin-lattice relaxation, there is no signal at the positions where enhanced intensity had been previously observed. The burst-pulse-acquisition cycle may be repeated over and over, with a gradual buildup of product ethylbenzene occurring with each burst. After $30 - 40$ bursts, this product can be observed in the ordinary NMR spectrum collected with a 90° pulse. However, this Curie-Law signal only appears at one of the two quartets and one of the two triplets which were observed under p-H_2 enhancement conditions. These multiplets are at the positions of ethylbenzene in this solvent, leading us to hypothesize that the positions in the spectrum which exhibited enhancement but not accumulation of product represented a transient bound species in the hydrogenation mechanism. The nearly equal intensities of the two species suggests that about half of the complex **4** of Fig. (VII-1) eliminates the alkane to form the starting material **1** while the other half is trapped in the "bound" intermediate **5**.

Further evidence on the distinct intermediate associated with the new pair of multiplets is obtained from the experiment depicted in SEQ-VII-1.

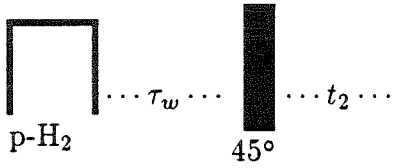

SEQ-VII-1

Fig. (VII-4) shows the decay of PASADENA J-order as a function of the delay τ_w between the p-H_2 burst and the acquisition pulse. After an initial slight increase, the J-order decays with different rates for the "free" and "bound" ethylbenzene. While the signal from the bound species is expected to decay with a single exponential (see Eq. (VII-2)), the same cannot be said for that of the free ethylbenzene, which will depend on multiple rates (see Eq. (VII-6)). The kinetic problem to be solved is suggested by fitting the data for $\tau_w > 3$ s to single exponentials. The values 1.94 s and 3.35 s are obtained for the bound and free J-order, respectively.

Fig. (VII-3) 200 MHz proton NMR spectrum of ethylbenzene formed by the addition in room-temperature solution of parahydrogen to styrene by the catalyst Rh(DIPHOS)$^+$. The spectrum shows that two distinct alkane species are formed in approximately equal quantities. The downfield multiplets of each type are at the frequency of the free alkane, while the upfield ones are attributed to an intermediate in a parallel pathway in which the nascent product becomes bound to the catalyst.

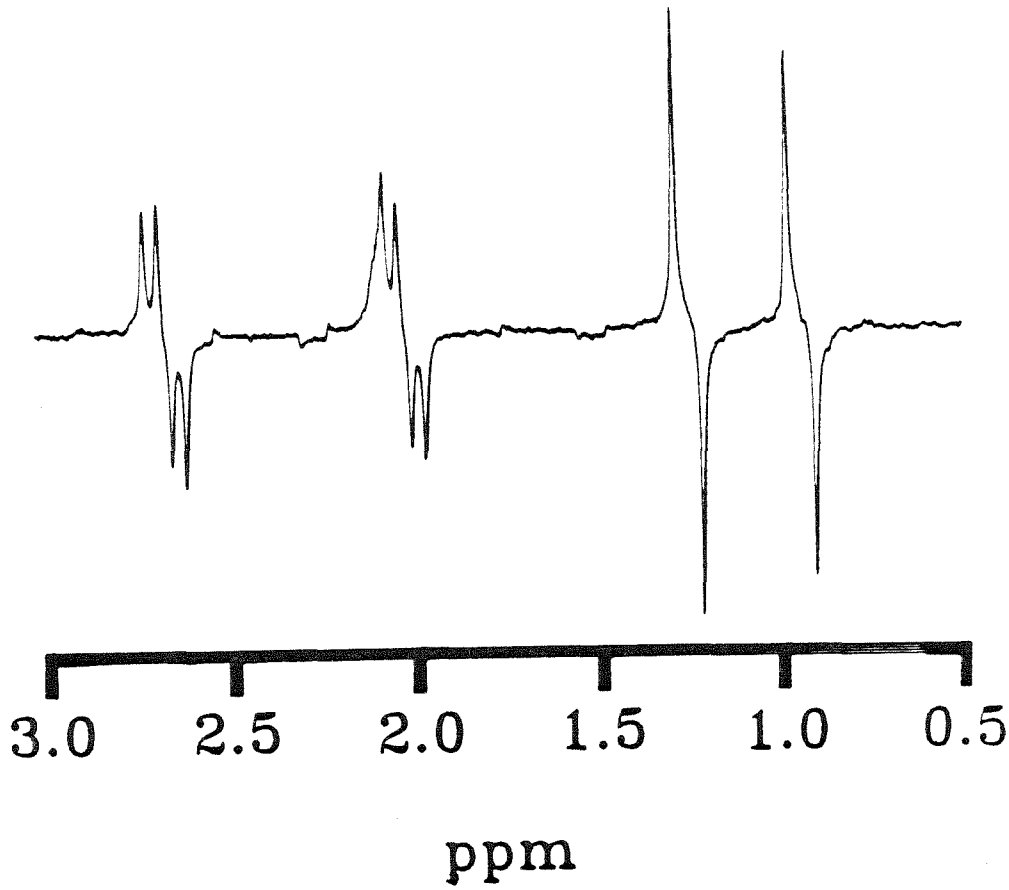

There are two simple explanations for this discrepancy; 1) the spin-lattice relaxation is more efficient on the bound species due to the slower rotational correlation time, and 2) the J-order of the bound species is reduced through chemical transfer of polarization to the free species on this time-scale. A superposition of these processes will be the working hypothesis.

§ VII-4. Kinetic Study of Rh(DIPHOS)(EB)$^+$ Decomposition

Exchange of polarization between magnetically inequivalent sites can be followed using the classic two-dimensional exchange sequence,[10,11] a modification of which is shown in SEQ-VII-2.

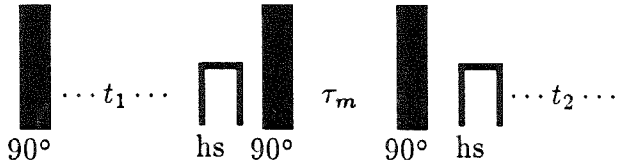

SEQ-VII-2

In this implementation, "hs" identifies a homospoil pulse, the purpose of which is to selectively admit only signal which originated as coherence during t_1 (see §VII-5.1). The sequence begins with the stimulation of single-quantum coherence by a preparation pulse. This is followed by coherent evolution during the period labelled t_1. The second pulse stores the coherence as population differences. During the *exchange* period, τ_m, some chemical transformation processes may occur, transferring populations from the eigenstates of the Hamiltonian characterizing the initial magnetic environment to the eigenstates of a second. A final pulse transforms the spin populations into observable transverse magnetization. Fourier transformation with respect to the evolution and acquisition time dimensions produces the two-dimensional spectrum, which permits correlation of the frequencies present in ω_1 with those of ω_2.

Four types of intensity maxima may occur in the two-dimensional spectrum resulting from SEQ-VII-2. These are classified as either *diagonal* or *cross-peaks.*

Fig. (VII-4) Decay of PASADENA J-order as a function of the delay between the H_2 burst and the rf pulse, τ_w (see SEQ-VII-1). The free alkane decay corresponds to "△," the bound to "○."

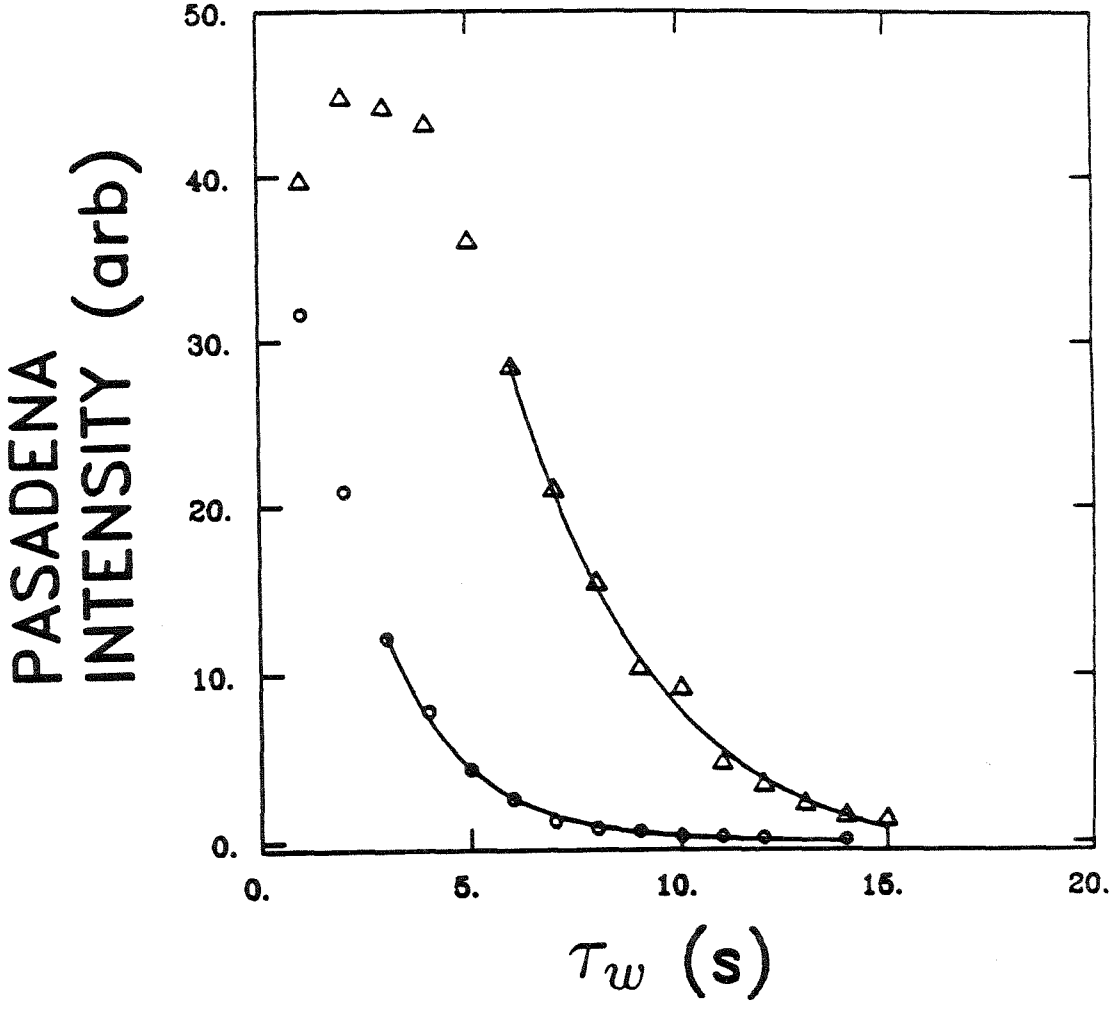

The diagonal peaks in the two site exchange spectrum represent spin populations which either did not undergo any dynamical transformation or else underwent an even number during τ_m. Otherwise, the chemical transformation process results in cross-peaks. A true exchange process can be inferred if the cross-peaks are symmetrical in magnitude with respect to the diagonal, i.e., an equilibrium situation prevails in which the rate of transformations site-1→site-2 is equal to the rate site-2→site-1. Under non-equilibrium conditions, a cross-peak appears predominantly or entirely on only one side of the diagonal. When spin polarization transfer occurs under non-equilibrium chemical conditions, it will be referred to as *polarization transfer by chemical reaction.*

The ratio of the cross-peak and diagonal-peak intensities can be related to the rate of the dynamical processes. However, due to the possibility for differences in the spin-lattice relaxation on the two species, the effects of spin-lattice relaxation and chemical transformation must be disentangled. By varying the length of the exchange period, a curve of cross-peak intensity versus exchange time can be constructed which may be fit to a model which accounts for both the possibility of inequivalent T_1 relaxation constants for each chemical species and the rate constant for the conversion of one into the other. This permits extraction of the values for all three parameters.

§ VII-4.1. Kinetic Modelling

Modelling expressions will now be derived which are generally applicable to the basic Jeener two-dimensional exchange sequence and variations thereof, including specific PASADENA two-dimensional polarization transfer by chemical reaction sequences designed to study the process

$$\text{Rh(DIPHOS)(EB)}^{+} \xrightarrow{k_6} \text{Rh(DIPHOS)}^{+} + \text{EB}$$

Let,

$j_f \equiv$ enhanced polarization on free ethylbenzene

$j_b \equiv$ enhanced polarization on bound ethylbenzene

$T_{1j}^b \equiv$ spin-lattice relaxation time of j_b

$T_{1j}^f \equiv$ spin-lattice relaxation time of j_f

$j_o^b \equiv$ initial polarization on bound ethylbenzene at $\tau_m = 0$

After a burst of p-H_2 has initiated the hydrogenation reaction which creates *J*-order, the subset of all Rh(DIPHOS)(EB)$^+$ molecules which were formed at or before a specified time can be coherence labelled with an rf pulse. The existence of coherence on a molecule allows it to be distinguished from other molecules which were formed after the pulse. Obviously, the duration of the pulse must be short compared to both the time-scale of the reaction as well as the period of the ensuing coherent evolution. The evolution period of the two-dimensional sequence is also made short compared to $1/k_6$. As in the conventional exchange sequence, the t_1 coherence is converted into population differences. These may be chemically transferred to other species during τ_m. Any possible contribution to the observed signal from population differences not originating as t_1 coherence can be eliminated by the use of appropriate pulsed d.c. field gradient techniques. Hence, for analytical purposes, the formation of $j_b(0)$ is nominally instantaneous at $\tau_m = 0$. Consequently, the rate equations are similar to Eq. (VI-13) and Eq. (VI-25) which were used in the modelling of the Rh(PPh_3)$_3$Cl NMR-kinetics.

During the exchange time, the disappearance of J order on Rh(DIPHOS)(EB)$^+$ obeys

$$\frac{dj_b}{d\tau} = -k_6 j_b - j_b R_b \tag{1}$$

where $R_b = 1/T_{1j}^b$. Integrating,

$$j_b(\tau) = j_b(0) e^{-(k_6 + R_b)\tau} \tag{2}$$

The amount of polarization which has been transferred from bound to free ethylbenzene is

$$j_b(0) - j_b(\tau) = j_b(0)\left(1 - e^{-(k_6+R_b)\tau}\right) \tag{3}$$

The ratio of the cross-peak intensity to the diagonal-peak intensity (representing bound ethylbenzene which remained bound throughout the exchange period), is

$$\frac{j_b(0) - j_b(\tau)}{j_b(\tau)} = e^{(k_6+R_b)\tau} - 1 \tag{4}$$

Notice that only the sum $k_6 + R_b$ occurs. An equation involving $j_f(t)$ is necessary to obtain an expression in which k_6 and R_b occur as independent factors. This can derived by using the constraint that the reduction of polarization on Rh(DIPHOS)(EB)$^+$ by chemical transfer must appear as an increase in the polarization on free ethylbenzene. In analogy with Eq. (VI-25),

$$\frac{dj_f(\tau)}{d\tau} = k_6 j_b(0) e^{-(k+R_b)\tau} - j_f R_f \tag{5}$$

where $R_f = 1/T_{1j}^f$. The solution is

$$j_f(\tau) = \frac{k_6 j_0^b}{k_6 + R_b - R_f} e^{-\tau R_f}\left[1 - e^{-(k+R_b-R_f)\tau}\right] \tag{6}$$

which describes the polarization originating on Rh(DIPHOS)(EB)$^+$ at $\tau_m = 0$. This polarization is manifested as a cross-peak in the two-dimensional spectrum. The cross-peak to bound diagonal-peak intensity ratio is therefore

$$\frac{j_f(\tau)}{j_b(\tau)} = \frac{k_6}{k_6 + R_b - R_f}\left[e^{(k_6+R_b-R_f)\tau} - 1\right] \tag{7}$$

Notice that in this expression, k_6 and $k_6 + R_b - R_f$ occur as separable factors, permitting parameterization and fitting to extract the chemical rate constant and the difference in the inverses of the spin lattice relaxation times. The values of T_{1J}^f and T_{1J}^b can be determined using the fitted k_6 from Eq. (VII-7) and the fitted value of $k_6 + R_b$ from Eq. (VII-3).

§ VII-5. Suppression of t_1 Noise

In the description of one-dimensional pulsed NMR experiments, the density operator is suddenly perturbed from equilibrium into a state of coherent evolu-

tion. The transverse magnetization frequencies, which are determined by the time independent internal Hamiltonian, are directly observed by the induction of an oscillating current in the detection coil.

The situation is different in the t_1 dimension of two-dimensional NMR experiments. Here, the time evolution is mapped out pointwise, its amplitude being determined not only by the internal Hamiltonian but also by a host of possibly random external factors as well, such as pulse amplitude jitter, static field drift and receiver instability. Such factors do not necessarily affect the S/N of the one-dimensional spectrum. If this spectrum represents a point in t_1, then the value of the coherence at that point is a linear combination of the "true" amplitude of the coherence and a contribution due to the random fluctuation in the experimental conditions. If the latter of these contributions is represented by a_{ij}, then the signal contribution from the ij*th* transition can be written as;[12]

$$\begin{aligned} S'_{ij}(t_1) &= \rho_{ij}\mathrm{I}_{+ji}(1 + a_{ij})e^{-i\omega_{ij}t_1} \\ &= S_{ij}(t_1) + N_{ij}(t_1) \end{aligned} \tag{8}$$

The uncorrelated random variations in a_{ij} for successive t_1 shots gives rise to Fourier components at all frequencies across the ω_1 domain. Furthermore, it can be shown that the average noise power spectral density scales with the magnitude of the true signal[12],

$$\langle |N_{ij}(\omega_1)|^2 \rangle = \frac{1}{2\pi}\langle |a_{ij}|^2 \langle |S_{ij}|^2 \rangle \tag{9}$$

The implications of this multiplicative property of the t_1 noise are particularly important in the design of two-dimensional PASADENA pulse sequences which depend on low t_1 noise to observe the transitions of interest. Variations in the p-H_2 burst characteristics represents an unconventional and dominating contribution to the random fluctuation a_{ij}.

The randomness in the p-H_2 bubbling is a current technical limitation on the t_1 noise of PASADENA experiments, and until sufficient reproducibility has

been achieved, optimal S/N of the ω_{ij} cross-peak transition cannot be obtained. With the present apparatus, the best that can be done is to eliminate all extraneous signals in ω_1 at the specific ω_2 at which the desired signal occurs. This will suppress the unwanted white noise contribution from irrelevant ω_1 transitions which happen to occur at the ω_2 of interest.

Three different sources of unwanted signal can be distinguished:

1. Residual populations which were not converted into coherence during the preparation period yet are converted into transverse magnetization by the mixing steps. Such magnetization appears as a peak at zero frequency in the ω_1 dimension.

2. Multiple-quantum coherence of an undesired order which occurs at non-zero ω_1 frequencies other than the those of the desired transitions in ω_1.

3. In the context of two-dimensional polarization transfer NMR, the essential kinetic information is contained in the ratio of the cross-peak to the diagonal-peak representing chemical intermediate formed before the first pulse and which remained as such during the exchange time. The peak representing chemical product formed before the first pulse occurs at the same position in ω_2 as the cross-peak. This product diagonal-peak is extraneous to the kinetic analysis and is detrimental to the S/N of the cross-peak.

The spectral contributions due to sources 1. and 2. can be eliminated by employing the pulsed field gradient methods which are described in §VII-5.1. A separate procedure, which relies on the ability to selectively prepare zero-quantum coherence from J-order, is used in the removal of source 3. The use of a simple

pulsed homospoil (discussed in §VII-5.1) is instrumental in achieving this.

§ VII-5.1. Pulsed Field Gradient Techniques

§ *The Homospoil*

In all of the experiments which will be presented, the pulsed homospoil, which consisted of a linear X field gradient, was applied immediately following the initial pulse. The effects of the homospoil on different orders of coherence can be understood by considering the following eigenoperator equation:

$$[\mathcal{H}_0, |i\rangle\langle j|] = \omega_{ij}|i\rangle\langle j| \tag{10}$$

where $|i\rangle\langle j|$ represents a coherence between the eigenstates $|i\rangle$ and $|j\rangle$. The magnetic field inhomogeneity is introduced as a spatial variation in the rotating frame Zeeman interaction:

$$\mathcal{H}_0'(\vec{r}) = \mathcal{H}_0 + \delta(\vec{r})\mathrm{I}_z \tag{11}$$

Substitution of $\mathcal{H}_0'$ for $\mathcal{H}_0$ into Eq. (VII-10),

$$[\mathcal{H}_0', |i\rangle\langle j|] = (\omega_{ij} + n_{ij}\delta(\vec{r}))\,|i\rangle\langle j| \tag{12}$$

where n_{ij} is the number of quanta in the transition, i.e. the order of the coherence. Consequently, the distribution of transition frequencies in the ensemble leads to dephasing of the coherence at a rate which depends on the strength of the gradient and the number of quanta in the transition. However, notice that for zero-quantum transitions, $n_{ij} = 0$, there is no linewidth dependence on the applied homospoil.

In the numerical density matrix calculations, the homospoil can be simulated by setting to zero all elements of the density matrix as written in the eigenbasis except for diagonal elements (populations) and zero-quantum coherence. This simple operation must be employed with caution, however, since the irreversibility implied by killing the matrix elements is artificial. An important aspect of dephasing in

field gradients which will prove useful in the design of n-quantum filters is that the dephasing can be reversed if the gradient is small enough so that diffusion of the molecules does not change their transition frequencies by an amount greater than the linewidth obtained without any gradients.

When $I_{zA}I_{zB}$ represents the initial density operator, pure zero-quantum coherence can be generated from a single 90° pulse followed by a homospoil. In contrast, Zeeman order requires at least two pulses to produce zero-quantum coherence. By selecting for zero-quantum coherence during τ, any contribution from Zeeman order representing accumulated product is eliminated, which is an important advantage.

§ *Coherence Transfer Echo Techniques*

Coherence transfer involves the delivery of amplitude from one coherence to a second coherence, i.e., exchange of off-diagonal elements of the density matrix. Coherence transfer is the principle upon which many (if not most) modern pulsed NMR experiments are based.

When the coherence $|i\rangle\langle j|$ is dephased due to some inhomogeneous interaction and then rephased as a coherence between a second pair of states $|k\rangle\langle l|$ (reversing the accumulated effect of the inhomogeneity), a *coherence transfer echo* results. Intentional inhomogeneity in the static magnetic field is used to shorten the duration of such echoes, thereby improving the discrimination between different coherence transfer pathways. Radiofrequency pulses are used to stimulate coherence transfer.

Consider the effect of a pulsed magnetic field gradient on a coherence. By Eq. (VII-12), the rate of dephasing is proportional to the order of the coherence. The times required for dephasing and echo formation are not the same if different orders of coherence are involved, a fact which can be exploited for selective observation of multiple-quantum coherence of a specified order. This technique is referred to as the *coherence transfer echo filter* (CTEF).[12,13]

The general form of the CTEF pulse sequence with arbitrary propagators U

and V is given in SEQ-VII-3.

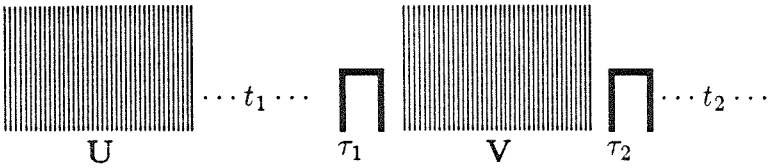

SEQ-VII-3

A signal expression will be derived to demonstrate the requirements on the field gradients. The results of this brief digression will be used to calculate the signal for the particular U and V which are employed in the two-dimensional exchange sequences of interest.

The density operator which results from SEQ-VII-3 is

$$\begin{aligned}\rho(t_U + t_1 + \tau_1 + t_V + \tau_2 + t_2) = &\exp(-i\mathcal{H}_0 t_2)\exp(-i\mathcal{H}_0'\tau_2)V\exp(-i\mathcal{H}_0'\tau_1)\\ &\exp(-i\mathcal{H}_0 t_1)U\rho(0)U^\dagger\exp(i\mathcal{H}_0 t_1)\\ &\exp(i\mathcal{H}_0'\tau_1)V^\dagger\exp(i\mathcal{H}_0'\tau_2)\exp(i\mathcal{H}_0 t_2)\end{aligned} \tag{13}$$

The complex transverse magnetization is computed from the usual trace relationship

$$S(t_U + t_1 + \tau_1 + t_V + \tau_2 + t_2) = \mathrm{Tr}\left[\rho(t_U + t_1 + \tau_1 t_V + \tau_2 + t_2)\mathrm{I}_+\right] \tag{14}$$

Since the trace is invariant to cyclic permutation of its operator product argument, the signal can be rewritten as

$$\begin{aligned}S(t_U + t_1 + \tau_1 + t_V + \tau_2 + t_2) = \mathrm{Tr}\big[&\exp(-i\mathcal{H}_0 t_1)U\rho(0)U^\dagger\exp(i\mathcal{H}_0 t_1)\\ &\mathrm{I}_+(-t_2 - \tau_2 - t_V - \tau_1)\big]\end{aligned} \tag{15}$$

where

$$\begin{aligned}\mathrm{I}_+(-t_2 - \tau_2 - t_V - \tau_1) = &\exp(i\mathcal{H}_0'\tau_1)V^\dagger\exp(i\mathcal{H}_0'\tau_2)\\ &\exp(i\mathcal{H}_0 t_2)\mathrm{I}_+\exp(-i\mathcal{H}_0 t_2)\\ &\exp(-i\mathcal{H}_0'\tau_2)V\exp(-i\mathcal{H}_0'\tau_1)\end{aligned} \tag{16}$$

and

$$\mathcal{H}_0' = \mathcal{H}_0 + \delta(\vec{r})\mathrm{I}_z \tag{17}$$

It is now useful to expand the trace of the signal in the eigenbasis.

$$S(t_U + t_1 + \tau_1 + t_V + \tau_2 + t_2) = \sum_{i,j} \langle i|\rho(t_1 + t_U)|j\rangle\langle j|\mathrm{I}_+(-t_2 - \tau_2 - t_V - \tau_1)|i\rangle \tag{18}$$

Using $[\mathcal{H}_0, \mathrm{I}_z] = 0$ and

$$\exp(i\theta\mathrm{I}_z)\mathrm{I}_+ \exp(-i\theta\mathrm{I}_z) = \mathrm{I}_+ \exp(i\theta), \tag{19}$$

the matrix element of the observable can be reduced to

$$\begin{aligned}
&\langle j|\mathrm{I}_+(-t_2 - \tau_2 - t_V - \tau_1)|i\rangle = \\
&\quad \exp(i\omega_{ij}\tau_1)\exp(i\delta(\vec{r})(n_{ij}\tau_1 + \tau_2)) \\
&\quad \langle i|V^\dagger \exp(i\mathcal{H}_0(t_2 + \tau_2))\mathrm{I}_+ \exp(-i\mathcal{H}_0(t_2 + \tau_2))V|j\rangle
\end{aligned} \tag{20}$$

The matrix element left unevaluated is the time-reversed observable operator which would result in the absence of field gradients. The factors containing the gradient dependence have been separated, revealing that if the following condition is met,

$$\frac{\tau_2}{\tau_1} = n_{ij}, \tag{21}$$

then the dephasing influence is completely removed. Otherwise, the signal would vanish upon integration over $\vec{r}$. Moreover, since only positive τ_1 and τ_2 are physically possible, only coherences with negative n_{ij} can be rephased. Consequently, the t_1 coherence of order n_{ij} is detected in quadrature through complex phase modulation of the echo signal. It can be verified by inspection that the dependence on the applied gradients vanishes even when the dephased and rephased coherences occur on different chemical species such as "b" and "f". Also note that if there is to be a non-vanishing cross-peak, the propagator V must include a stochastic

polarization transfer operator which exchanges populations between the "b" and "f" states.

§ VII-5.2. Diffusion in Magnetic Field Gradients

It has been shown that the effects of evolution in an inhomogeneous field are reversible so long as diffusion can be neglected. While zero-quantum coherence is not affected, the sensitivity to field inhomogeneity increases with the number of quanta in the transition because the higher frequencies associated with a greater number of spin flips permit phase differences among spin subpopulations to accumulate faster. This dephasing process has the appearance of a transverse relaxation process, but with a different time dependence. Specifically, the gradients during τ_1 and τ_2 diminish the amplitude of the coherence transfer echo signal by a factor[12]

$$\exp\left[-\tau_1/T_2^n - \tau_2/T_2 - n^2\gamma^2G^2D\tau_1^2/12 - \gamma^2G^2D\tau_2^2\right] \tag{22}$$

Notice also that a distinction has been made in Eq. (VII-22) between transverse relaxation of n-quantum coherence, T_2^n, and the transverse relaxation of single-quantum coherence, T_2. Likewise, the spin-lattice relaxation rate of the operators representing populations stored during the exchange period will depend on the particular operators representing the n-quantum coherence from which they originated.

The dual issues of multiple-quantum order sensitivity to diffusion in field gradients and the possibility for operator dependent relaxation mechanisms must be carefully considered in the design of two-dimensional exchange experiments, since optimal sensitivity is of the essence.

§ VII-6. Pulse Sequence Development

The convergence toward the optimal PASADENA two-dimensional "exchange" type pulse sequence for the kinetic study of the bound intermediate was an iterative process guided by the interplay of experimental data and theoretical considerations,

both numerical and analytical. Rather than to immediately state the end-result, a bit of the historical development will be chronicled, since the evolutionary process which led to the optimized sequence is itself of some didactic value.

§ VII-6.1. Zero-Quantum, Two-Dimensional Polarization Transfer

The originally proposed two-dimensional PASADENA sequence is shown in SEQ-VII-4.

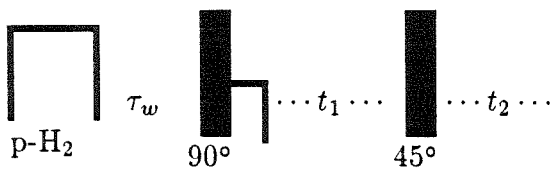

SEQ-VII-4

As in one-dimensional PASADENA experiments, the reaction is initiated by bubbling p-H_2 through the solution for 1 s. After a delay of 2 s, the initial density operator is represented by $I_{zA} \cdot I_{zB}$, where the subscripts A and B represent the methyl and methylene groups. However, since all of the essential spin physics is contained in the analysis for the two spin analog, we consider this reduced system to avoid clouding the relevant issues with algebraic tedium. Numerical simulations were used for much of the generalization to the A_2X_3 system of experimental interest.

Zero and double-quantum coherences are initiated by the first 90°_y rf pulse. Neglecting constants,

$$I_{z1}I_{z2} \xrightarrow{90^\circ I_y} I_{x1}I_{x2} \tag{23}$$

A pulsed homospoil removes the double-quantum coherence, leaving the density operator represented by pure zero-quantum coherence.

$$I_{x1} \cdot I_{x2} \xrightarrow{\text{homospoil}} \frac{1}{2}(I_{x1}I_{x2} + I_{y1}I_{y2}) \tag{24}$$

The high-field, weak coupling Hamiltonians for the bound and free ethylbenzene are defined as

$$\mathcal{H}_0^b = \omega_{z1}^b \mathrm{I}_{z1} + \omega_{z2}^b \mathrm{I}_{z2} + J_{12}^b \mathrm{I}_{z1}\mathrm{I}_{z2}$$
$$\mathcal{H}_0^f = \omega_{z1}^f \mathrm{I}_{z1} + \omega_{z2}^f \mathrm{I}_{z2} + J_{12}^f \mathrm{I}_{z1}\mathrm{I}_{z2} \qquad (25)$$

The zero-quantum coherence evolves at the chemical shift difference

$$\rho(\tau) = (\mathrm{I}_{x1}\mathrm{I}_{x2} + \mathrm{I}_{y1}\mathrm{I}_{y2}) \cos \Delta^{b,f}\tau + (\mathrm{I}_{y1}\mathrm{I}_{x2} - \mathrm{I}_{x1}\mathrm{I}_{y2}) \sin \Delta^{b,f}\tau \qquad (26)$$

where $\Delta^{b,f} = \omega_{z1}^{b,f} - \omega_{z2}^{b,f}$, as usual. The zero-quantum spectrum can then be obtained using a 45° mixing pulse. The zero-quantum magnitude spectrum of PASADENA enhanced ethylbenzene is shown in Fig. (VII-5) along with a numerical density matrix simulation. The source of the (1,3,3,1) quartet structure for the five spin system is evident by summation of the subspectra resulting from the effects of all possible J-coupling local fields on the pairwise zero-quantum transitions.

SEQ-VII-4 can be converted to a polarization transfer type sequence by inserting a 90° pulse to store coherence as populations at the end of the evolution period,

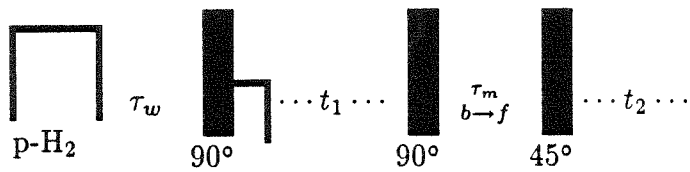

SEQ-VII-5

The experimental data for two different exchange times, 0.75 s and 3.0 s, are shown in Fig. (VII-6a) and Fig. (VII-6b), respectively. The intensity of the bound diagonal is seen to decrease considerably in going to the longer exchange time while the free diagonal remains nearly the same. The absence of any cross-peaks at either $\omega_1 = \omega_{zA}^b, \omega_2 = \omega_{zA}^f$ or $\omega_1 = \omega_{zB}^b, \omega_2 = \omega_{zB}^f$ implies that the source of this intensity loss is predominantly relaxation and not chemical transfer

Fig. (VII-5) Top: Numerically simulated PASADENA zero-quantum magnitude spectrum of ethylbenzene obtained using the sequence SEQ-VII-4. Bottom: Experimental realization of the zero-quantum magnitude spectrum. The lines were deliberately "folded over" to reduce the number of required t_1 points.

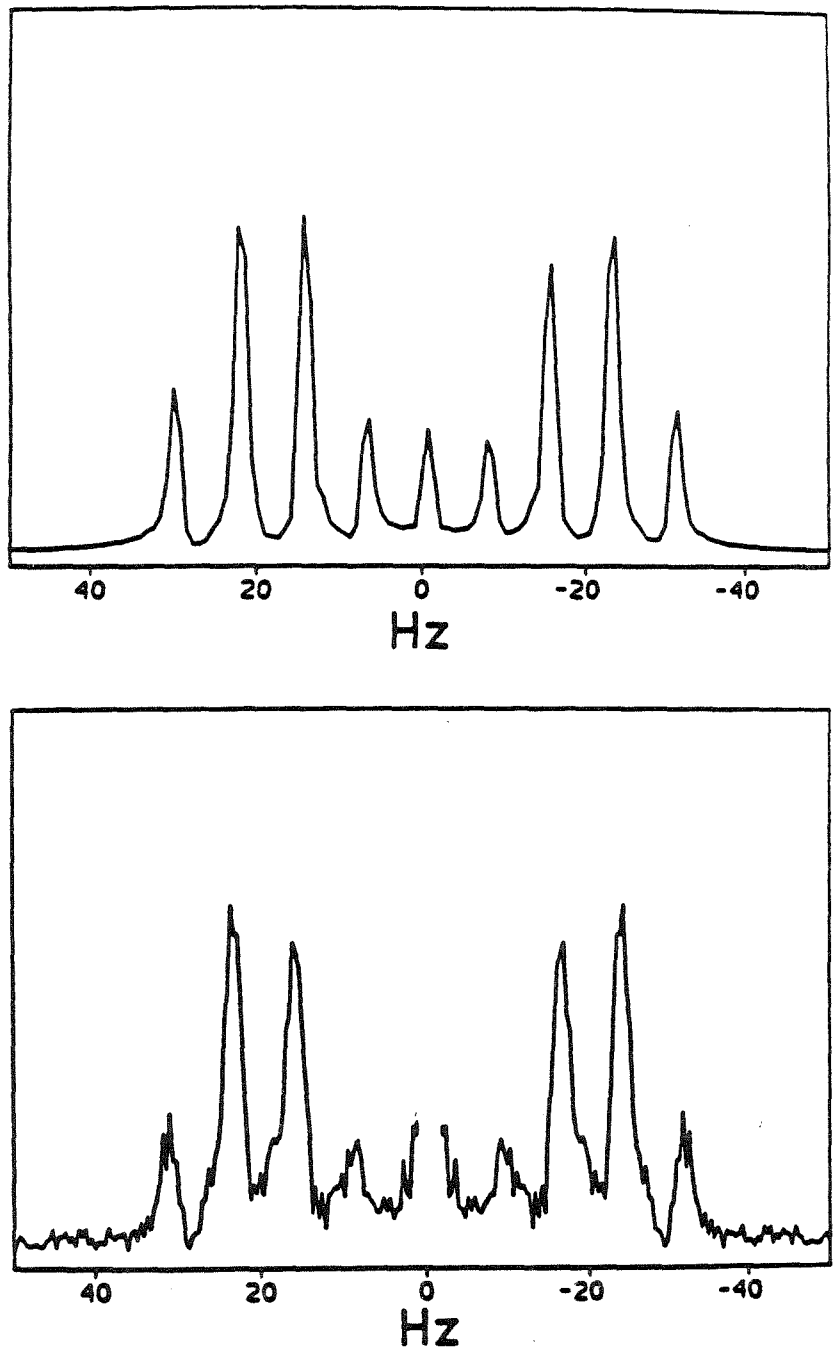

of polarization. The prominent ω_1 ridges are indicative of t_1 noise. The major source of these ridges is the enormous peak at $\omega_1 = 0$, which is caused by residual populations converted by the second and third pulses of the sequence into transverse magnetization. Apparently, the sensitivity of the experiment is diminished to such an extent that observation of the relatively low intensity cross-peaks is impossible.

§ VII.6.2. Double-Quantum Two-Dimensional Polarization Transfer

Elimination of the d.c. peak in ω_1 was the motivation for incorporation of a CTEF into the sequence. This required a secondary modification, however, since field gradients have no effect on zero-quantum coherence. Instead, double-quantum coherence was employed in both the preparation and evolution periods, as shown in SEQ-VII-6.

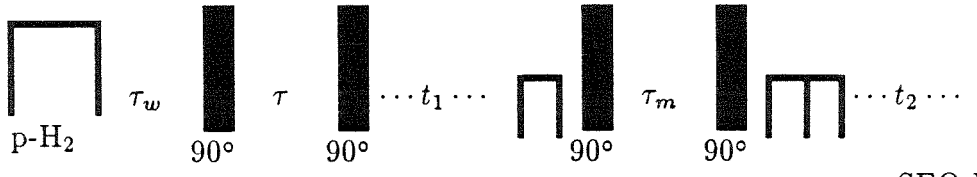

SEQ-VII-6

The spectra which were obtained with this sequence showed weak diagonal-peak intensities for $\tau_m = 2$ s. This may be rationalized on the basis of the increased sensitivity of double-quantum coherence to diffusion effects. A second possibility is that the population differences created from double-quantum coherence relax more rapidly than those formed from zero or single-quantum coherence. Either of these factors would account for the lack of signal, making double-quantum coherence unusable in the two-dimensional PASADENA experiments.

To investigate the importance of these potential loss mechanisms, the sequence SEQ-VII-7 was employed. Note that the initial condition here is equilibrium mag-

Fig. (VII-6) Two-dimensional PASADENA magnitude spectra resulting from the Rh(DIPHOS)$^+$ catalyzed hydrogenation of styrene in d_6-acetone corresponding to the pulse sequence SEQ-VII-5, with τ_w = 2.5 s, a 1 s p-H_2 burst, and two different values of τ_m. In part b., τ_m = 3.0 s. The faster decay of the bound alkane polarization compared to the free alkane is evident by the nearly complete disappearance of the former when τ_m changes from 0.75 to 3.0 s.
(VII-6a) τ_m = 0.75 s.

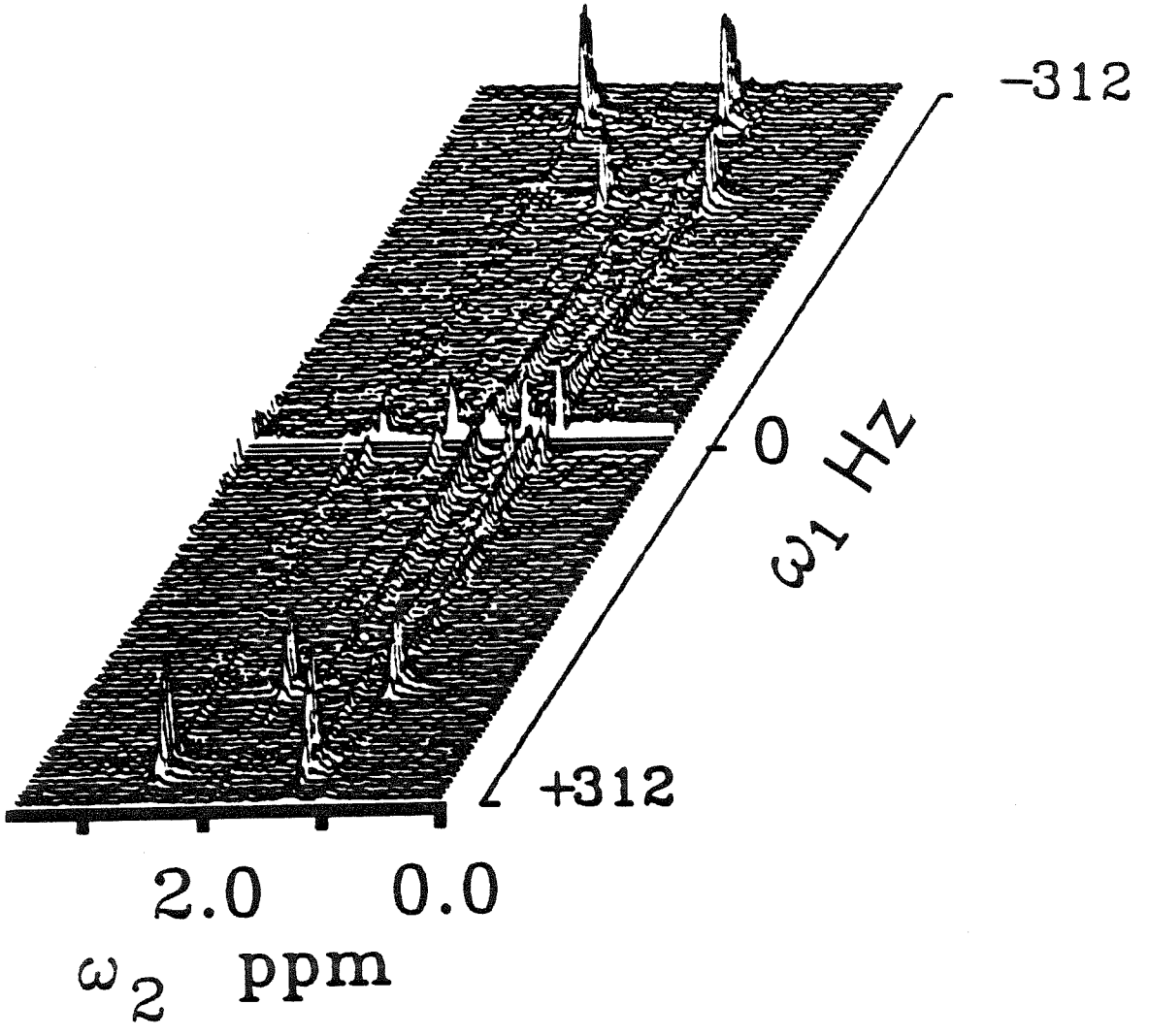

Fig. (VII-6b) $\tau_m = 3.0$ s

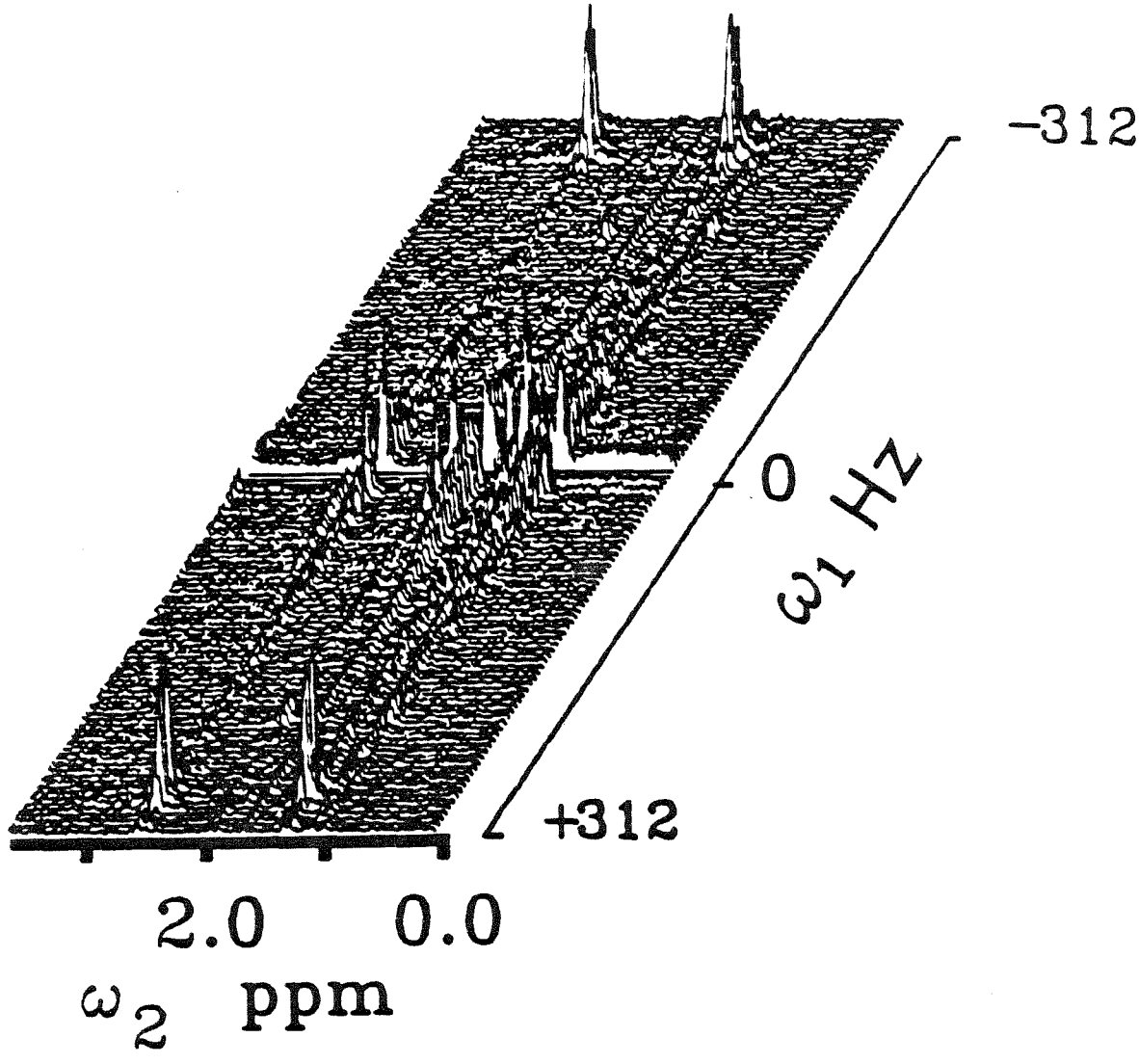

netization.

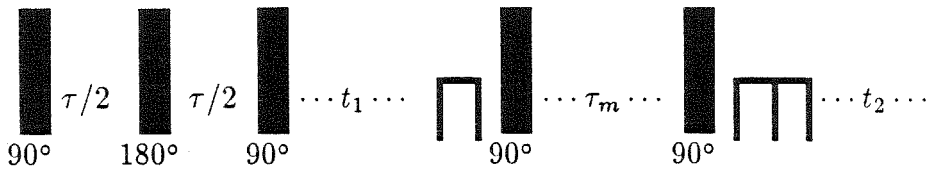

SEQ-VII-7

The 180° pulse was inserted into the preparation period to remove the chemical shift evolution and receiver frequency offset of the double-quantum coherence. The mixing period τ_m was varied from 0.1 s to 2.0 s. The resulting double-quantum peaks are shown in Fig. (VII-7a–f). The lower peak in these stacked plots is due to leakage of single-quantum coherence through the CTEF. The decay of the two-dimensional integrated magnitude was fit to an exponential form as shown in Fig. (VII-8), with a decay constant of 0.52 s. When the point at $\tau_m = 2$ s was repeated but with the homospoil turned off, the stacked spectrum of Fig. (VII-7g) results. Strikingly, the single-quantum peak jumps up in intensity while the double-quantum peak remains at the same low level. From this data, it may be firmly concluded that the source of double-quantum intensity loss is not due to diffusion at all, but rather from relaxation of the particular type of population differences which were stored from double-quantum coherence. When the analogous experiment to the one just described is repeated for single-quantum coherence created from equilibrium Zeeman order, the decay constant obtained was very close to the value obtained for T_1 by the conventional $180° - \tau - 90° - t_2$ sequence.

§ VII-6.3. Single-Quantum Two-dimensional Polarization Transfer

The findings of §VII-6.2. led to the proposal of the sequence SEQ-VII-8 in which single-quantum coherence is used in both the evolution and detection periods. There are several experimental advantages to putting zero-quantum coherence in the preparation period; zero-quantum coherence is independent of receiver offset

Fig. (VII-7) Two dimensional double-quantum spectra of ethlybenzene in d_6-acetone obtained using SEQ-VII-7 for increasing values of τ_m: a. $\tau_m = 0.01$ s; b. $\tau_m = 0.1$ s; c. $\tau_m = 0.4$ s; d. $\tau_m = 0.8$ s; e. $\tau_m = 1.4$ s, f. $\tau_m = 2.0$ s. The double coherence was prepared from Curie-Law Zeeman order. The smaller multiplet in the foreground of each spectrum is due to leakage of single-quantum coherence through the coherence transfer echo filter. In part g, the homospoil was disabled and the experiment with $\tau_m = 2.0$ s was repeated. The small double-quantum peak was essentially unchanged from part f, but the single-quantum peak jumped up in intensity.

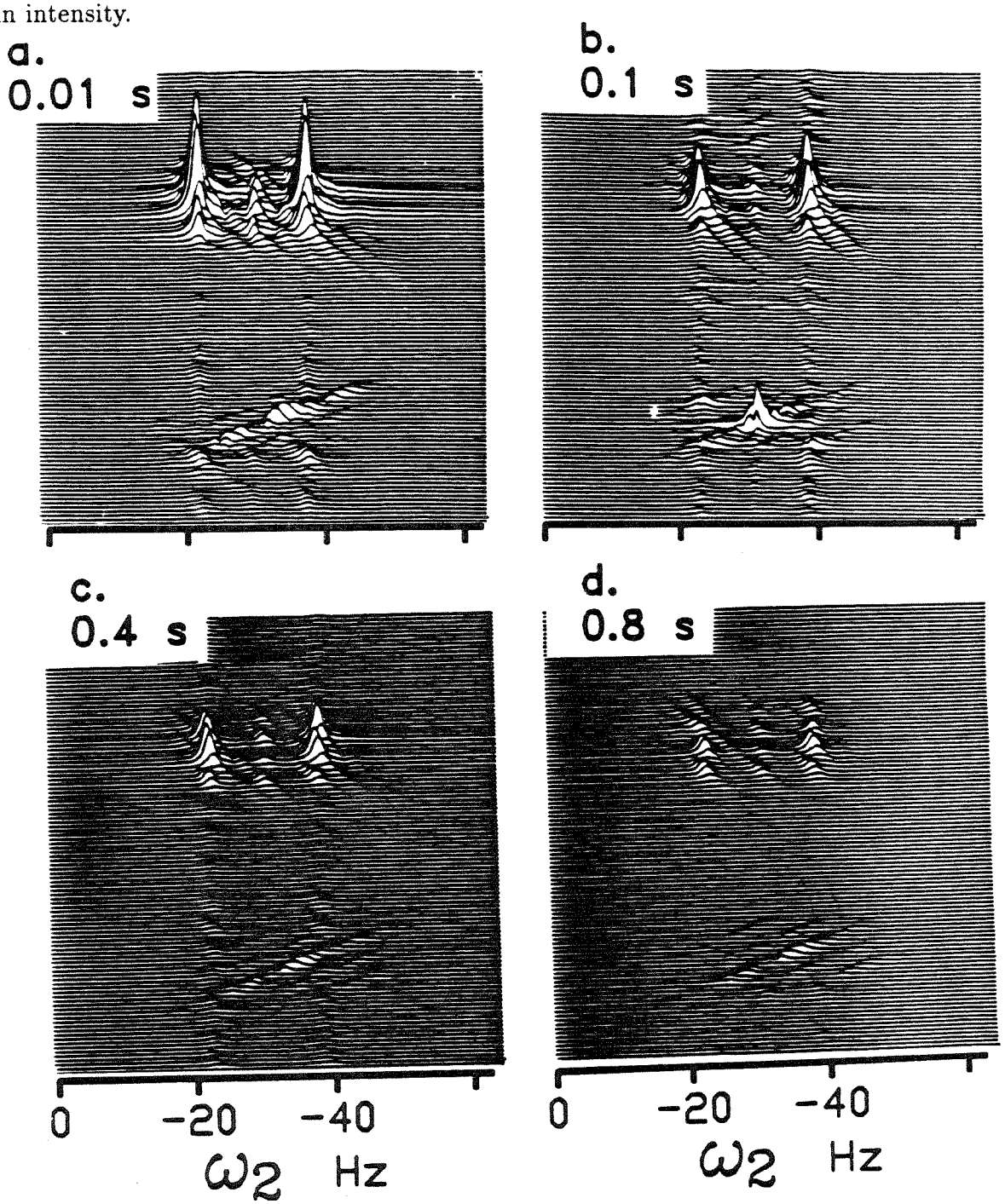

Fig. (VII-7) (continued)

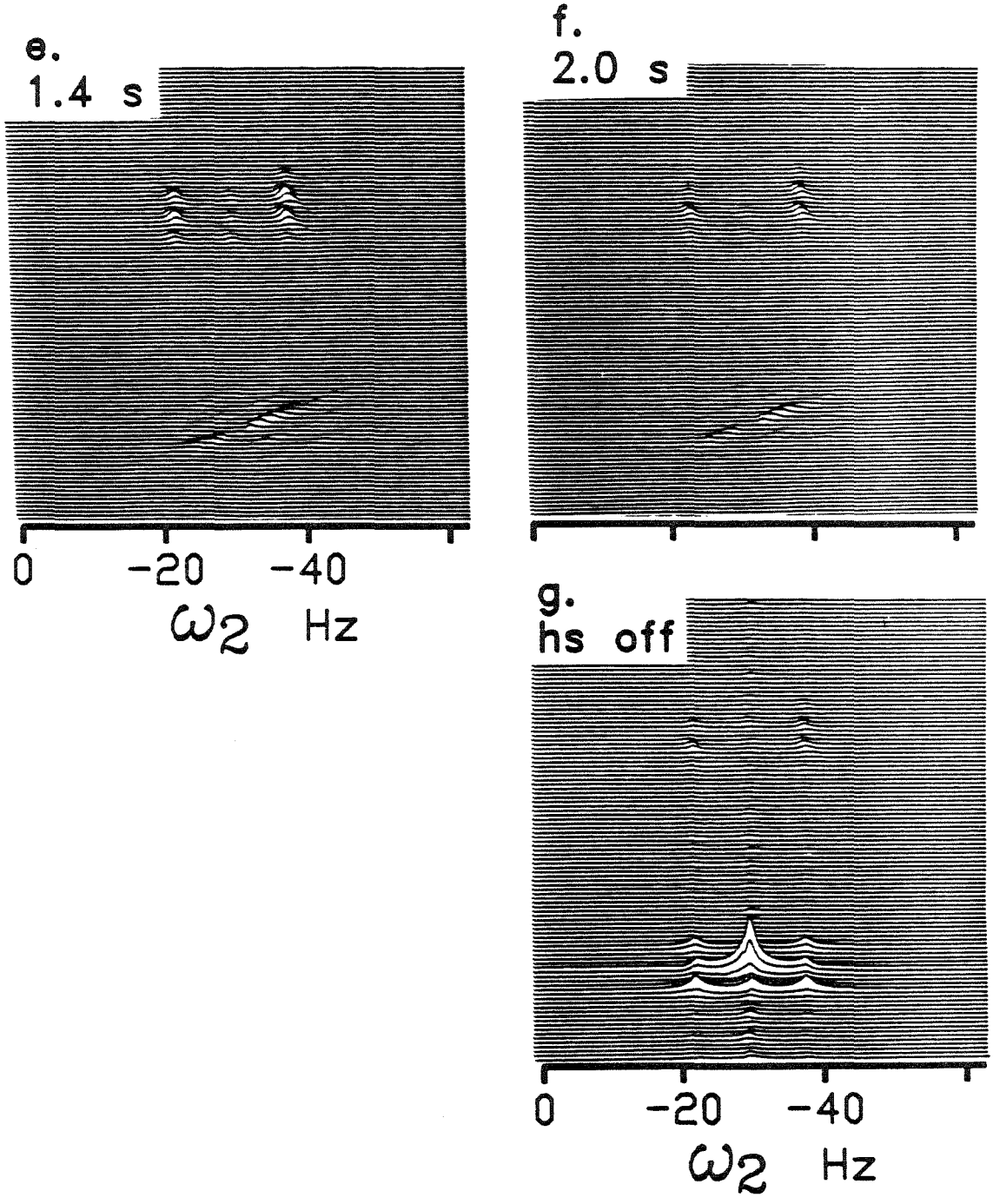

Fig. (VII-8) Plot of the double integral over ω_1 and ω_2 of the double-quantum multiplet magnitude as a function of the mixing time, τ_m (experimental data indicated by o. A decay constant of $T_1^{DQ} = 0.52$ s yields the single exponential fit represented by the solid line.

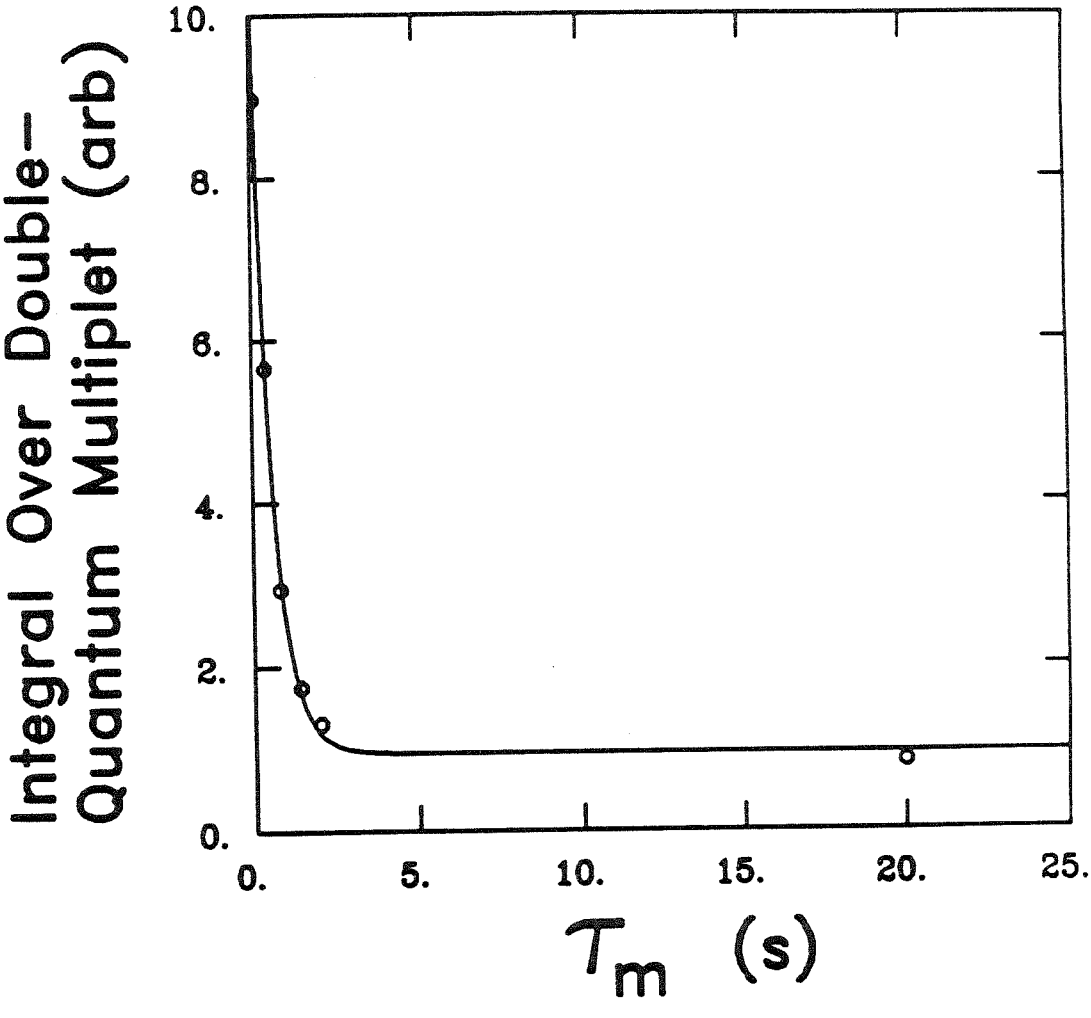

and can be selectively prepared by a single pulse followed by a homospoil.

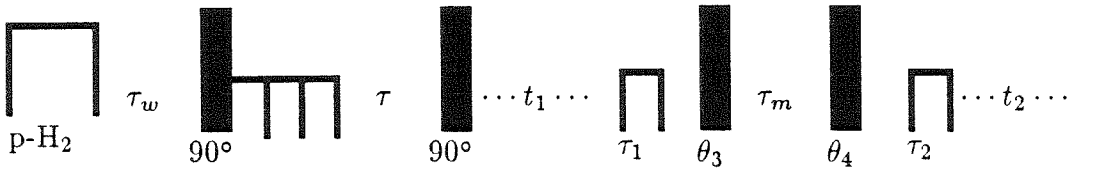

SEQ-VII-8

Conversion into single-quantum coherence is clearly optimized by a second 90°_y pulse. The evolution through t_1 needs to include only single-quantum operators, since the coherence transfer echo will filter away all other orders. Specifically, Eq. (VII-20) states that only $n = -1$ operators lead to any eventual signal, given $\tau_1 = \tau_2$. To obtain a density operator consisting of only this negative order coherence, the level shift operators $\mathrm{I}_x = \frac{1}{2}(\mathrm{I}_+ + \mathrm{I}_-)$ and $\mathrm{I}_y = \frac{1}{2}(\mathrm{I}_+ - \mathrm{I}_-)$ could be substituted into the density operator expression and all terms containing I_+ discarded. However, to reduce the number of terms which propagate, both positive and negative orders will be retained. This leads to a signal expression with terms containing a phase which depends on the gradient offset, $\delta(\vec{r})$. Such terms vanish when integrated over the sample volume, so there is no harm in propagating them through the sequence. The θ_y pulse which follows the evolution period leads to the following population terms in the density operator for the bound ethylbenzene:

$$\rho(\tau + t_1 + \tau_1) = \left[\sum_i \langle i|\rho(\tau)|i\rangle|i\rangle\langle i|\right] \xrightarrow{90^\circ \mathrm{I}_y,\ \mathcal{H}_0^b(t_1),\ \mathcal{H}_0^{b\prime}(\tau_1),\ \theta_3 \mathrm{I}_y}$$

$$= +\mathrm{I}_{z1}\frac{\sin\Delta^b}{2}\tau\sin\theta_3\sin\left[\frac{J^b}{2}(t_1+\tau_1)\right]$$

$$\left\{\sin\delta(\vec{r})\tau_1\sin[\omega_{z1}^b(t_1+\tau_1)] - \cos\delta(\vec{r})\tau_1\cos[\omega_{z1}^b(t_1+\tau_1)]\right\}$$

$$-\mathrm{I}_{z2}\frac{\sin\Delta^b}{2}\tau\sin\theta_3\sin\left[\frac{J^b}{2}(t_1+\tau_1)\right]$$

$$\left\{\sin\delta(\vec{r})\tau_1\sin[\omega_{z2}^b(t_1+\tau_1)] - \cos\delta(\vec{r})\tau_1\cos[\omega_{z2}^b(t_1+\tau_1)]\right\}$$

$$+\mathrm{I}_{z1}\mathrm{I}_{z2}\sin\Delta^b\tau\sin\theta_3\cos\theta_3\cos\left[\frac{J^b}{2}(t_1+\tau_1)\right]$$

$$\times \left\{ \sin\delta(\vec{r})\tau_1(\cos[\omega^b_{z2}(t_1+\tau_1)] - \cos[\omega^b_{z1}(t_1+\tau_1)]) \right.$$
$$\left. + \cos\delta(\vec{r})\tau_1(\sin[\omega^b_{z2}(t_1+\tau_1)] - \sin[\omega^b_{z1}(t_1+\tau_1)]) \right\} \tag{28}$$

Eq. (VII-28) has been written to emphasize that the population differences stored during the exchange time can be written as a linear superposition of Zeeman and J-order, the weight of each type being dependent on the pulse angle θ_3. The creation of J-order could be prevented by using $\theta_3 = 90°$, thereby maximizing Zeeman order. However, notice that the t_1 dependence of such populations contains the factor $\sin(J^b(t_1+\tau_1)/2)$. The A/E multiplet lineshape arises from the Fourier transformation of this factor.

Setting $\tau_1 = \tau_2$, the detected cross-peak signal is

$$\begin{aligned}
S_{b\to f}(\tau+t_1+2\tau_1+\tau_m+t_2) = \\
&\frac{1}{4}\sin\Delta^b\tau\cos\left[\frac{J^b}{2}(t_1+\tau_1)\right]\sin\left[\frac{J^f}{2}(t_2+\tau_1)\right]\sin\theta_3\cos\theta_3\sin\theta_4\cos\theta_4 \\
&\times\left\{\exp\left[-i((\omega^b_{z1}-\omega^f_{z1})\tau_1+\omega^b_{z1}t_1-\omega^f_{z1}t_2)\right]\right. \\
&\quad-\exp\left[i((\omega^f_{z1}-\omega^b_{z2})\tau_1+\omega^f_{z1}t_2-\omega^b_{z2}t_1)\right] \\
&\quad+\exp\left[-i((\omega^b_{z1}-\omega^f_{z2})\tau_1+\omega^b_{z1}t_1-\omega^f_{z2}t_2)\right] \\
&\quad\left.-\exp\left[-i((\omega^b_{z2}-\omega^f_{z2})\tau_1+\omega^b_{z2}t_1-\omega^f_{z2}t_2)\right]\right\} \\
&+\frac{1}{4}\sin\Delta^b\tau\sin\theta_3\sin\theta_4\sin\left[\frac{J^b}{2}(t_1+\tau_1)\right]\cos\left[\frac{J^f}{2}(t_2+\tau_1)\right] \\
&\times\left\{\exp[-i(\omega^b_{z2}t_1-\omega^f_{z2}t_2)]-\exp[-i(\omega^b_{z1}t_1-\omega^f_{z2}t_2)]\right\}
\end{aligned} \tag{29}$$

The bound diagonal signal can be derived from this expression by setting $\omega^f_{zi} \mapsto \omega^b_{zi}$ and $J^f \mapsto J^b$,

$$\begin{aligned}
S_{b\to b}(\tau+t_1+2\tau_1+\tau_m+t_2) = \\
&\frac{1}{4}\sin\Delta\tau\cos\left[\frac{J^b}{2}(t_1+\tau_1)\right]\sin\left[\frac{J^b}{2}(t_2+\tau_1)\right]\sin\theta_3\cos\theta_3\sin\theta_4\cos\theta_4
\end{aligned}$$

$$\times \Big\{ \exp\big[-i\omega^b_{z1}(t_1-t_2)\big] - \exp\big[i\big(\omega^b_{z1}t_2 - \omega^b_{z2}t_1 + (\omega^b_{z1}-\omega^b_{z2})\tau_1\big)\big]$$

$$+ \exp\big[-i\big(\omega^b_{z1}t_1 - \omega^b_{z2}t_2 + (\omega^b_{z1}-\omega^b_{z2})\tau_1\big)\big] - \exp[-i\omega^b_{z2}(t_1-t_2)]\Big\}$$

$$+\frac{1}{4}\sin\Delta\tau\sin\theta_3\sin\theta_4\sin\left[\frac{J^b}{2}(t_1+\tau_1)\right]\cos\left[\frac{J^b}{2}(t_2+\tau_1)\right]$$

$$\times\left\{\exp[-i\omega^b_{z2}(t_1-t_2)] - \exp[-i\omega^b_{z1}(t_1-t_2)]\right\} \qquad (30)$$

The orthogonal nature of the multiplet lineshapes represented by each term of the cross-peak expression has a special significance. Recall that for the one-dimensional PASADENA signals, if the magnitude of J is on the order of the transition linewidth, then some diminishment of the signal intensity is expected. In the limit of zero coupling, no PASADENA effect at all was expected. However, in two-dimensional polarization transfer PASADENA, it is possible to obtain an undiminished enhancement even if the coupling is zero on one of the species involved, as long as the coupling on the other species is resolved. For example, if $J_b = 0$ but $|J_f| > 1/T_2^f$, the choice $\theta_3 = \theta_4 = 45°$ would still permit the indirect observation of the enhanced transitions associated with the "b" species. Alternatively, enhancement of the uncoupled "f" species transitions could be facilitated by the choice $\theta_3 = \theta_4 = 90°$.

For the resolved couplings of bound and free ethylbenzene, $J^b_{AB} = J^f_{AB}$, so that PASADENA signals are observed regardless of the choice of θ_3 and θ_4. Yet there are additional reasons for careful specification of these flip angles. In practice, the resolution of two-dimensional PASADENA experiments is usually worse in the ω_1 dimension than it is in ω_2. The finite lifetime of the catalytic activity decreases over the course of the experiments, limiting the number of t_1 points to approximately 256 in the Rh(DIPHOS)$^+$ system before the signal disappears into the noise. This is illustrated in Fig. (VII-9), which is a plot of the PASADENA magnitude integrated over the bound (intermediate) ethylbenzene triplet in ω_2 versus the point in t_1. This data was obtained using the pulse sequence SEQ-VII-8 with $\theta_3 = \theta_4 = 90°$ and $\tau = 409$ ms. As expected from Eq. (VII-30), the signal obtained for this particular

choice of pulse angles is seen to "grow in" from zero at $t_1 = 0$. The loss of catalytic activity has the appearance of a transverse relaxation factor in t_1. Consequently, the resolution was limited to 3.5 Hz in the ω_1 dimension. The linewidth in ω_2 was 2 Hz, limited only by the magnetic field homogeneity and not changes in the catalytic activity.

The complete two-dimensional frequency spectrum of the same data shown in Fig. (VII-9) is shown in Fig. (VII-10). The efforts which have been extended in the direction of pulse sequence design have been rewarded (compare Fig. (VII-10) and Fig. (VII-6)). The peak at $\omega_1 = 0$ has been almost completely suppressed, dramatically reducing the t_1 noise and permitting the unmistakable observation of the weak cross-peak representing the proposed bound→free pathway. The two-dimensional magnitude lineshape of the methyl triplet has been simulated using a five spin numerical density matrix calculation. This may be compared with the corresponding experimental lineshape in Fig. (VII-11). The cause of the slight "ripple" on the experimental data, which defies simulation, is unknown.

The S/N of the cross-peak is prohibitively small to permit its measurement for the sufficiently large range of τ_m necessary to obtain a theoretical fit using Eq. (VII-7). However, it is still possible to obtain an estimate of the rate based on this single measurement of the cross-peak/diagonal ratio. Since the bound diagonal intensity decays during τ_m as a single exponential with a rate $k_6 + R_b$, the value of this combined constant can be extracted from a plot of cross-peak versus τ_m. In addition, if $\theta_4 = 90°$ is selected, then the calculations reveal that only Zeeman order is present during τ_m, and hence it is valid to assume that $1/R_f$ is equivalent to the spin lattice relaxation time of Zeeman order as measured by the $180° - \tau - 90° - t_2$ sequence. Using these three pieces of information, it is possible to invert Eq. (VII-7) and solve for k_6. However, there is insufficient data at present to complete the analysis outlined above.

An upper limit on the rate is still obtainable by assuming that the decay

Fig. (VII-9) Experimental data representing the evolution of the single-quantum coherence, derived from PASADENA J-order, during t_1 (magnitude shown). The decay of the coherence is due primarily to the gradual loss of catalytic activity.

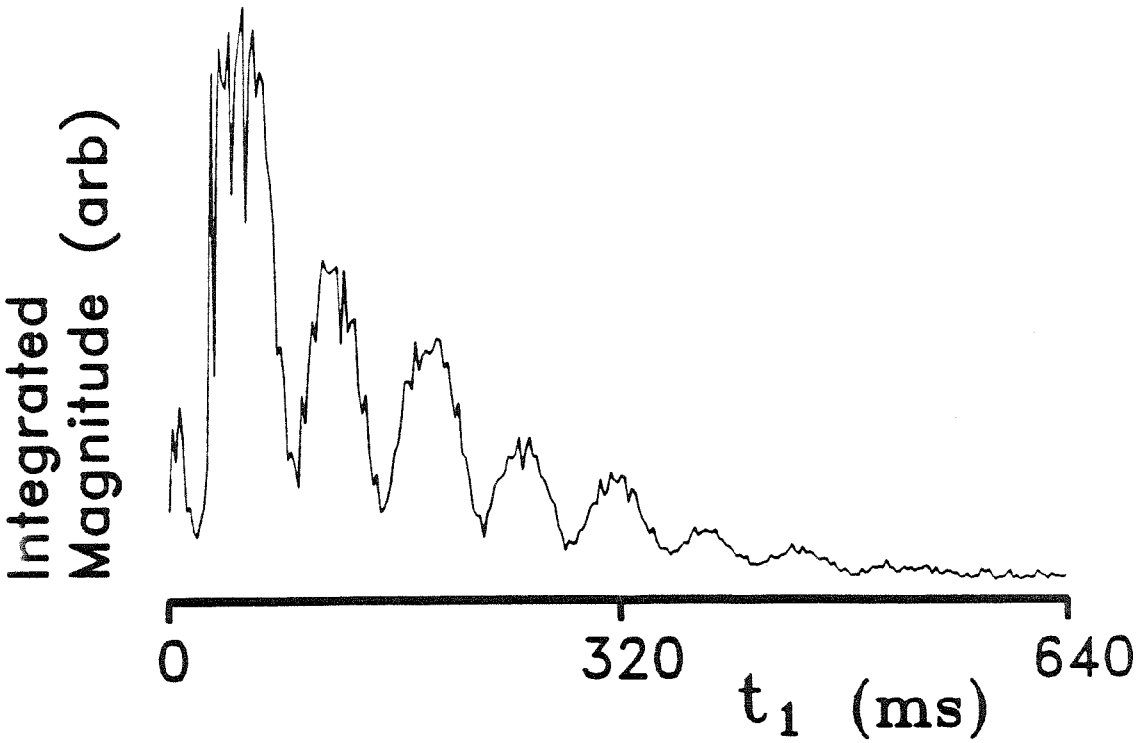

Fig. (VII-10) The 200 MHz two-dimensional magnitude spectrum resulting from the PASADENA chemical polarization transfer sequence SEQ-VII-8, with τ_w = 2.0 s, a 2 s H_2 burst and $\theta_3 = \theta_4 = 90°$. Single-quantum transitions occur in both frequency dimensions. A cross-peak (off-diagonal) due to the release of the bound alkane from the catalyst during τ_m is observed at $\omega_1 = 60$ Hz and $\omega_2 = -70$ Hz (circled). The (diagonal) multiplet at $\omega_1 = 60$ Hz and $\omega_2 = -130$ Hz arises from alkane which was bound prior to the first pulse of the sequence and remained bound through the t_2 acquisition. The (diagonal) peak at $\omega_2 = -70$ Hz and $\omega_1 = 70$ Hz represents alkane which was free before the first.

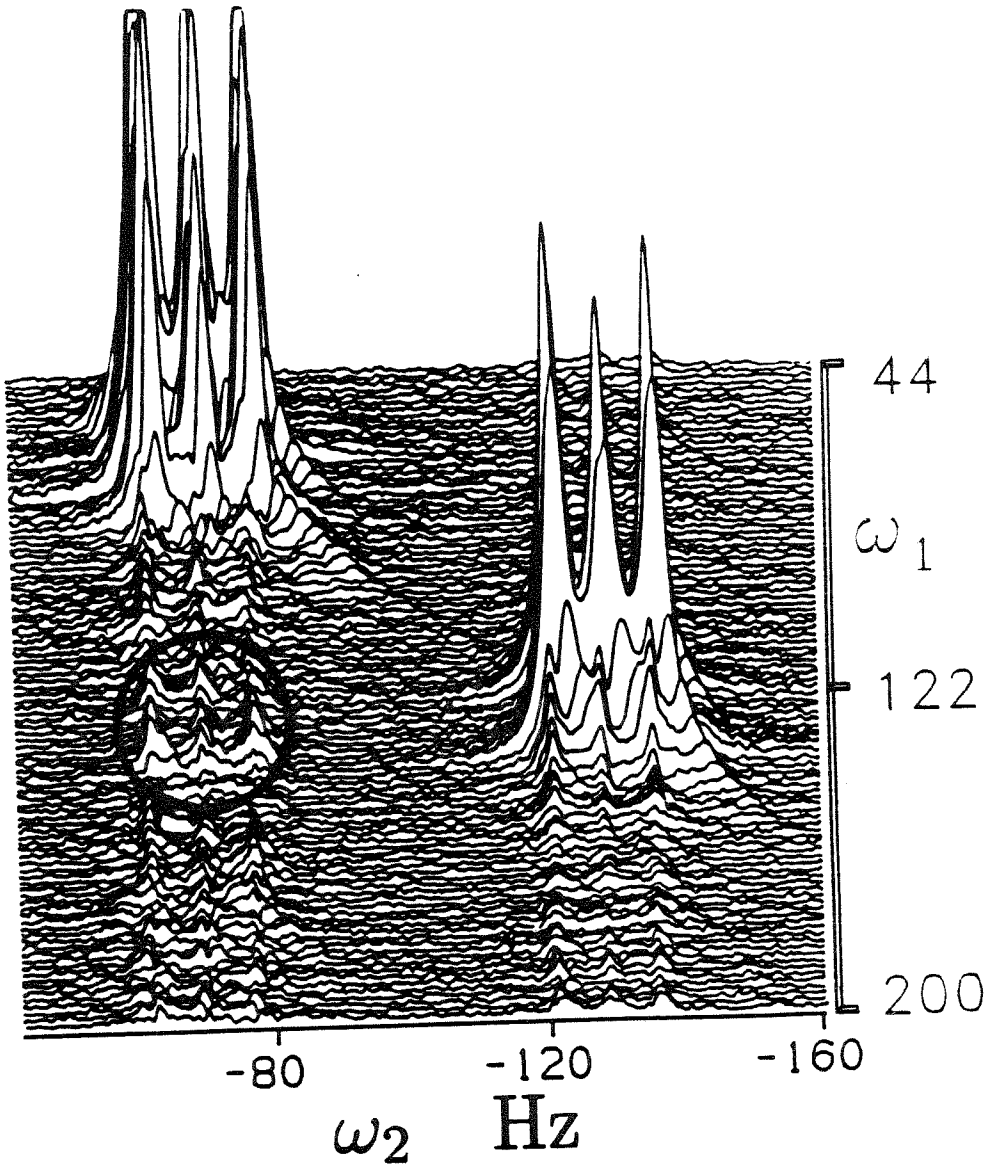

Fig. (VII-11) Top: Numerical density matrix simulation of the two dimensional PASADENA magnitude lineshape of the ethylbenzene triplet for the pulse sequence SEQ-VII-8 with $\theta_3 = \theta_4 = 90°$. The Hamiltonian was parameterized by $\omega_A = -126.0$ Hz, $\omega_B = 91.0$ Hz, $J_{AB} = 7.5$ Hz. Bottom: The corresponding experimental data, also shown in Fig. (VII-10), but re-scaled here to allow comparison with the theoretical lineshape.

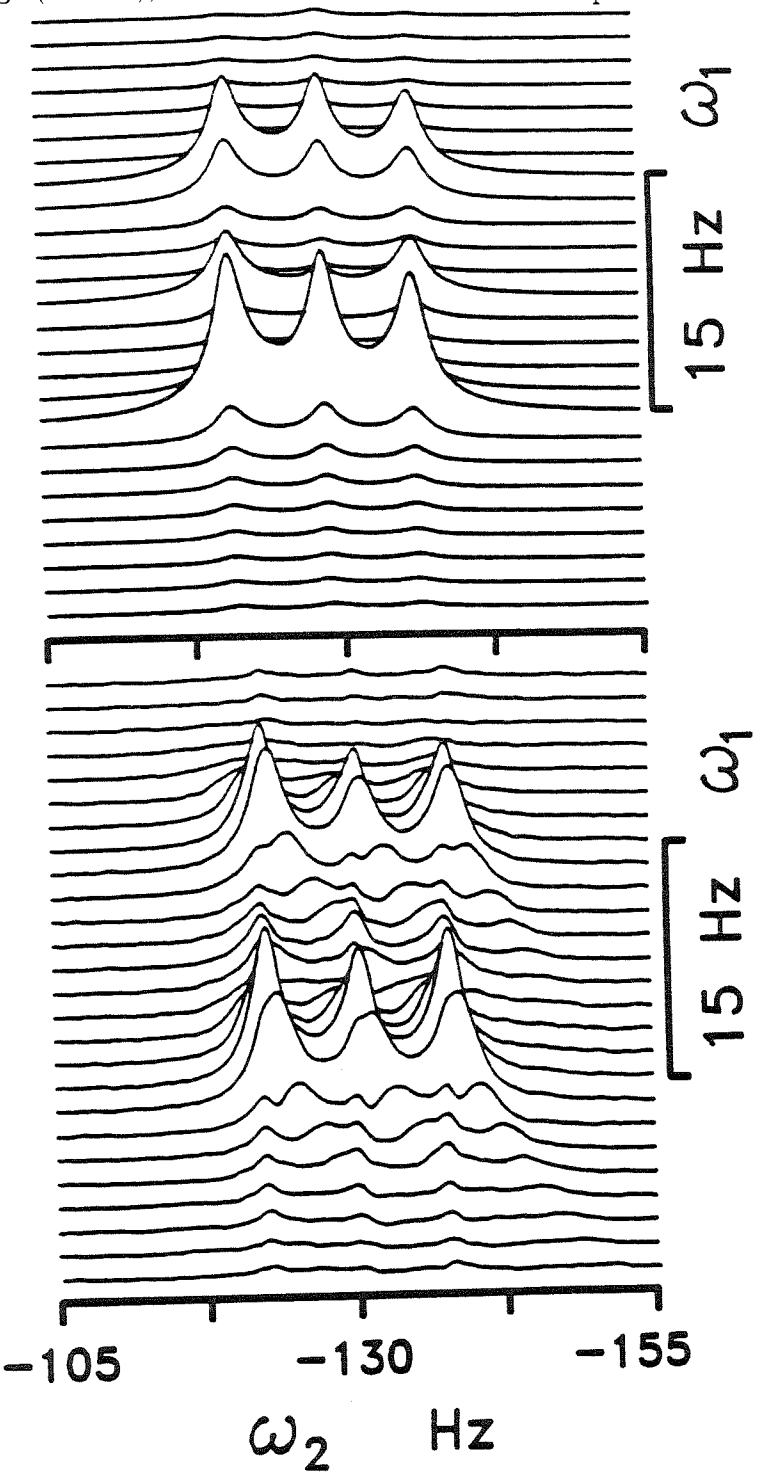

constant for populations during τ_m with $\theta_3 = \theta_4 = 90°$ may be approximated by a single exponential decay constant for the J-order, as was measured in §VII-3. Based on the T_1 and T_{1J} values measured in Chapter VI for ethylbenzene, the value of $k_6 + R_b$ extracted from the data of Fig. (VII-4) is predicted to be an overestimate. The value of the spin lattice relaxation time of Zeeman order, $T_1 = 5.0$ s, was measured by the $180° - \tau - 90° - t_2$ sequence. Inverting Eq. (VII-7),

$$k_6 = \frac{\frac{j_b(\tau)}{j_f(\tau)}(k_6 + R_b - R_f)}{e^{(k_6+R_b-R_f)\tau} - 1}$$

After substituting

$$\frac{j_b(\tau = 2.0)}{j_f(\tau = 2.0)} = 0.14$$

as measured from Fig. (VII-10), $R_f = 0.2$ s^{-1} and $k_6 + R_b = 0.52$ s^{-1} from the data of Fig. (VII-4), the upper limit $k_6 \leq 0.05$ s^{-1} results. If the spin lattice relaxation time on the bound species is actually longer, a lower rate would suffice to obtain the same cross-peak intensity.

The limited resolution obtainable in the ω_1 dimension raises a second issue involving the choice of θ_3 and θ_4 which will maximize the signal intensity by minimizing the destructive interference. The t_1 dependence of the $I_{z1}I_{z2}$ formed during τ_m is through the factor $\cos(J(t_1 + \tau_1)/2)$, which yields pure absorption or pure emission at each multiplet in the ω_1 domain, while the t_2 dependence of the signal originating from this product operator is through the factor $\sin(J(t_2 + \tau_1)/2)$. The corresponding time dependencies are in the reverse order for Zeeman order present during τ_m. In other words, the A/E lineshape will always occur to some extent in both frequency domains. If the linewidth is greater in the ω_1 dimension, then it may be of some advantage to maximize the weight of the signal arising from $I_{z1}I_{z2}$. This objective is achieved by prudent pulse angle specification, i.e., $\theta_3 = \theta_4 = 45°$. However, these gains may be overshadowed by the loss of signal due to the faster relaxation of J-order than Zeeman order on ethylbenzene, as was encountered in Chapter VI.

Indeed, the time at which the maximal cross-peak intensity occurs will be a function of the pulse angles used. Maximization of the cross-peak intensity (Eq. (VII-7)) leads to

$$t_{max} = \frac{\ln[R_f(k_6 + R_b)]}{k_6 + R_b - R_f} \tag{31}$$

For $\theta_3 = \theta_4 = 45°$, an estimate of $t_{max} = 2.5$ s can be obtained by using the exponential fit to the data presented in Fig. (VII-4) and the substitutions $k_6 + R_b \approx 0.52$ s and $R_f \approx 0.30$.

Fig. (VII-12) shows the spectrum which results when this choice of angles and τ_m are used in SEQ-VII-8. Projections on ω_1 of integrals over a range of ω_2 containing the free styrene quartet and triplet are shown in Fig. (VII-13a,b), respectively. The positions at which cross-peaks arising from chemical transfer of polarization would be expected are indicated by arrows.

A second type of cross-peak is clearly present in the projections shown in Fig. (VII-13a,b). Polarization is apparently exchanged between the enhanced methyl and methylene protons of ethylbenzene within molecules of the same species, while none is exchanged between different species. This may be attributed to a cross-relaxation by the Overhauser effect,[14] the observation of which is somewhat remarkable given the low molecular weight of ethylbenzene. The observability here is another indication of the high degree of spin order induced by parahydrogen addition.

§ VII-6.4. Suppression of Extraneous Diagonal Peaks

Extraneous diagonal peaks in the two-dimensional spectrum can lead to poor S/N for the peaks of interest when they share the same detected frequency. Obviously, this is only a problem when both the desired and undesired peaks arise from t_1 coherences involving the same number of quanta; otherwise, coherence transfer echo filtering (§VII-5.1) would be applicable.

One approach to this problem is to select the preparation time τ (see SEQ-

Fig. (VII-12) The 200 MHz two-dimensional magnitude spectrum resulting from the PASADENA chemical polarization transfer sequence SEQ-VII-8, with τ_w = 2.0 s, a 2 s H_2 burst and $\theta_3 = \theta_4 = 45°$. Single-quantum transitions occur in both frequency dimensions. The diagonal is indicated by the dashed line, upon which the two pairs of diagonal peaks appear. The cross-peaks due to dipolar cross-relaxation (Overhauser effect) are indicated by dashed boxes.

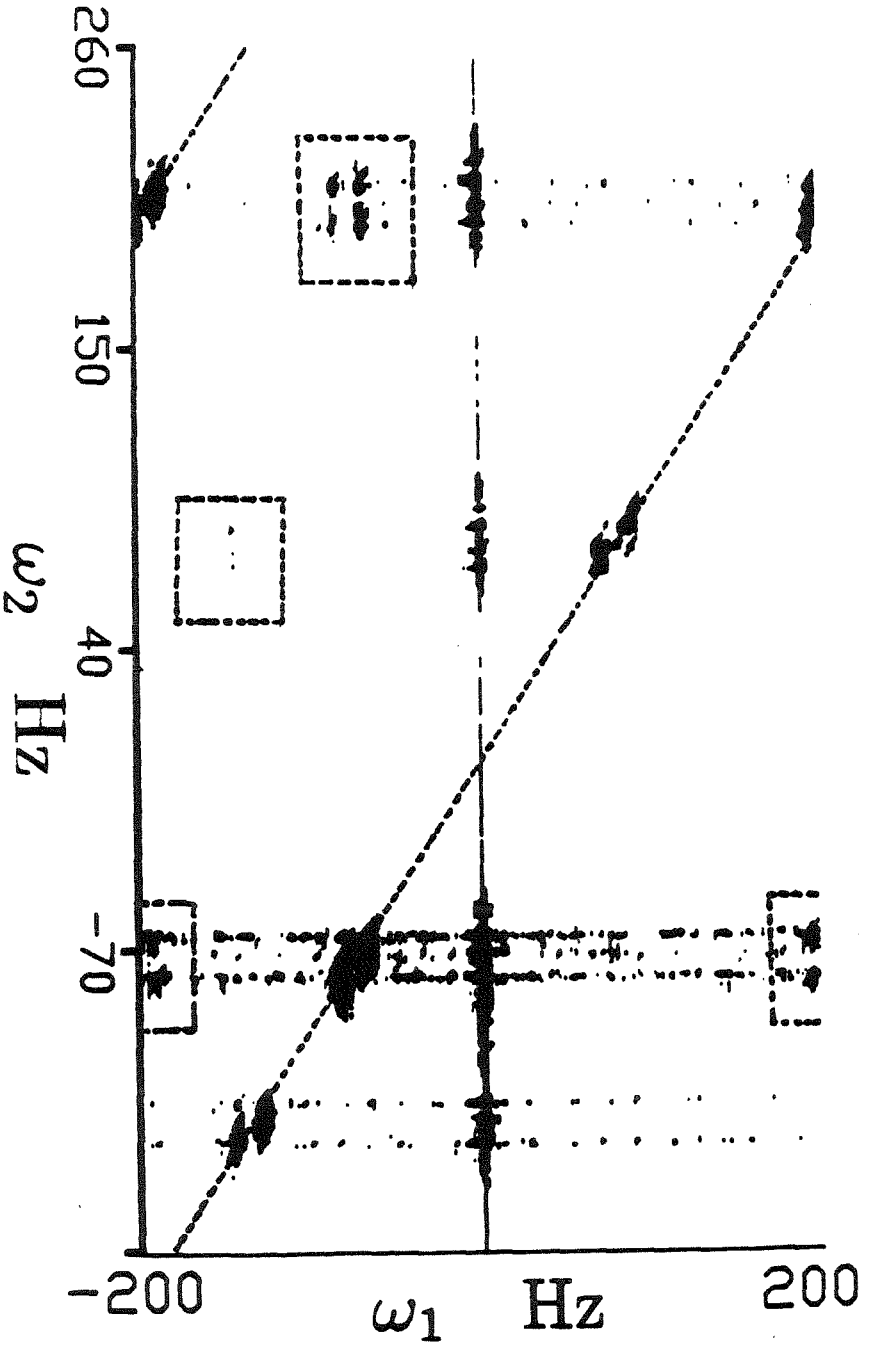

Fig. (VII-13a) Projection of the integrated quartet magnitude of free ethylbenzene onto ω_1. The peak at the Nyquist frequency in this spectrum occurs along the diagonal in Fig. (VII-12). The doublet centered near $\omega_1 = 80$ Hz is the result of dipolar cross-relaxation between the methyl and methylene spins. If there is a cross-peak due to chemical polarization transfer in this spectrum, it occurs below the level of the t_1 noise at the position indicated by the arrow.

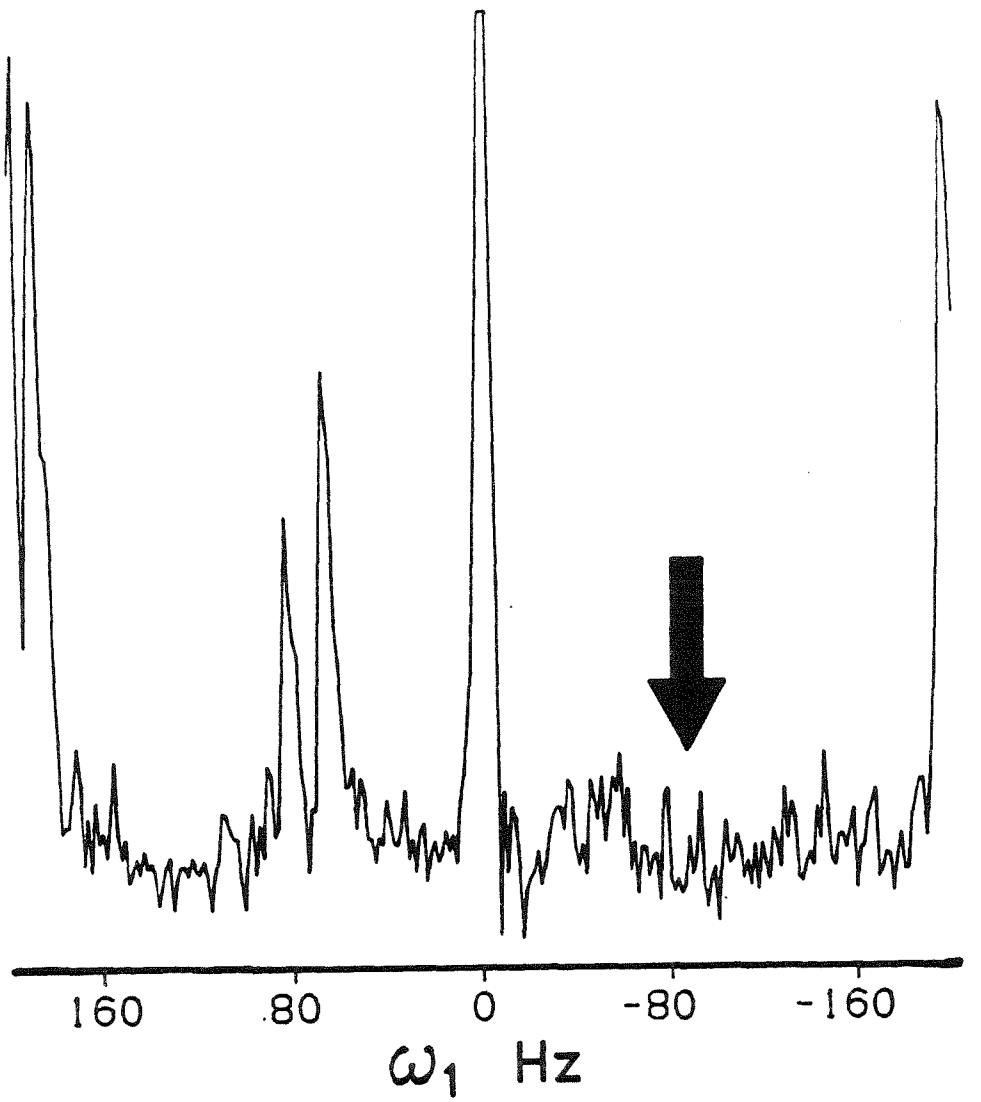

Fig. (VII-13b.) Projection of the integrated bound ethylbenzene triplet onto ω_1. The undesired peak at $\omega_1 = 0$ results from leakage of coherence through the coherence transfer echo filter.

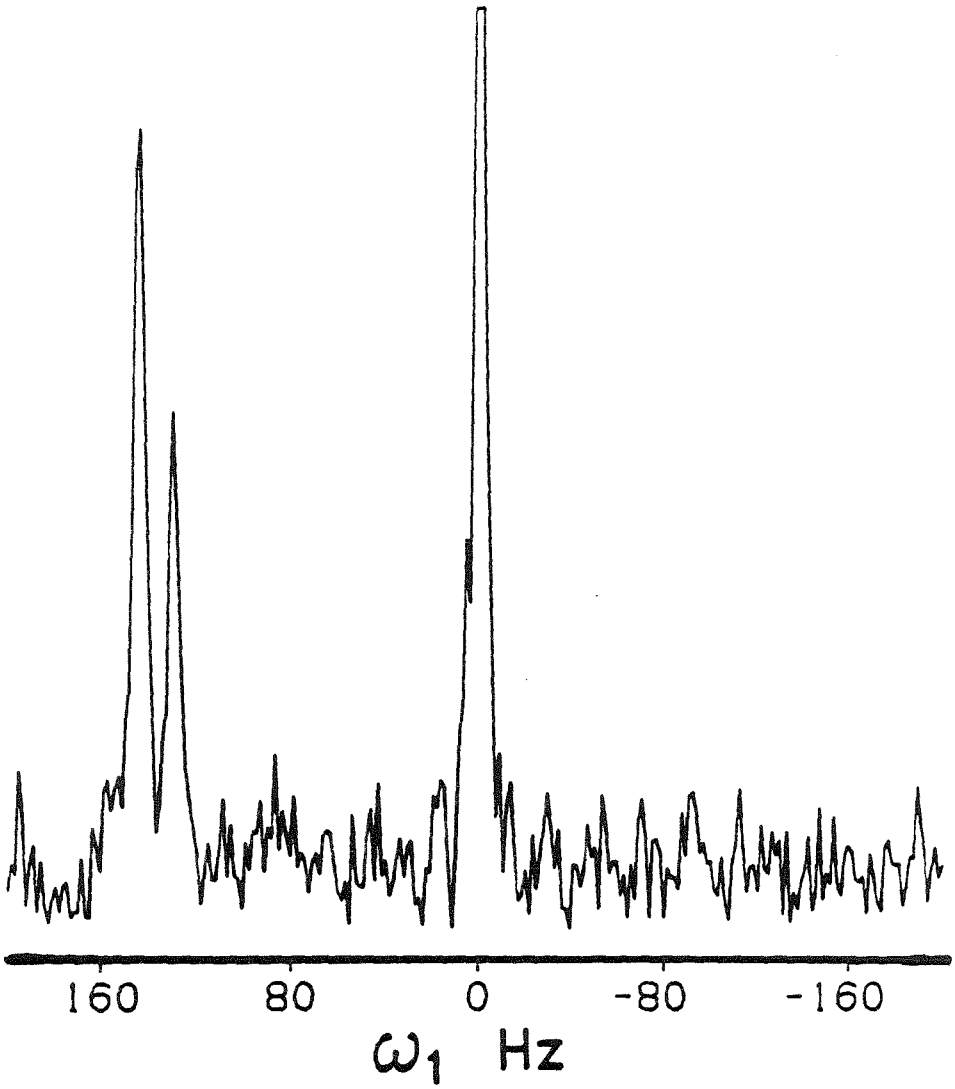

VII-8) such that the detected signal power averaged over the t_1 and t_2 domains is simultaneously maximized for the coherences of interest and minimized for those which should be suppressed. For the two spin-1/2 system, the analytical form of the signal is known and the τ dependence of the average power can be immediately calculated. While the analogies between the two and five spin dynamics has been very useful, at this juncture nothing less than the complete five spin calculation is necessary for proper selection of the preparation time.

The signal is first written in the usual eigenbasis expansion;

$$S(t_U + t_1 + t_V + t_2) = \sum_{ij} \rho_{ij}(t_U + t_1 + t_V) \mathrm{I}_+^{ji} \exp[-i\omega_{ij} t_2] \tag{32}$$

The summation is over the eigenstates of either the bound or free ethylbenzene spins, depending on whether the signal describes the diagonal or cross-peak. The signal power is proportional to the modulus squared of the signal,

$$\begin{aligned} |S(t_U + t_1 + t_V + t_2)|^2 = & \\ & \left(\sum_{ij} \rho_{ij} \mathrm{I}_+^{ji} \exp[-i\omega_{ij} t_2] \right) \left(\sum_{kl} \rho_{kl}^* (\mathrm{I}_+^{lk})^* \exp[i\omega_{kl} t_2] \right) \\ & = \sum_{ij} \sum_{kl} \rho_{ij} \rho_{kl}^* \mathrm{I}_+^{ij} \mathrm{I}_-^{lk} \exp[-i(\omega_{ij} - \omega_{kl}) t_2] \end{aligned} \tag{33}$$

The t_1 dependence of the density matrix elements will be used to make explicit the t_1 dependence on the signal power.

$$\begin{aligned} \rho_{ij}(t_U + t_1 + t_V) &= \langle i | V \exp(-i\mathcal{H}_0^b t_1) \rho(t_U) \exp(i\mathcal{H}_0^b t_1) V^\dagger | j \rangle \\ &= \langle i | V \left[\sum_{rs} \rho_{rs}(t_U) | r \rangle \langle s | \exp(-i\omega_{rs} t_1) \right] V^\dagger | j \rangle \end{aligned} \tag{34}$$

where the density operator has been expanded as

$$\rho(t_U) = \sum_{rs} \rho_{rs}(t_U) | r \rangle \langle s | \tag{35}$$

In the polarization transfer by chemical reaction sequence, the period t_V contains two rf pulses separated by a mixing time during which polarization is transferred and the pulsed homospoils which comprise the CTEF. The end result of V is the transfer of amplitude from the coherence $|r\rangle\langle s|$ to $|i\rangle\langle j|$, which occur on different chemical species in the case of the cross-peak. Hence,

$$V|r\rangle\langle s|V^\dagger = V_{rs,ij}|i\rangle\langle j| \tag{36}$$

Inserting into Eq. (VII-34),

$$\rho_{ij}(t_U + t_1 + t_V) = \sum_{rs} \rho_{rs}(t_U) V_{rs,ij} \exp[-i\omega_{rs} t_1] \tag{37}$$

Substituting ρ_{ij} into Eq. (VII-33),

$$|S(t_U + t_1 + t_V + t_2)|^2 = \sum_{ij}\sum_{kl} \mathrm{I}_+^{ji}\mathrm{I}_-^{lk} \exp[i(\omega_{kl} - \omega_{ij})t_2] \times \sum_{rs}\sum_{tu} \rho_{rs}\rho_{tu}^* V_{rs,ij} V_{tu,kl}^* \exp[i(\omega_{tu} - \omega_{rs})t_1] \tag{38}$$

The quantity which is to be maximized for the cross-peak and minimized for the free diagonal is the power time average over t_1 and t_2.

$$\begin{aligned} P_{ave}(t_U, t_V) &\propto \langle |S(t_U + t_1 + t_V + t_2)|^2 \rangle \\ &= \sum_{ij}\sum_{kl} \mathrm{I}_+^{ji}\mathrm{I}_-^{lk} h_{ij,kl} \sum_{rs}\sum_{tu} \rho_{rs}\rho_{tu}^* V_{rs,ij} V_{tu,kl}^* h_{rs,tu} \end{aligned} \tag{39}$$

where

$$\begin{aligned} h_{ij,kl} &= \frac{1}{T_{ij,kl}} \int_0^{T_{ij,kl}} \exp(2\pi i t_2) dt_2 \qquad T_{ij,kl} = \frac{2\pi}{(\omega_{ij} - \omega_{kl})} \\ h_{rs,tu} &= \frac{1}{T_{rs,tu}} \int_0^{T_{rs,tu}} \exp(2\pi i t_1) dt_1 \qquad T_{rs,tu} = \frac{2\pi}{(\omega_{rs} - \omega_{tu})} \end{aligned} \tag{40}$$

These expressions account for the possibility of interference only between different transitions which are degenerate. This treatment is valid only for the limit of infinitely narrow lines. For transitions with a realistic linewidth, interference between nearly degenerate transitions must be included. Thus

$$h_{ij,kl} = \begin{cases} 1, & \text{if } |\omega_{ij} - \omega_{kl}| < \text{linewidth;} \\ 0, & \text{otherwise} \end{cases} \tag{41}$$

This general form is suitable for numerical density matrix simulation of the average signal power dependence on the preparation time τ_m. The implementation of Eq. (VII-39) is an important next step for further improvement in the S/N of the cross-peaks.

§ VII-7. Summary and Conclusions

In this chapter, a general methodology was developed for the incorporation of p-H_2 enhancement of transitions into the framework of mechanistic studies of hydrogenation reactions by two-dimensional chemical dynamic NMR. The single greatest technical difficulty stemmed from t_1 noise, and much of the discourse has been focused on the reduction of it. The vital considerations in pulse sequence design were discussed, including relaxation, diffusion, coherence filtering, polarization transfer by chemical reaction, and optimal coherence preparation.

While optimal signal in ω_1 has proven mandatory for the observation of rates slow on the time-scale of longitudinal relaxation, less stringent requirements would be necessary if the rates were faster. In all NMR experiments, relaxation ultimately determines the slowest rates which can be measured. At least with enhanced polarization, this time-scale can be further extended for the same S/N.

Perhaps the most significant advantage of employing an enhancement scheme such as PASADENA to mechanistic investigations is the ability to observe chemical intermediates in solution which would not otherwise be observed. A prototypical example has been presented, with the observation of a cross-peak correlating a previously unobserved rhodium bound ethylbenzene complex with the final hydrogenated product. While it may be concluded that the slow rate associated with this pathway is indicative of its relative unimportance in the overall mechanism, there is excellent potential for the observation of key intermediates in other reactions. The critical complexes in catalytic mechanisms are usually those which rapidly react to form the next species in the pathway, preventing them from accumulating to large enough concentrations to be observed by conventional means. This is where

the highest potential lies for the PASADENA method and the techniques derived herein.

§ VII-8. References

1. J. Halpern, *Science* **217**, 401 (1982)
2. J. Halpern, A. S. C. Chan, D. P. Riley and J. J. Pluth, *Adv. in Chem. Ser.* **173**, 16 (1979)
3. J. Halpern, *J. Organomet. Chem.* **250** 485 (1983)
4. J. Halpern, A. S. C. Chan, D. P. Riley and J. J. Pluth, *J. Am. Chem. Soc.* **99**, 8055 (1977)
5. J. Halpern and A. S. C. Chan, *J. Am. Chem. Soc.* **102**, 838 (1980)
6. R. R. Schrock and J. A. Osborn, *J. Am. Chem. Soc.* **98**, 2134 (1976)
7. R. R. Schrock and J. A. Osborn, *J. Am. Chem. Soc.* **98**, 2143 (1976)
8. R. R. Schrock and J. A. Osborn, *J. Am. Chem. Soc.* **98**, 4450 (1976)
9. D. C. Roe, *J. Am. Chem. Soc.* **105**, 7770 (1983)
10. J. Jeener, B. H. Meier, P. Bachmann and R. R. Ernst, *J. Chem. Phys.* **71**, 4546 (1979)
11. B. H. Meier and R. R. Ernst, *J. Am. Chem. Soc.* **101**, 6441 (1979)
12. D. P. Weitekamp, *Adv. Mag. Reson.* **11**, 111 (1983)
13. A. A. Maudsley, A. Wokaun and R. R. Ernst, *Chem. Phys. Lett.* **55**, 9 (1978)
14. T. C. Eisenschmid, J. McDonald and R. Eisenberg, *J. Am. Chem. Soc* **111**, 7267 (1989)

Chapter VIII

Enhancement of Surface NMR by Para-Hydrogen Addition

§ Introduction

The possibility of extending p-H_2 NMR enhancement to the condensed phase will be explored in this chapter. Spectral calculations will be presented for an isolated magnetically inequivalent, dipolar-coupled two proton system, which will be referred to as the *oriented spin system.* The lineshape is powder averaged to investigate the degree of destructive interference that is anticipated to result from the overlap of antiphase components from different orientations. The dependence of the enhanced spectral energy on the ratio of dipolar coupling strength to chemical shift difference will be examined. The ordinary and PASADENA lineshapes will be compared in terms of their sensitivity to parameters in the anisotropic Hamiltonian. Finally, the theoretical enhancement factors for a model system will be presented for parameters which optimize the size of the effect.

§ VIII-1. Two Proton System

For the simulations, the spin Hamiltonian for the addition site will be taken as that of a magnetically isolated pair in high field with a definite orientation, as

might occur at a solid surface. The orientation of the internuclear vector relative to the magnetic field direction (z-axis) is described by the polar angle ϑ and azimuthal angle ϕ. The observed chemical shifts $\omega_{zi}(\vartheta, \phi, \Omega_i)$ depend also on the principal components of each shielding tensor and the set of Euler angles $\Omega_i = \{\alpha_i, \beta_i, \gamma_i\}$ relating its principal axis system to that of the dipolar coupling.[1,2]

The rotating-frame spin Hamiltonian including chemical shifts, dipolar and scalar couplings is

$$\mathcal{H}_{int} = \omega_{z1}\mathrm{I}_{z1} + \omega_{z2}\mathrm{I}_{z2} + D[\mathbf{I}_1 \cdot \mathbf{I}_2 - 3\mathrm{I}_{z1}\mathrm{I}_{z2}] + J\mathbf{I}_1 \cdot \mathbf{I}_2, \tag{1}$$

where $D = \frac{\omega_D}{2}(3\cos^2\vartheta - 1)$ and $\omega_D = \gamma^2\hbar/r^3$. The diagonalization of this Hamiltonian led to the transition frequencies and eigenstates in Eq. (III-2) and Eq. (III-15).

The initial density matrix describing the spins at the moment of addition to a surface site has previously been derived (see Eq. (III-27)). When the distribution of reaction times is wide compared to the period of the coherent evolution on the surface, it was determined that the off-diagonal elements of the density matrix are eliminated, leading to the density operator expression of Eq. (III-27). This will be a realistic model of the dynamics in most samples, in view of the decay of coherent oscillations associated with a powder distribution of proton dipolar couplings (ca. 10^{-4} s).

Substitution of this averaged operator and the Hamiltonian of Eq. (VIII-1) into the eigenbasis expansion of the trace (Eq. III-14) led to the PASADENA signal of Eq. (III-29), which is the starting point for the simulation of the numerical NMR lineshape simulations which follow. But first, explicit expressions for the orientational dependence of the chemical shifts, $\omega_{zi}(\vartheta, \phi, \Omega_i)$, must be found.

§ VIII-1.1 Tensorial Chemical Shift Interactions

For the oriented system, the spin interactions are tensorial in character.[1,2] The

full chemical shift Hamiltonian for the *ith* spin has the form

$$\mathcal{H}^i_{\rm CS} = \gamma^i_n \mathbf{I}_i \cdot \sigma^i \cdot \mathbf{H} \tag{2}$$

where $\mathbf{H}$ is the magnetic field vector and σ is the chemical shielding tensor. The behavior of tensorial interactions under rotations is most easily managed using spherical tensor operators. In irreducible spherical tensor notation, the chemical shielding Hamiltonian of a given nucleus has the form

$$\mathcal{H}^i_{\rm CS} = \gamma^i_n \sum_{l=0,2} \sum_{m=-l}^{+l} (-1)^m \sigma^i_{l,-m} \mathrm{T}^i_{lm} \tag{3}$$

where T^i_{lm} and $\sigma^i_{l,-m}$ are components of irreducible tensor operators and γ^i_n is the nuclear gyromagnetic ratio. The shielding tensor can be expressed in terms of its principal values (σ^i_{XX}, σ^i_{YY} , σ^i_{ZZ}) and elements of the Wigner rotation matrix $\mathcal{D}^l_{m'm}(\alpha, \beta, \gamma)$,

$$\sigma^i_{l,-m} = \sum_{m'} \mathcal{D}^l_{m',-m}(\alpha_i, \beta_i, \gamma_i) \quad \rho^i_{lm'} \tag{4}$$

where

$$\rho^i_{00} = \frac{1}{3} \mathrm{Tr}\, \sigma = \frac{1}{3}(\sigma^i_{XX} + \sigma^i_{YY} + \sigma^i_{ZZ}) = \sigma^i_0 \tag{5}$$

$$\rho^i_{20} = \sqrt{\frac{3}{2}}(\sigma^i_{ZZ} - \sigma^i_0) = \sqrt{\frac{3}{2}}\delta^i \tag{6}$$

$$\rho^i_{2\pm 2} = \frac{1}{2}(\sigma^i_{YY} - \sigma^i_{XX}) = \frac{1}{2}\eta^i \delta^i \tag{7}$$

Substituting Eq. (VIII-4) into Eq. (VIII-3),

$$\begin{aligned} \mathcal{H}^i_{\rm CS} &= \gamma^i_n \sum_{l=0,2} \sum_{m=-l}^{+l} (-1)^m \mathrm{T}^i_{lm} \sum_{m'} \mathcal{D}^l_{m',-m} \quad \rho^i_{lm'} \\ &= \gamma^i_n \mathrm{T}^i_{00} \rho^i_{00} \\ &+ \sum_{m=-2}^{+2} (-1)^m \mathrm{T}^i_{2m} \sum_{m'} \mathcal{D}^2_{m',-m} \quad \rho^i_{2m'} \end{aligned} \tag{8}$$

In high field, the spectrum is affected by only the secular terms ($l = \{0, 2\}, m = 0$);

$$\begin{aligned}\mathcal{H}^i_{\rm CS} &= \omega_{0i}\mathrm{I}_{zi}\left\{\sigma^i_0 + \sqrt{\frac{2}{3}}\delta^i\left[\sqrt{\frac{3}{2}}\mathcal{D}^2_{00} + \frac{\eta^i}{2}\left(\mathcal{D}^2_{20} + \mathcal{D}^2_{-20}\right)\right]\right\} \\ &= \omega_{0i}\mathrm{I}_{zi}\left[\sigma^i_0 + \sigma^i_{20}\right] \end{aligned} \tag{9}$$

where the following have been used:

$$\mathrm{T}^i_{00} = H_0\mathrm{I}_{zi} \qquad \mathrm{T}^i_{20} = \sqrt{\frac{2}{3}}H_0\mathrm{I}_{zi} \tag{10}$$

The Euler angles $\Omega_i = \{\alpha_i, \beta_i, \gamma_i\}$ relate the principal axis system of the ith shielding tensor (CAS) with the laboratory coordinate system (LAB), the z-axis for which is defined by the direction of the static magnetic field.

For the purpose of relating the spectra to molecular structure, yet a third frame, fixed in the molecule, is useful. The chemical shift tensor is extremely sensitive to the local molecular electronic structure surrounding the nucleus. In single crystals, the principal axis system of the chemical shift may be related to some lattice frame, which might be defined by the particular molecular frame. This known molecular frame can then be related to the laboratory frame in which the components of spin are observed.

In the analysis of polycrystalline solids, commonly referred to as "powders," it is necessary to account for all possible transition frequencies resulting from the distribution of orientations. This requires evaluation of the "powder average" integral. For protons, the dipolar coupling and chemical shielding tensors dominate the nuclear spin Hamiltonian. Their respective principal axis systems are not necessarily coincident, although their relative orientation is fixed for all random lab orientations. Because the eigenstates depend on the relative magnitude of the three interactions, care must be exercised to maintain the relative orientations of the dipolar and chemical shielding principal axis systems ("DAS" and "CAS," respectively) when computing the powder average. The spectrum correctly calculated in this way is not equivalent to the one obtained by averaging over each interaction individually.

To incorporate the intermediate molecular frame, σ^i_{20} is written in terms of its components in the DAS frame and the Wigner rotation matrix elements:

$$\begin{aligned}
&\sigma^i_{20}(LAB) \\
&\quad = \sum_{m'} \mathcal{D}^2_{m'0}(\Omega')\sigma^i_{2m'}(DAS) \\
&\quad = \sum_{m'} \mathcal{D}^2_{m'0}(\Omega') \sum_{m''} \mathcal{D}_{m''m'}(\Omega_i)\rho^i_{2m''} \\
&\quad = \sum_{m'} \mathcal{D}^2_{m'0}(\Omega')\delta^i \left[\sqrt{\frac{3}{2}}\mathcal{D}^2_{0m'}(\Omega_i) + \frac{1}{2}\eta^i \left[\mathcal{D}^2_{2m'}(\Omega_i) + \mathcal{D}^2_{-2m'}(\Omega_i)\right]\right] \qquad (11)
\end{aligned}$$

A simplification is afforded by using the formula

$$\mathcal{D}^2_{m'0}(\alpha,\beta,\gamma) = (-1)^{m'}(4\pi/5)^{1/2}Y_{2m'}(\beta,\gamma) \qquad (12)$$

which shows that this particular matrix element is independent of α. Conventionally, the orientation of the dipolar tensor is expressed as a function of the polar angles, ϑ and ϕ. The polar and Euler angles are related according to $\beta' = \vartheta$ and $\gamma' = \pi - \phi$. Substituting these relationships into Eq. (VIII-12),

$$\begin{aligned}
\mathcal{D}^2_{m'0}(\alpha,\vartheta,\pi-\phi) &= (-1)^{m'}(4\pi/5)^{1/2}Y_{2m'}(\vartheta,\pi-\phi) \\
&= (-1)^{m'}(4\pi/5)^{1/2} \begin{cases} (5/16\pi)^{1/2}(1-3\cos^2\vartheta, & m'=0; \\ \pm(15/8\pi)^{1/2}\cos\vartheta\sin\vartheta e^{\pm i(\pi-\phi)}, & m'=\pm1; \\ -(15/32\pi)^{1/2}\sin^2\vartheta e^{\pm 2i(\pi-\phi)}, & m'=\pm2. \end{cases} \\
&= (-1)^{m'}(4\pi/5)^{1/2}Y_{2,-m'}(\vartheta,\phi) \qquad (13)
\end{aligned}$$

Inserting this expression into Eq. (VIII-11), the line position of the *ith* nucleus for an arbitrary orientation of the DAS and CAS is

$$\begin{aligned}
\omega_{zi} &= \omega_0 - (8\pi/15)^{1/2}\delta^i \sum_{m'} Y_{2,-m'}(\vartheta,\phi) \\
&\quad \times \left[\left(\frac{3}{2}\right)^{1/2} \mathcal{D}^2_{0m'}(\Omega_i) + \frac{1}{2}\eta^i \left[\mathcal{D}^2_{2m'}(\Omega_i) + \mathcal{D}^2_{-2m'}(\Omega_i)\right]\right] \qquad (14)
\end{aligned}$$

Each proton will have its own set of Euler angles which rotate the chemical shift principal axis system into coincidence with the dipolar frame.

§ VIII-2. Powder Averaging

The PASADENA and Curie-Law signals have been derived for an arbitrary crystallite orientation which is specified by the angles ϑ and ϕ. Given a uniform orientation of the sites, as in a single crystal, the four transitions would be fully resolved, making destructive interference amongst the lines an impossibility. Hence, the PASADENA enhancement is potentially optimal for single crystal surfaces. Single crystal surface NMR, which is prohibitively insensitive by conventional ambient temperature NMR, is a potentially fruitful area of applicability of PASADENA techniques, but the emphasis here is on the more readily accessible polycrystalline case.

To simulate a powder spectrum, the signal must be integrated over all possible orientations. By taking advantage of the symmetry of $D(\vartheta)$ and $\sum_{m'} Y_{-2m'}(\vartheta,\phi)$ with respect to ϑ, the limits of the integral can be reduced to the angular range $\{\vartheta = 0 \rightarrow \pi/2\}$ and $\{\phi = 0 \rightarrow 2\pi\}$, i.e. the positive-z hemisphere.

Powder averaging may be performed in either the time or frequency domain. In the frequency domain, the form is

$$S(\Omega_1,\Omega_2,\omega) = \int_0^{2\pi}\int_0^{\frac{\pi}{2}} S(\Omega_1,\Omega_2,\vartheta,\phi,\omega)\sin\vartheta\; d\vartheta\; d\phi \qquad (15)$$

Substitution of the Fourier transform of Eq. (III-29) or Eq. (III-30) into Eq. (VIII-15) produces a rather unwieldy integral. Instead of attempting to find an analytical form, an efficient linear interpolation method will be employed for its evaluation.

§ VIII-2.1. Numerical Powder Average

At least three approaches are possible for evaluating the powder average integral. The brute force method is to evaluate and accumulate the signal at thousands

of orientations. This is not the method of choice. On the order of 64,000 evaluations are necessary for even coarse results. Another obvious approach is to apply numerical quadrature algorithms.† For functions with azimuthal symmetry which vary in one dimension only, direct numerical integration is slow, but yields satisfactory results. For two-dimensional integrals over the full range of ϑ and ϕ, this method is unacceptably slow.

A recent method involving linear interpolation achieves a many-fold increase in speed and accuracy over the above techniques.[4] The algorithm begins with the definition of an equilateral triangular grid, which is superimposed over the quadrant of a sphere, as shown in Fig. (VIII-1). The number of intersections of the grid along an edge of the triangle is an integer determined by the desired accuracy and speed of the spectral calculation. The intersections on the triangular grid can then be identified by three indices, $\{i, j, k\}$. This triple of indices is converted into a polar coordinate using the formulas

$$r = i^2 + j^2 + k^2; \qquad \vartheta = \arccos(k/r) \qquad \phi = \arccos\left(\frac{i}{r\sqrt{1 - k^2/r^2}}\right) \tag{16}$$

The lineshape function is now evaluated at every intersection on the grid and the values are stored in an array for rapid future access. If multiple transitions are to be averaged and co-added, it is most efficient to compute the frequencies and intensities for all transitions simultaneously, which requires the orientations specified by the grid intersections to be transformed into polar coordinates only once instead of once for each transition. For each triangle, a "tent" is constructed in frequency space as shown in Fig. (VIII-2). The area of the tent is normalized by taking the peak height as $2/(\omega_{\max} - \omega_{\min})$. Next, the area of the tent is made proportional to the average of the three intensities at the vertices of the tent. The intensities of the vertex orientations are themselves weighted by the solid angle correction factor, which insures that all orientations contribute equally. This factor

† Available in Numerical Recipes in C,[3] the NAG library, or the IMSL library).

Fig. (VIII-1) A triangular grid is constructed to define the orientations at which the transition frequencies and intensities are computed. For orientations other than those of the vertices, the lineshape factors are determined by linear interpolation. (adapted from Ref. 4)

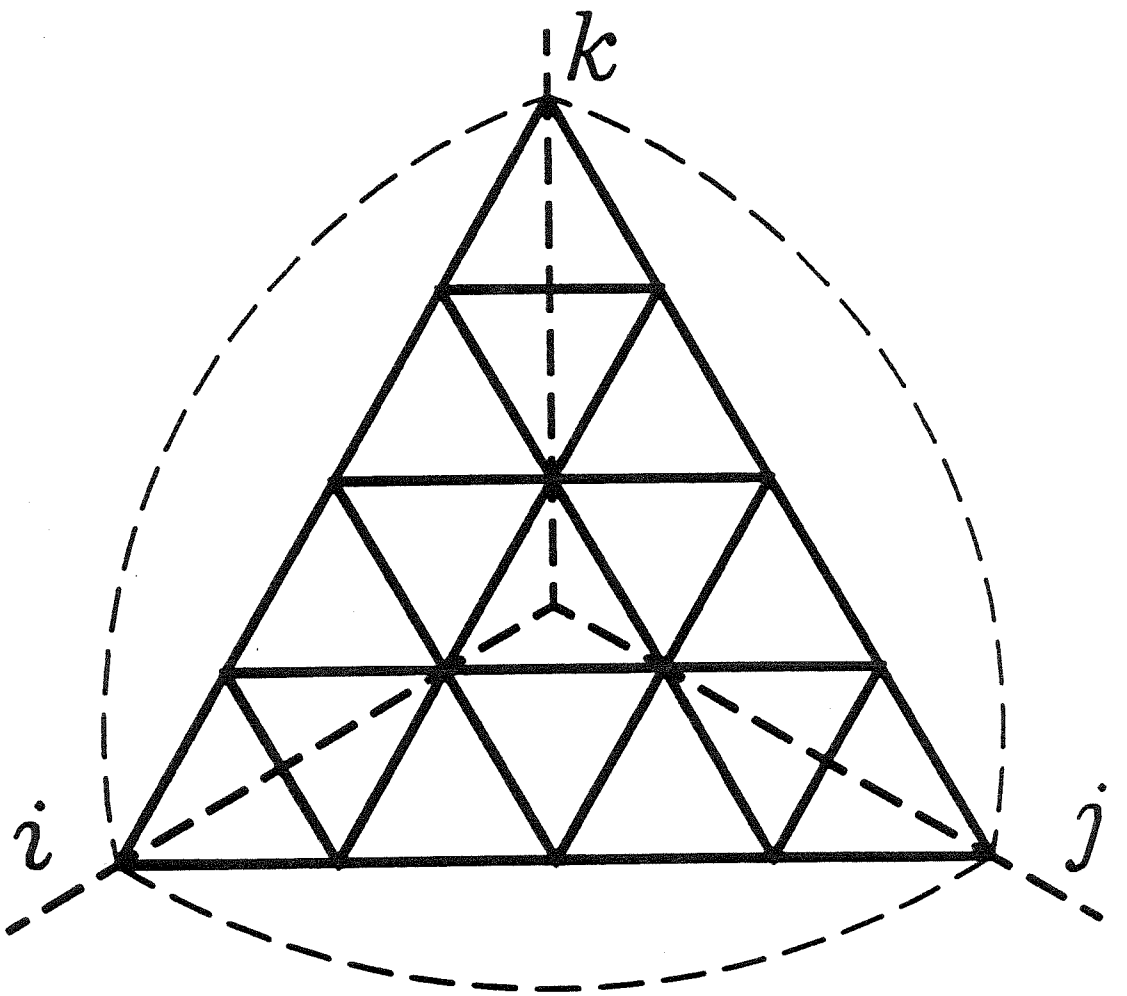

can be well approximated as

$$\text{solid angle correction} = 1/r^3 \tag{17}$$

In the final step, the tent for each transition is added to an array by linear interpolation of the intensities at the vertices. The contribution to each frequency interval represented by an element of the array is proportional to the height of the tent over that interval. The spectrum is gradually built-up by the accumulation of many tents in the array.

§ VIII-3. Simulations

In Fig. (VIII-3), the spectrum was simulated for two different orientations of the principal axis system for the first spin, $\alpha_1 = 0°$ and $\alpha_1 = 30°$, while the orientation for the second spin remained fixed. For comparison, the powder spectra derived from Zeeman order for the same spin system and parameters are shown. The phase and amplitude variations across the powder PASADENA spectrum leads to destructive interference of NMR intensity. The PASADENA spectra tend to be somewhat more sensitive to the relative orientation of the shielding tensors than are their conventional counterparts, since a purely absorptive lineshape cannot reflect changes due to cancellation effects.

Cancellation, or destructive interference, is a prominent feature of the solid PASADENA signals. The loss of intensity through this channel is also an important factor in the liquid state experiments as well, if the J-coupling is not resolved. In the oriented spin system, the problem is compounded because the dipolar coupling reverses its sign at the magic angle orientation of $\approx 54.7°$. At that juncture, the multiplet may switch from being mostly A/E (absorptive/emisive) to E/A in character, so that the potential exists for substantial destructive interference.

The degree of cancellation will depend on the spin Hamiltonian parameters in a complex way. One important factor is the size of the dipolar coupling compared to the isotropic chemical shift difference, $\Delta_0 = \omega_0(\sigma_0^1 - \sigma_0^2)$. To demonstrate this

Fig. (VIII-2) The frequency range of an intensity "tent" is defined by the minimum and maximum of the three transition frequencies computed at the orientations defined by the vertices of a triangle on the grid shown in Fig. (VIII-1). The position of the tent peak is determined by the intermediate frequency, and its area is made proportional to the average of the three intensities. The amplitude of the spectral contribution at each point within the tent is given by the amplitude of the tent at the frequency of the point. (adapted from Ref. 4)

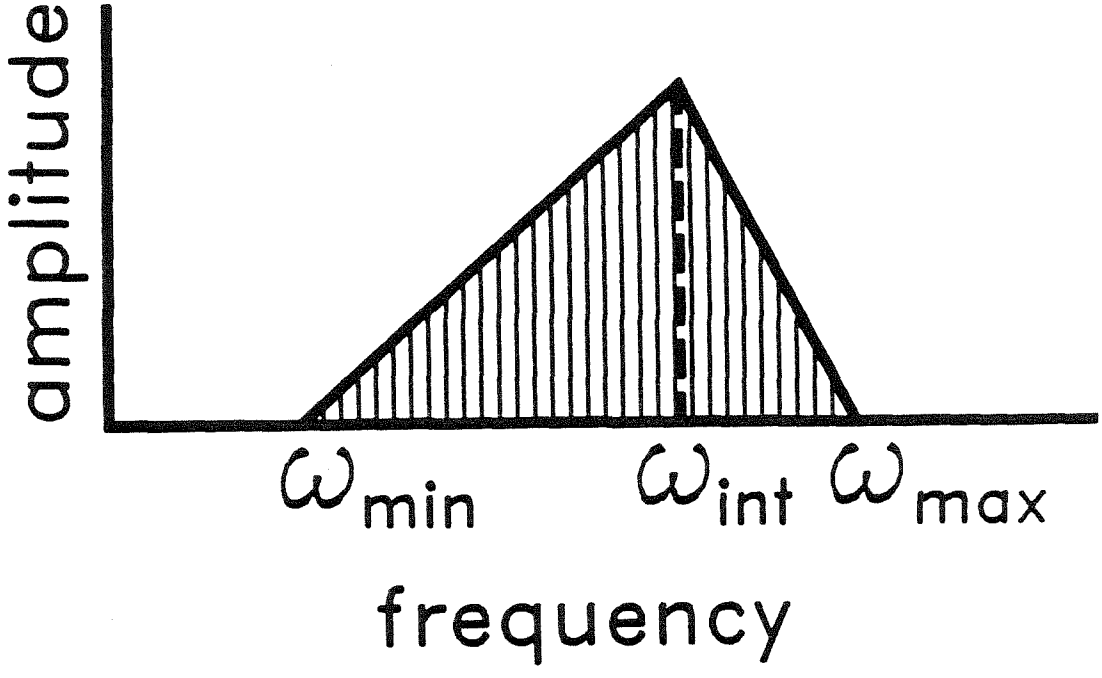

Fig. (VIII-3) Surface PASADENA powder lineshape simulations at two different orientations of the principal axis system of one of the protons of a two-spin system with an internal Hamiltonian parameterized by the following parameters (in Hz): $\nu_0\sigma^1_{XX} = -5000$, $\nu_0\sigma^1_{YY} = -3000$, $\nu_0\sigma^1_{ZZ} = -1000$, $\nu_0\sigma^2_{XX} = 1000$, $\nu_0\sigma^2_{YY} = 3000$, $\nu_0\sigma^2_{ZZ} = 5000$ and $\omega_D/2\pi = 2857$. The corresponding conventional spectra (pure absorption) are shown for comparison.

$$\rho(0) = \sum_i \langle i| \left(\frac{1}{4} - f\mathbf{I}_1 \cdot \mathbf{I}_2 \right) |i\rangle|i\rangle\langle i|$$

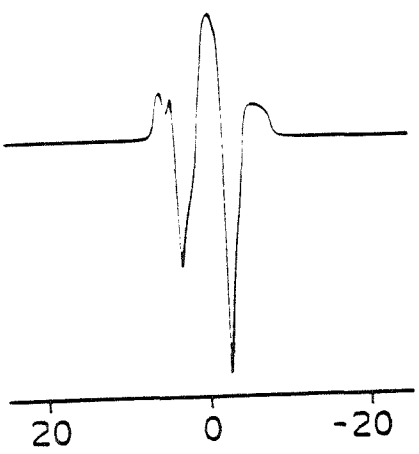

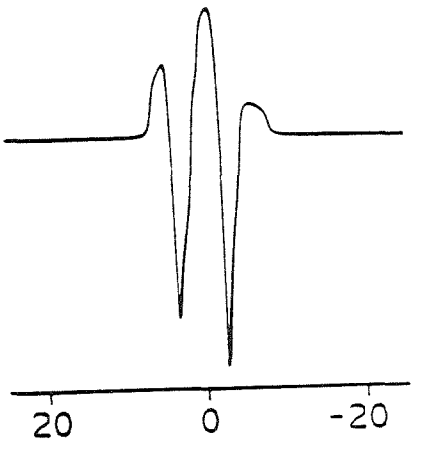

$\Omega_1 = \{10°, 0, 0\}$
$\Omega_2 = \{0, 0, 0\}$

$\Omega_1 = \{30°, 0, 0\}$
$\Omega_2 = \{0, 0, 0\}$

$$\rho(0) = bI_z$$

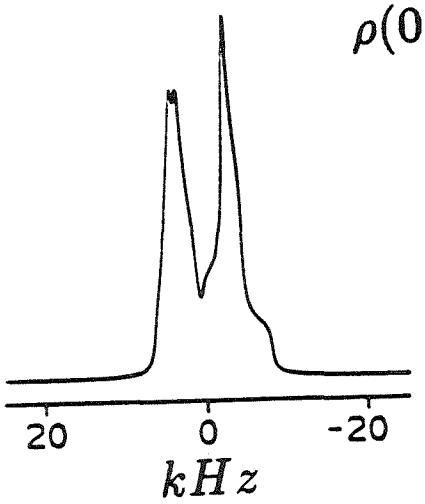

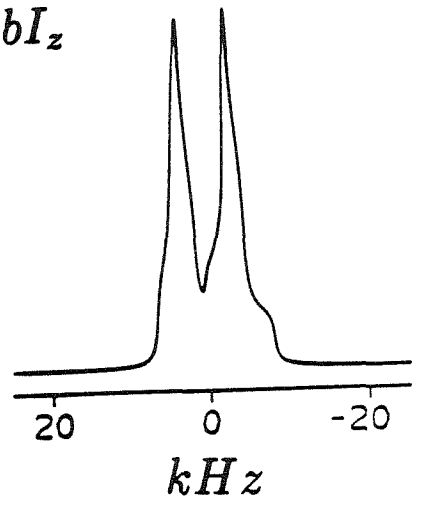

trend, Fig. (VIII-4) shows the integrated magnitude of the powder pattern plotted as a function of the dipolar coupling parameter ω_D. Without any coupling, there is zero enhancement. On the other extreme, the enhancement approaches zero as the spins become magnetically equivalent at very large couplings. Minimum cancellation occurs when $\omega_D \approx \Delta_0/2$.

Defining the enhancement for powder patterns as the ratio of the frequency domain amplitude maxima of the PASADENA and the Curie-Law spectra at 300 K and $H_0 = 4.7$ T, the maximum enhancement was found to be ≈ 6233. This is 20% of the ideal enhancement expected for weak, resolved coupling.† It is concluded that substantial gains in sensitivity are theoretically possible for oriented systems, despite losses due to destructive interference.

In practice, the spin system of interest will not usually have internal Hamiltonian parameters which lead to the ideal PASADENA enhancement. For protons, the dipolar coupling is likely to be too large. Substantial enhancements could be achieved in such systems by employing multiple-pulse sequences such as WAHUHA,[4] with judicious delay misadjustment, to scale down the size of the coupling to an optimal value.

---

† The enhancement figure is based $\chi_p = 1$ and rf-pulse angles of 45° and 90° for the PASADENA and Curie-law derived spectra, respectively.

Fig. (VIII-4) Plot showing the dependence of the integral of the magnitude spectrum on the relative size of the dipolar coupling and chemical shift difference. The integrated magnitude is a measure of the destructive interference due to the antiphase character of the lineshape.

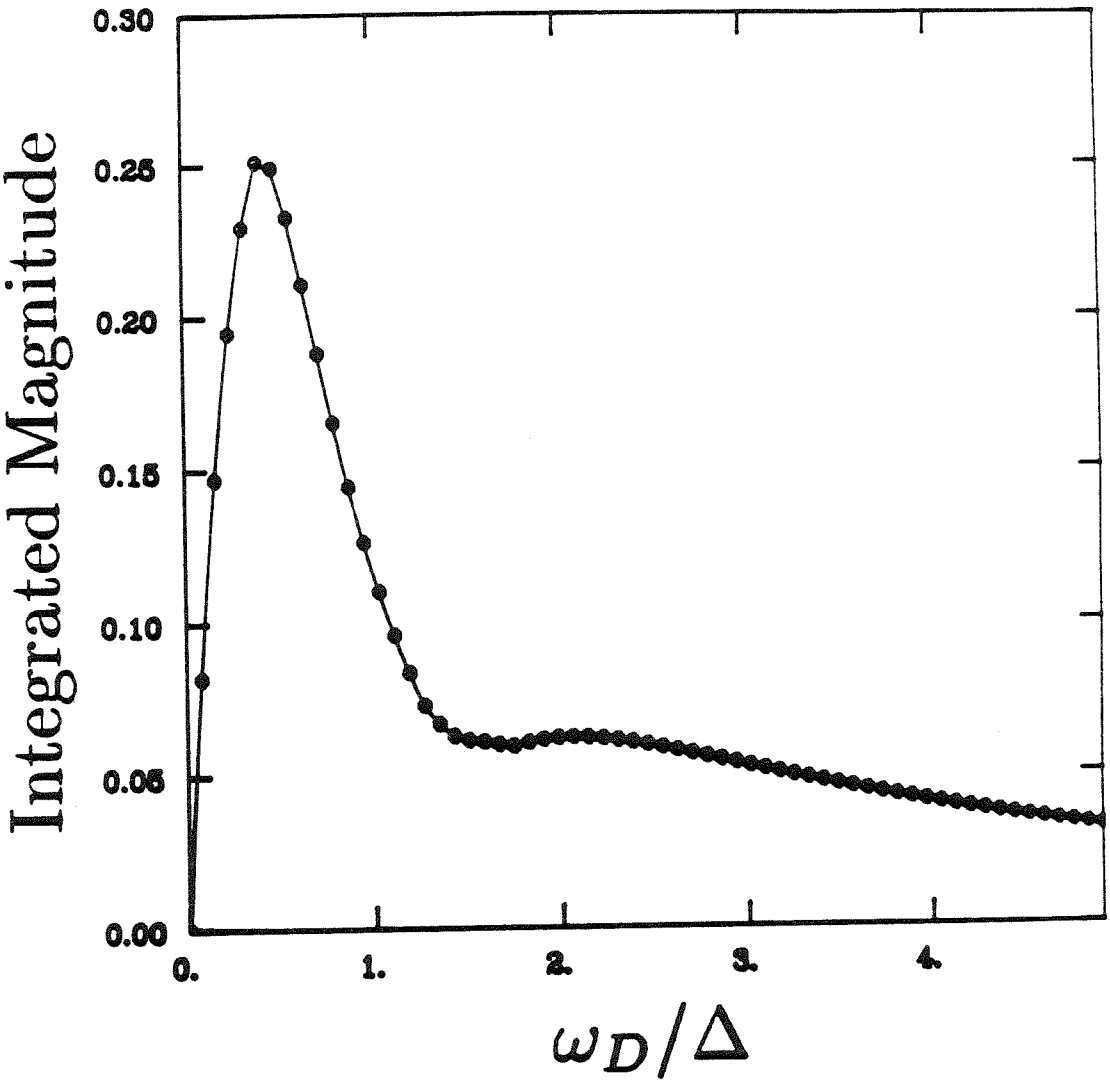

§ VIII-4. References

1. M. Mehring, Principles of High Resolution NMR in Solids, second edition, Springer-Verlag, New York (1983)
2. U. Haeberlen, High Resolution NMR in Solids, Selective Averaging, Academic Press, New York (1976)
3. W. H. Press, B. P. Flannery, S. A. Teukolsky and W. T. Vetterling, Numerical Recipes in C, Cambridge University Press, New York (1988)
4. D. W. Alderman, M. S. Solum and D. M. Grant, *J. Chem. Phys.* **84**, 3717 (1986)
5. J. S. Waugh, L. M. Huber and U. Haeberlen, *Phys. Rev. Lett.* **20**, 180 (1968)

Chapter IX

Radiowave Application Yields Modulated Ortho Number Desorbed

§ Introduction

It is proposed that the nuclear magnetic resonance of sites which release dihydrogen can be obtained by measuring the branching fraction to the ortho or para form.[1,2] The motivation is to transform the sensitivity problem from that of detecting weak rf signals into the more amenable one of establishing the para mole fraction of free H_2. In this chapter, it is shown with a density operator formalism that the para or ortho mole fraction reports directly on the zero-quantum coherence of the precursor and that other spin operators may be observed indirectly. Spectra are simulated for the case of a surface site at which release of H_2 occurs.

The poor sensitivity of nuclear magnetic resonance is attributable to two distinct deficiencies. The equilibrium spin ordering is weak at the temperatures where chemical reactions occur and the usual observable, the rf signal from precessing nuclear spin magnetization, is degraded by thermal noise. For the case of proton NMR at room temperature, perfect spin ordering would represent an enhancement by a factor of about 10^4, so further improvement must come from the detection process. There is in fact far more room for improvement here, since even with perfect or-

dering, rf detection falls short of the single molecule limit by an additional factor of 10^{12}. In the PASADENA effect, the coupling of nuclear spin to rotational states through the symmetrization postulate has been exploited to address the first problem of increasing the spin order for systems that add dihydrogen into magnetically inequivalent sites.[1] Applications to the study of homogeneous catalysts in solution were described in earlier chapters. Other PASADENA studies have appeared in the literature.[3–7] In the present, we describe how the connection between NMR and spin statistics, provided by magnetic inequivalence and chemical reaction, creates a more sensitive detection observable, the fraction of para or ortho species formed. These proposed methods are well described by the acronym RAYMOND (*r*adiowave *a*pplication *y*ields *m*odulated *o*rtho *n*umber *d*esorbed).

§ IX-1. Nuclear Magnetic Resonance by Measuring Reaction Yield of Spin Symmetry Species

Consider an ensemble of dihydrogen molecules produced by a chemical reaction at time t. Recall that the singlet (para) and triplet (ortho) nuclear spin states of dihydrogen interconvert slowly in the absence of a further reaction[8] and so the parahydrogen mole fraction χ_p will be considered a constant of the motion throughout whatever measurement process is used to determine it. We will assume also that total nuclear spin angular momentum is conserved in the reaction which carries the protons from the precursor of NMR interest to the observable pool of dihydrogen. Finally, we assume that the numbers of ortho and para species formed from an unpolarized ensemble are in the statistical ratio 3:1, implying that the rate is independent of the rotational state of the eliminated molecule. This is a worst case assumption in that if it were not true, total H_2 release could be used as an observable for surface NMR. It is however expected to be a good high-temperature approximation, since the ortho/para ratio in the gas phase dihydrogen partition functions is within 0.4% of 3 at 300 K. All of the above assumptions are kinetically reasonable. Equilibrium arguments are not relevant, because the situations of

interest will be precisely those in which, subsequent to initiation of rf irradiation, the precursor passes irreversibly to products in a time short compared to its spin-lattice relaxation time T_{1J}.

Suppose that the precursor of NMR interest is the site at which two protons combine to form a dihydrogen molecule. Then the expectation value proposed is

$$\chi_p(t) = \mathrm{Tr}\{\rho(t)(\frac{1}{4} - \mathbf{I}_1 \cdot \mathbf{I}_2\}, \tag{1}$$

where $\rho(t)$ is the two-spin density operator for the ensemble of such pairs at the time of dihydrogen formation. By the above hypotheses, these operators also describe the analyzed dihydrogen. As in Chapter VIII, the spin Hamiltonian for the site will be taken as that of a magnetically isolated pair in high field with a definite orientation, as might occur at a solid surface. The rotating-frame spin Hamiltonian including chemical shifts, dipolar and scalar couplings was given by Eq. (VIII-1).

Two different types of nuclear spin ensembles will be considered for the precursor molecules. The more familiar case is one characterized by a Zeeman spin temperature in the Curie-Law high-temperature limit. This temperature may be the lattice temperature or may result from some nonequilibrium preparation, for example, rapid lattice heating to the reaction temperature or deposition from a spin-polarized molecular fluid or beam.

The other case considered is depicted in Fig. (IX-1).
The precursor ensemble is prepared by molecular addition of p-H_2, irradiated with Larmor frequency rf, and monitored for χ_p as a function of the desorption time of the released H_2. This is a convenient way of producing a highly spin-ordered ensemble, but requires that the sites can be occupied by molecular addition. If binding were rapid compared to the spin evolution on the surface, the initial condition would be simply $\rho(0) = \frac{1}{4} - f\mathbf{I}_1 \cdot \mathbf{I}_2$, where $f = \frac{1}{3}(4\chi_p(0) - 1)$. More typically, practical delivery of the dihydrogen to the surface will result in the arrival time of a given molecule being randomly distributed over a period of at least 10^{-3} s. Upon binding, the sudden introduction of magnetic inequivalence initiates off-diagonal

Fig. IX-1 Illustration of the NMR detection process involving reversible molecular addition of parahydrogen to a surface. Parahydrogen adds pairwise to magnetically inequivalent sites AB. The evolution period is controlled by the multiple-pulse sequence R. The NMR frequencies are detected as a modulation of the mole fraction of p-H_2 released.

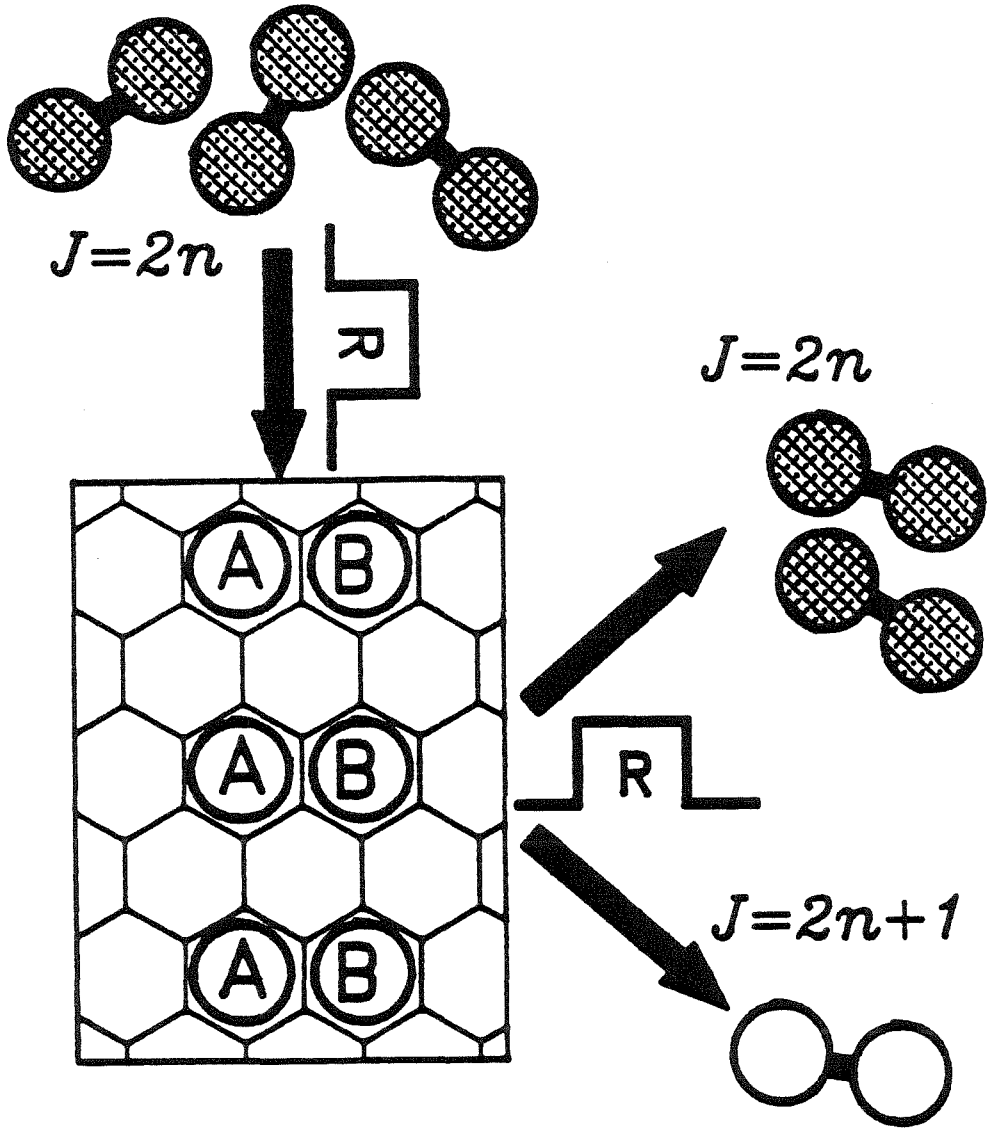

zero-quantum evolution, which for the case of the four-level system of Eq. (VIII-1) is at the frequency

$$\omega_{23} = [(J + D)^2 + \Delta^2]^{1/2}, \tag{2}$$

The random arrival times and the distribution of this frequency over a powdered sample will both lead to dephasing. Thus, as discussed in Chapters III, IV, V and VIII, a realistic expectation is that only populations will be needed to describe the subsequent evolution. Recall from §III-4. that the time averaged initial density operator in this case is given by

$$\langle \rho(0,\kappa) \rangle = \frac{1}{4} - f\left[\frac{1}{2}\sin\kappa\cos\kappa(\mathrm{I}_{z1} - \mathrm{I}_{z2}) + \frac{1}{3}\cos^2\kappa(3\mathrm{I}_{z1}\mathrm{I}_{z2} - \mathrm{I}_1 \cdot \mathrm{I}_2) + (1 - \frac{2}{3}\cos^2\kappa)\mathrm{I}_1 \cdot \mathrm{I}_2\right] \tag{3}$$

where $\kappa = \tan^{-1}((J + D)/\Delta)$.

If this initial condition is subjected to a resonant rf pulse (SEQ-IX-1) described by the rotating-frame propagator $\exp(-i\theta \mathrm{I}_y)$, the resulting response calculated according to Eq. (IX-1), with nonoscillating terms omitted, is the zero-quantum interferogram

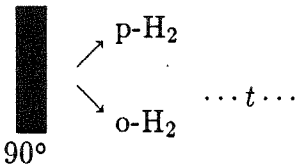

SEQ-IX-1

$$\chi_p(t) = \frac{f}{8}\left[\frac{\Delta^2}{[\Delta^2 + (J + D)^2]^2}\right][2(J + D)^2(1 - \cos\theta) + \Delta^2\sin^2\theta]\cos(\omega_{23}t) \tag{4}$$

While the sequence SEQ-IX-1 which leads to Eq. (IX-4) is experimentally simple, it is wasteful in the sense that some of the initial spin order of the p-H_2 is lost. To obtain the maximum possible intensity, the incoherent off-diagonal evolution, which is spontaneously initiated upon molecular addition, must be suppressed until the binding reaction is substantially complete. This is possible by the application

of an appropriate multiple-pulse train, as denoted by **R** in Fig. (IX-1). In liquids, a train of π pulses would suffice. For a dipolar coupled system, sequences[9,10] which eliminate both chemical shift and dipolar terms are needed. These produce an average Hamiltonian containing only the scalar coupling. Thus the full spin order of each molecule can be preserved until the zero-quantum evolution of the ensemble is coherently initiated by terminating the line-narrowing sequence as in SEQ-IX-2.

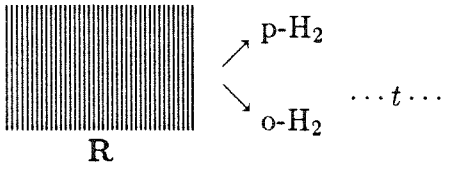

SEQ-IX-2

For the detection of zero quantum coherence, two possible variations in the experimental procedure can be envisioned. In SEQ-IX-3, the coherence is mapped by incrementation of the evolution period as in two-dimensional NMR, with one point of the function $\chi_p(t)$ being collected for each repetition of the adsorption cycle.

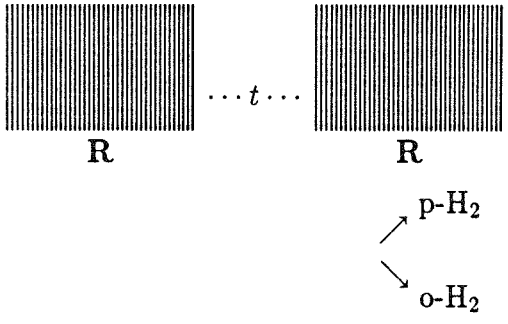

SEQ-IX-3

Following the evolution period t, the pulse train **R** is again applied, synchronously terminating evolution for all molecules that subsequently desorb. All of the proton pairs in the sample are released to the gas phase and contribute to a single point of $\chi_p(t)$, yielding maximal pointwise sensitivity. The cycle is repeated for as many points as required by the desired spectral resolution.

This pointwise approach would be unnecessary if the sensitivity of the detection scheme were sufficient to measure those molecules desorbed in each interval Δt of the evolution period, with Δt dictated by the Nyquist sampling condition. In this case, the experiment would be one dimensional; all points t could be measured for each adsorption cycle. The fraction of molecules desorbing during the decay of the coherence would be kept small to minimize lifetime broadening of the surface spectrum.

In either scheme, the error in χ_p can be reduced by independently measuring the amount of ortho and parahydrogen, and applying a normalization correction for any variation in the total amount of hydrogen detected. Such a procedure would also allow for detection of a systematic effect of total H_2 release on spin order, which would occur if the branching to the two forms from an unpolarized ensemble was not in the statistical ratio of 3:1. The desorption rate could be enhanced locally or over the whole sample by sudden heating.

When **R** is applied during the addition step as in SEQ-IX-2 or SEQ-IX-3 so that the initial density operator is that of the gas adsorbed, then χ_p is

$$\chi_p(t) = \frac{f+1}{4} + f\frac{(J+D)^2 + \Delta^2\cos(\omega_{23}t)}{2[(J+D)^2+\Delta^2]} \tag{5}$$

The ratio of the amplitudes of the oscillatory signals of Eq. (IX-5) and Eq. (IX-4) is

$$\frac{4[\Delta^2 + (J+D)^2]}{\Delta^2\sin^2\theta + 2(J+D)^2(1-\cos\theta)}, \tag{6}$$

which shows how the improvement due to **R** depends on the pulse angle and Hamiltonian parameters. For example, if $|\Delta| \gg |J+D|$, then a fourfold improvement results with a $\pi/2$ pulse. This ratio, calculated in the two-spin limit, likely underestimates the advantage of line-narrowing during binding that would be seen when the spins of interest have extraneous neighbors to which spin diffusion would

otherwise occur.

§ IX-2. Simulations

§ IX-2.1. Liquids

The complex $[Ir(PPh_2C_2H_4PPh_2P)_2]^+$, shown below, is a specific example of a system which rapidly adds and photochemically releases H_2 (with almost unity quantum yield) upon irradiation with ultraviolet light.

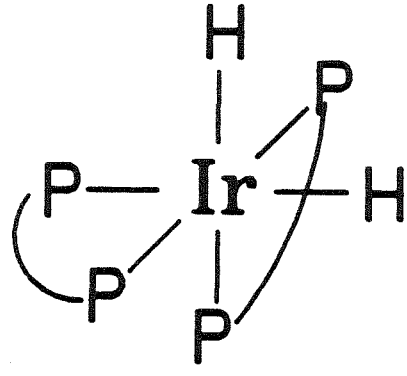

In the dihydride form, the protons are chemically but not magnetically equivalent due to unequal *cis* and *trans* scalar coupling with phosphorous. The experimental spectrum consists of two quartets separated by the $J_{HP}^{trans} = 110$ Hz coupling of each proton with the *trans* ^{31}P. The $J_{HP}^{cis} = 14$ Hz couplings with the three *cis* ^{31}P nuclei gives rise to a quartet. The proton-proton coupling is less than 2 Hz, as measured from the experimental NMR spectrum.

With J_{HH} unresolved, this system would not yield any PASADENA enhancement, yet this is not a requirement for the observation of zero quantum coherence by the current technique. In this weak coupling limit, with $D = 0$, the signal expressions in Eq. (IX-4) and Eq. (IX-5) can be reduced to (non-oscillating components excluded)

$$\chi_P(t) \approx \frac{f}{8} \sin^2\theta \cos\left[\left(J^2 + \Delta^2\right)^{1/2} t\right] \tag{7}$$

and

$$\chi_P(t) \approx \frac{f}{2} \cos\left(J^2 + \Delta^2\right)^{1/2} t \tag{8}$$

Hence, the RAYMOND spectrum of $[Ir(PPh_2C_2H_4PPh_2P)_2]^+$ will contain a line at the effective "chemical shift" difference. A numerical density matrix simulation of the spectrum involving observation through the branching ratio confirms that the predicted single transition does indeed occur at $\pm(J_{HP}^{cis} - J_{HP}^{trans})$.

The measured hydride T_1 of 0.25 s serves as an estimate for the time limitation imposed on the entire addition-evolution-elimination cycle, raising the technical question of how rapidly the gaseous H_2 can be dissolved into and then removed from the solvent.

§ IX-2.2. Solids

To illustrate the general lineshape features expected for the spectrum of a polycrystalline solid, the signal $\chi_P(t)$ will be averaged to simulate a distribution of orientations of the spin system as in a powder sample. The integration over ϑ and φ is performed in the frequency domain using the linear interpolation method described in Chapter VIII.[11] In Fig. (IX-2a), the conventional weak coupling ($D = J = 0$) lineshape derived from Zeeman order and detected as complex transverse magnetization is shown as a point of reference. The two sites are resolved by their chemical shifts and the discontinuities of each powder pattern reveal the principal components of that shielding tensor. Fig. (IX-2b) is the corresponding RAYMOND spectrum, obtained as the powder-averaged Fourier transform of Eq. (IX-4). It shows a single powder pattern in which the discontinuities occur at the principal components of the difference of the shielding tensors of the two spins. When the orientations of the shielding tensors differ ($\Omega_1 \neq \Omega_2$), these components provide information on their relative orientation. The pattern is symmetric about the carrier frequency, since the signal is entirely real. Note that unlike the PASADENA effect, a coupling between spins is not needed for RAYMOND.

Fig. (IX-2) Comparison of ordinary NMR and zero-quantum RAYMOND. All spectra are powder pattern simulations with the following parameters (in Hz) determining the spin Hamiltonian (Eq. (VIII-1)): Principal shift tensor components: $\nu_0\sigma^1_{xx} = -6000$, $\nu_0\sigma^1_{yy} = -2000$, $\nu_0\sigma^1_{zz} = -1000$, $\nu_0\sigma^2_{xx} = 1000$, $\nu_0\sigma^2_{yy} = 2000$, $\nu_0\sigma^2_{zz} = 5000$; orientation of shift tensor principal axis system relative to dipolar principal axis system: $\Omega_1 = \Omega_2 = \{0,0,0\}$. Parts a,b. $\omega_D = 0$. Parts c,d. $\omega_D = 30,000$ Hz, $r = 5.4$ Å. Parts a. and c. are ordinary NMR spectra, while the corresponding spectra b. and d. are calculated by Fourier transformation of Eq. (IX-4). The powder averages were convoluted with a Lorentzian lineshape with a FWHM of 200 Hz in a. and b. and 2000 Hz in c. and d.

$$\rho(0) = \sum_i \langle i| \left(\frac{1}{4} - f\mathbf{I}_1 \cdot \mathbf{I}_2 \right) |i\rangle|i\rangle\langle i|$$

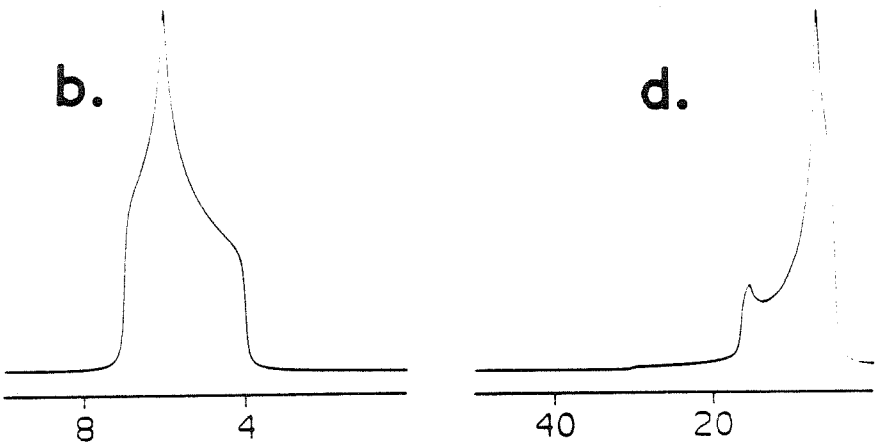

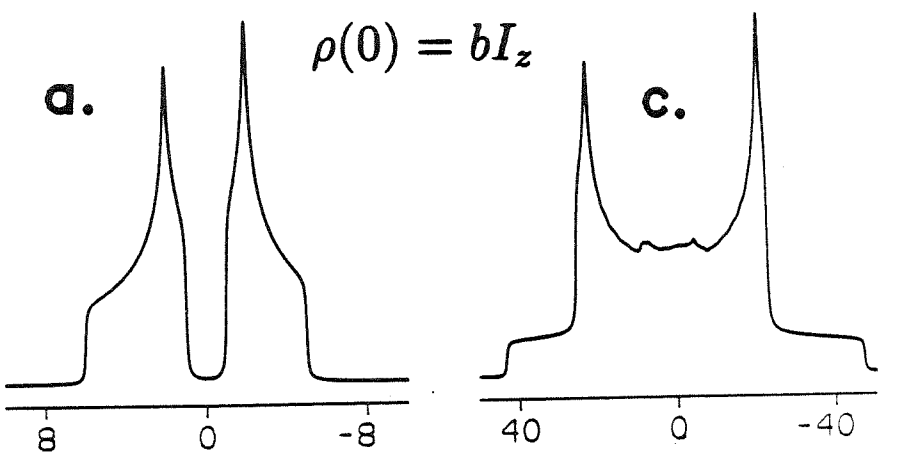

The strong coupling case detected by magnetization (PASADENA) is illustrated by Fig. (IX-2c) and the corresponding RAYMOND spectrum is in Fig. (IX-2d). Note the change in frequency scale. The RAYMOND lineshape in this case is sensitive to the spin coupling as well as the chemical shift difference tensor, but the intensity is strongly peaked near the magic-angle where $D = 0$.

The use of RAYMOND detection does not require that the initial condition be scalar order. The use of the ubiquitous Zeeman order would open up a wider range of applications. Magnetization along the field axis can be converted into RAYMOND-observable zero-quantum coherence with two $\pi/2$ pulses as in SEQ-IX-4.

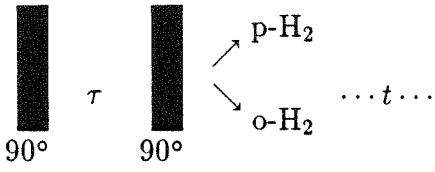

SEQ-IX-4

In the weak coupling limit, the time dependence of the p-H_2 mole fraction is

$$\chi_p(t) = \sin\theta \sin\frac{J\tau}{2} \sin\bar{\omega}\tau \left[\cos\theta(\cos(\Delta t) - 1)\cos\frac{\Delta\tau}{2} - \sin(\Delta t)\sin\frac{\Delta\tau}{2}\right] \qquad (9)$$

with θ being the tip angle of the second pulse ($\theta = \pi/2_y$ in SEQ-IX-4 and $\bar{\omega} = (\omega_{z1} + \omega_{z2})/2$). The two terms in square brackets can be acquired separately by appropriate selection of the preparation time τ. The lineshape due to the first term is purely absorptive, while the second yields both absorption and emission.

Most of the difference in information content between the conventional and RAYMOND spectra of Fig. (IX-2) is simply that zero-quantum spectra are being detected in the latter case. RAYMOND may also be used to detect single or multiple-quantum coherence by encoding these pointwise in $\chi_p(t)$. Illustrative two-dimensional2 pulse sequences starting with scalar or Zeeman order are illustrated in SEQ-IX-5 and SEQ-IX-6, respectively. Thus the full set of NMR information is

available with this new observable.

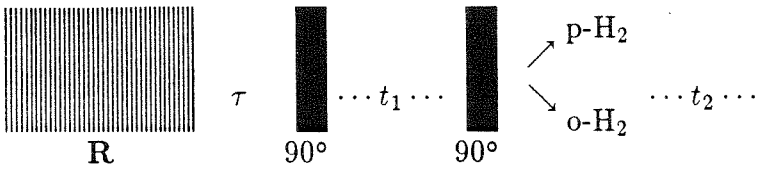

SEQ-IX-5

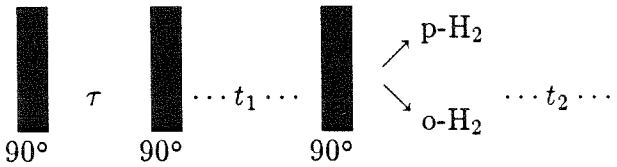

SEQ-IX-6

The key experimental question is how to detect the ortho and para mole fractions with high sensitivity and precision. The precision will determine how high the initial spin ordering must be before a detectable modulation of $\chi_p(t)$ will be practical. Because of the long lifetime for relaxation between ortho and para species, a great variety of methods are possible,[12–14] but the practical choice is debatable.

§ IX-3. References

1. C. R. Bowers and D. P. Weitekamp, *Phys. Rev. Lett.* **57**, 2645 (1986)
2. C. R. Bowers and D. P. Weitekamp, *J. Am. Chem. Soc.* **109**, 5541 (1987)
3. C. R. Bowers, D. H. Jones, N. D. Kurur, J. A. Labinger, M. G. Pravica, and D. P. Weitekamp, *Adv. Magn. Reson.* **14**, 269 (1990)
4. C. R. Bowers and D. P. Weitekamp, in preparation.
5. M. G. Pravica and D. P. Weitekamp, *Chem. Phys. Lett.* **145**, 255 (1988)
6. T. C. Eisenschmid, R. U. Kirss, P. P. Deutsch, S. I. Hommeltoft, R. E. Eisenberg, J. Bargon, R. G. Lawler, and A. L. Balch, *J. Am. Chem. Soc.* **109**, 8089 (1987)
7. R. U. Kirss, T. C. Eisenschmid and R. E. Eisenberg, *J. Am. Chem. Soc.* **110**, 8564
8. A. Farkas, Orthohydrogen,Parahydrogen and Heavy Hydrogen, Cambridge University Press, London (1935)
9. D. P. Weitekamp, J. R. Garbow and A. Pines, *J. Chem. Phys.* **77**, 2870 (1982)
10. H. M. Cho, C. J. Lee, D. N. Shykind and D. P. Weitekamp, *Phys. Rev. Lett.* **55**, 1923 (1985)
11. D. W. Alderman, M. S. Solum and D. M. Grant, *J. Chem. Phys.* **84**, 3717 (1986)
12. E. E. Marinero, C. T. Rettner, R. N. Zare, and A. H. Kung, *Chem. Phys. Lett.* **95**, 486 (1983)
13. S. T. Pratt, P. M. Dehmer and J. L. Dehmer, *J. Chem. Phys.* **85**, 3379 (1986)
14. P. J. Pizarro and D. P. Weitekamp, *Phys. Rev. Lett.*, submitted.

Appendix A

Dual Interface

Spectrometer Control Object

§ Introduction

The interfacing software used in the Weitekamp laboratory† is known as the *Dual Interface Spectrometer Control Object*, or DISCO. This software is flexible enough to implement practically any conceivable NMR experiment, yet it is straightforward to use. The object of this appendix is to communicate the key functional concepts and to describe the commands, parameters and programming syntax.

§ A-1. The Spectrometer

Three devices are interfaced to the DEC μVAX computer through a GPIB-IEEE. These are a Nicolet digital oscilloscope, an Interface Technology digital word generator and a PTS-500 digital synthesizer. Two interface boards have been installed in the μVAX. A single DISCO process can select either board through a software command (hence the first two words of the acronym).

Either of two Nicolet oscilloscope modes can be used to control the digitization

† Written by the Author

rate. In the automatic mode, the acquisition is triggered by a single logic pulse with the digitization rate set by the front panel knob. In the "EP" mode, a trigger pulse must be supplied to collect each sample. The EP mode is particularly useful for multiple-pulse experiments in solids where sampling occurs during the "windows" of the sequence and/or when the analog integrator is being used. A greater degree of flexibility in setting the spectral width is also afforded by this mode, since the front panel time-per-point knob has only a limited number of positions. An acquisition loop in the pulse program is necessary for sampling in EP mode.

The PTS-500 digital synthesizer can be both frequency and amplitude controlled remotely through DISCO. Incrementation of the frequency over a desired interval is also possible through DISCO, permitting experiments such as ENDOR or indirect detection NMR methods. The frequency incrementation may also be used in conjunction with other DISCO loop and time period incrementation features to perform "slice selection" in three-dimensional NMR imaging.

The Interface-Technology RS-670 digital word generator (ITI) is the nerve center of the spectrometer hardware. The ITI can control 16 TTL logic channels with a maximum frequency of 40 MHz, 32 channels at 20 MHz or 64 channels at 10 MHz. Both 16 and 32 bit versions of DISCO exist. A maximum of 4096 digital words can be stored in ITI memory, along with 16 loop counters and 32 tables of words which group the words. The individual digital words are most conveniently programmed in the binary base. The output of the ITI word goes to a distributor box with BNC connectors. The TTL logic gates control all the rf switches, power amplifier blanking, receiver deblanking, oscilloscope triggering, integrator functions and miscellaneous devices associated with specialized experiments. For example, the pressurized p-H_2 bubbling apparatus used in PASADENA experiments.

The ITI is a stand-alone instrument. Pulse programs can be written, run and stored on its $5\frac{1}{4}''$ floppy drive. However, the necessary functions for sophisticated NMR experiments involve incrementation of loop values, word time periods, cycling

of the words themselves and frequency stepping. These functions are not within the capability of a single program of the ITI, but are facilitated by DISCO.

§ A-2. Disco Pulse Programming

Pulse programming with DISCO was designed to emulate pulse programming on the ITI. This makes it particularly convenient to switch between programming locally through the front panel or remotely from the μVAX. The "edit/edt" program is spawned from DISCO to permit efficient editing of the pulse program. The following subsections describe the syntax for the basic elements of the pulse program. Beginning with the digital "WORD," the program structure will be discussed at increasingly higher levels, corresponding to higher level loops. The overall loop structure of DISCO is illustrated in Fig. (A-1).

While the DISCO sequence files emulate the ITI, there are several important differences. There are constraints on the time values programmed on the ITI, requiring the use of several words to obtain the desired time period. In contrast, the words in DISCO can have any time value (within memory limits). The DISCO word time values are automatically broken down into ITI compatible time values when the sequence is loaded. The second major difference is the availability in DISCO pulse program of special commands which perform the tasks required in complex NMR experiments. These are discussed in sections §A-2.a–g.

§ A-2.a. The WORD

The basic programming unit is the digital word, which is expressed in a binary format. Each bit of the word corresponds to a TTL logic channel which may be set high or low for a specified amount of time. The syntax for specifying a digital word in a DISCO pulse program is

Fig. (A-1) The Loop Structure of DISCO

VAX VMS
VAX VMS Spectrometer Batch Queue
DCL ".com" file loop
DCL level commands (e. g. @, run, copy, rename, etc.)
DCL-DISCO level commands (e.g. lwg, set, out, read, write, dcl, etc.)
DISCO-PTS frequency step loop
DISCO-ITI sequence increment loop
DISCO recycle or INC loop
DISCO WCYCLE and TCYCLE loop
ITI MAJOR loop
ITI MIDDLE loops
ITI TABLE loops
ITI WORDS
acquisition trigger
EP-mode sampling
Integrator control
rf-switches, blanking
p-H_2 flow control
miscellaneous
[NICOLET averaging]
[Output file created]
[State of Hibernation]

FORMAT:

WORD ⟨word value⟩ ⟨time value⟩;

EXAMPLE:

WORD 1010101010101010 300.0e-3;

§ A-2.b. The INC

Frequently in NMR, the duration of pulses, delays, etc., are incremented. In the context of the ITI, this requires some way of incrementing the time value of the word. This role is fulfilled by the INC operator which successively acts on the time value of the word just preceding it, each time incrementing its value by a specified amount. The increment can be positive or negative (the total time value must be positive, of course). The time values for multiple words can be simultaneously incremented in a single pulse program. This permits such useful possibilities as one pulse growing into an adjacent pulse, or synchronous incrementation of a group of pulses or delays belonging to different TABLES or MIDDLE loops. Complicated pulse programs can be constructed with relative ease.

The number of increments specified is the number of times the pulse sequence will be executed for a given PTS frequency. If there are no INCs, then the *REP* parameter (§(A-4) determines the number of recycles. If the number of time value increments is different for each word, the execution will terminate when the smaller number has been reached. The maximum number of incremented words allowed per table (see below) is 20 and the maximum number of tables is 32 (however, only 16 at a time can be accessed by the sequence).

FORMAT:

WORD	⟨word value⟩	⟨initial time⟩;
INC	⟨# increments ⟩	⟨increment⟩;

EXAMPLE:

WORD	0101010101010101		1.0e-5;
INC	40	2.0e-5;	

§ A-2.c. The TCYCLE

The TCYCLE consists of a table of time values, each of which is substituted into the ITI sequence in a cyclic fashion. This feature is useful for designating a collection of closely spaced data points where the measured quantity of interest is changing rapidly. Fewer points are measured where the second derivative is small. Hence, the TCYCLE is useful in T_1 experiments. The TCYCLE feature was employed to obtain the data shown in Fig. (VI-6). The maximum number of TCYCLEs is currently 20.

FORMAT:

TCYCLE	⟨word value⟩	⟨# time values⟩;
⟨time$_1$⟩	⟨time$_2$⟩	...
⟨time$_n$⟩;		

EXAMPLE:

TCYCLE	000101000000110		5;
1.05	1.1	1.3	
2.0	3.0;		

§ A-2.d. The WCYCLE

The WCYCLE was created expressly for phase cycling, although many other

uses for it can be envisioned. It consists of a table of word values which are cyclically substituted and down-loaded onto the ITI, just as in the TCYCLE. Both types of cycles can be used in the same pulse program simultaneously. The WCYCLE word time values can be incremented by the INC operator. Note that there is only one loop for all TCYCLEs and WCYCLEs, so that if the number of cycle words and the number of cycle times differ, the substituted time and word values for successive iterations will lose their initial synchronization. The maximum number of WCYCLE words is currently 20.

FORMAT:

WCYCLE ⟨# word values⟩ ⟨time value⟩;
⟨$word_1$⟩
⟨$word_2$⟩
⋮
⟨$word_n$⟩

EXAMPLE:

```
WCYCLE          4                   6.0e-6;
0000000010000000
0000000001000000
0000000000100000
0000000000010000;
```

---

§ A-2.e. TABLES

The WORDs, INCs, TCYCLEs and WCYCLEs are elements of TABLEs. The TABLE has a label referred to as the "table id." The tables are found in the "TABLES:" section of the pulse program file. The end of this section is indicated by an "END_TABLE:". The tables may appear in any order.

FORMAT:

TABLES:

TABLE ⟨table id⟩;
[KEY 5432109876543210;]
WORD, TCYCLE or WCYCLE
[INC]
WORD, TCYCLE or WCYCLE
[INC]
⋮

TABLE ⟨table id⟩;
[KEY 5432109876543210;]
WORD, TCYCLE or WCYCLE
[INC]
WORD, TCYCLE or WCYCLE
[INC]
⋮

⋮

END_TABLE:

§ A-2.f. The SEQUENCE

The order in which the tables are executed when the ITI is triggered is dictated by the SEQUENCE section of the pulse program. There are three levels of looping on the ITI; MAJOR, MIDDLE and TABLE loops. The maximum loop value is 4095. Continuous (infinite) loops can only be programmed through the front panel of the ITI.

The number of iterations of a loop can be incremented in DISCO. This incrementation is associated with the next to the outermost loop within DISCO (see Fig. (A-2)). An error message will result if the user tries to program incrementation

that will result in a negative loop value or values greater than 4095.

The ability to increment sequence loops is a powerful feature which is ideally suited for multiple-pulse solid-state NMR experiments which require incrementation of the number of times some complicated subcycle is repeated. The subcycle can be programmed in multiple tables, multiple incremented tables, middle loops containing multiple tables, etc. The loop increment for TABLE, MIDDLE or MAJOR loops can also be negative, resulting in successive decrementation of the number of iterations. The optional negative sign on the loop value indicates that this loop, MAJOR, MIDDLE or TABLE, is to be incremented. The first value used is the absolute value of the loop value specified. The parameters in square brackets have no effect unless the loop value is specified as a negative integer.

FORMAT:

SEQUENCE:

MAJOR	⟨[-]loop value⟩	[⟨# increments⟩]	[⟨increment⟩];	
MIDDLE	⟨[-]loop value⟩	[⟨# increments⟩]	[⟨increment⟩];	
TABLE	⟨table id⟩	⟨[-]loop value⟩	[⟨# increments⟩]	[⟨increment⟩];
TABLE	⟨table id⟩	⟨[-]loop value⟩	[⟨# increments⟩]	[⟨increment⟩];
⋮				
MIDDLE	⟨[-]loop value⟩	[⟨# increments⟩]	[⟨increment⟩];	
TABLE	⟨table id⟩	⟨[-]loop value⟩	[⟨# increments⟩]	[⟨increment⟩]
⋮				
MIDDLE	0;			

EXAMPLE:

```
SEQUENCE:
MAJOR       1024;
MIDDLE      -32         16          10;
TABLE       01          1;
TABLE       03;
MIDDLE      10;
TABLE       02          -10         8           4;
MIDDLE      0;
```

§ A-2.g.

The program elements discussed in §A-2a through §A-2f are used to construct the total pulse program, which exists as a text file on the μVAX. The overall program structure is shown below.

FORMAT:

[TITLE: ⟨title of arbitrary length and # lines⟩;]

SEQUENCE:
⋮

[KEY:
⟨commenting feature to record device-channel assignments⟩;]

TABLES:
⋮
END_TABLE:

END;

A simple example sequence is shown in Fig. (A-3), corresponding to the pulse sequence of SEQ-VI-1.

Fig. (A-3) Example pulse program corresponding to SEQ-VI-1, written in the DISCO format. This program was employed to obtain the data of Fig. (VI-3), making use of the TCYCLE to increment τ_w nonlinearly. The short KEY codes for the devices represent; solenoid valves–A, B, C; rf power amplifier–ENI; transmitter control rf switch–RF; rf switches in four-phase box–X, Y, X|, Y|; receiver deblanking–RD; Nicolet scope trigger–NIC.

```
TITLE: PASADENA pulse sequence, TCYCLE of delay before 45 degree pulse;

SEQUENCE:
MAJOR          1;
MIDDLE         1;
TABLE          01              1;
TABLE          05              1;
TABLE          02              1;
TABLE          03              1;
TABLE          04              4;
MIDDLE         0;

KEY:

15  14  13  12  11  10  9   8   7   6   5   4   3   2   1   0
    A   B   C   EP  ENI RF  RD  Y|  X|  Y   X   NIC;

TABLES:

TABLE          01;
KEY            5432109876543210;
WORD           0000000000000000                1.0e-6;
WORD           0001000000000000                2.0;            CHARGE!
WORD           0000000000000000                0.5;            DELAY
WORD           0000100000000000                2.0;            BURST !
```

Fig. (A-3), continued

```
TABLE          05;
TCYCLE         0000000000000000 20;
    1.0  1.06 1.12 1.18 1.24 1.3  1.6
    1.9  2.2  2.5  2.8  3.1  3.4  3.7  4.4
    5.4  7.0  10.0 15.0 25.0;
TABLE          02;
KEY            5432109876543210;
WORD           0000010000000000          20.0e-6;      ENI warm up
WORD           0000010000010010          7.0e-6;       45 deg pulse

TABLE          03;
KEY            5432109876543210;
WORD           0000000000001000          1.0e-6;       trigger scope

TABLE          04;
KEY            5432109876543210;
WORD           0000000100000000          1.2;          acquire

END_TABLE:

END:
```

§ A-3. DISCO Commands

The following lower case commands can be entered at the |s⟩ prompt.

GPIB

clib	Clear and allocate GPIB of the current spectrometer.

PTS-500

loc	Put the PTS-500 into local operation mode.
rem	Put the PTS-500 into remote operation mode.

Nicolet Digital Oscilloscope

ni	Initialize the Nicolet.
np	The Nicolet "NP" command (see the Nicolet manual).
nw	Nicolet NW interfacing command (gets the wave form data, see the Nicolet manual).
nd	Nicolet data transfer to the μVAX in binary format (see the Nicolet manual).

ITI RS-670

lwg	Load word generator with current pulse sequence.
ltable ⟨*table id*⟩	Loads individual tables.
twg	Trigger word generator. Begins the NMR experiment by initiating the outermost loop within DISCO (see Fig. (A-1)).
rum	Rapid update mode. Repeatedly displays Fourier transform of continually updated FID. This is useful when shimming in the frequency domain. The shortest delay between successive displays is about 2 s. (*rum* works only on the Workstation and Lanpar terminals).

DISCO Parameter Control

show	Displays current DISCO parameters.

set x y	Sets th value of the parameter x to the value y. See §A-4. for a description of DISCO parameters.
ep	Edit current parameter file directly.
read	Reads parameters into DISCO from current parameter file.
write	Updates parameter file with current DISCO parameters.

Pulse Program

rpf	Read current pulse program file into memory.
es	Edit current sequence.

Fourier Transform and Plotting

fft	Fourier transform with graphics. Sub-menu options permit display of real, imaginary or magnitude spectra. Interactive phasing and cursor functions are also available.

Data Files

out	Output data to file with current data file name.
inp	Input data from file with current data file name.

Miscellaneous

dcl ⟨*dcl command*⟩	Spawn DISCO subprocess.
hare	Spawns D. R. Hare's FT4105 program as a DISCO subprocess.
exit,quit,bye	Causes DISCO to terminate.
control-C	Cancels execution of an executing pulse program after the current cycle has been completed.
help	Online help.

§ A-4. DISCO Parameters

The disco parameters are displayed by entering the *show* command. Parameter identifiers appearing in capitals can be changed using the *set x y* command. Lower case parameter identifiers displayed by the *show* command are informative only

and cannot be set through the software. The *SW* and *NPT* parameters cannot be directly changed either, but are capitalized to emphasize that they may be changed indirectly.

Spectrometer Choice

SPEC	Defines which spectrometer is being accessed. Each spectrometer is connected to one of the GPIB boards installed in the μVAX. The names of the spectrometers are DIRAC and ELVIS (the latter of which does not yet exist, although several sightings have recently been made in the lab!). The spectrometer must be specified before issuing a *clib* command.

Pulse Program

SEQ	The pulse program file name.
MIN	The recycle loop delay, in seconds.
REP	The number of iterations of the recycle loop.

Nicolet Digital Oscilloscope

parameters under software control

#1W	Specifies which Nicolet wave form will be transferred to the real DISCO data buffer. *#1W* is used as a parameter of the Nicolet *nd* data transfer command.
#2W	Analogous to #1W.
FIR	Specifies the first data point to be transferred.
LAS	Specifies the last data point to be transferred.
STEP	Specifies transfer of every *STEPth* point of the data. When equal to 1, every point is transferred between *FIR* and *LAS*.
WAC	Wave form acquisition mode (see Nicolet manual). Specifies whether LIVE, HOLD NEXT or HOLD LAST will be executed on the Nicolet scope when the *twg* command is issued.

parameters which are informative only

tim	Reports the time/point knob setting.

sw	Reports the computed spectral width based on *tim* and *STEP*.
cha	Reports the Volts/division knob setting for channel A.
chb	Reports the Volts/division knob setting for channel B.

Fourier Transform

NFFT	This is othe number of points in the fast Fourier transform. If *NFFT*>*NPT*, the buffer is zero filled.
LIN	Specifies the value of the Lorentzian line broadening factor.
IFFT	The sign of i in the Fourier transform. This must be set to either 0 or -1.
BAS	"*set bas* 1" specifies subtraction of DC offset from the FID. "*set bas* 0" disables the baseline correction.

Data Files

FIL	"*set fil* 0" disables creation of data files. "*set fil* 1" creates files.
OUT	Specifies the data file name for input or output.
TITLE	Character string header to be written into data files which are created.

PTS-500

FREQ	Specifies synthesizer frequency in Hz.
OFF	Specifies an offset from *FREQ* which defines a range over which the frequency will be incremented in remote mode by DISCO, but only if *NFREQ*> 1.
NFREQ	The number of incrementations of the synthesizer frequency. The PTS must be in remote mode.

Phase Correction for Plotting

LPH, RPH	Value of the phase in degrees at the left and rightmost edge of the frequency domain spectrum.
LPG, RPG	Left and right gross phase correction calculated from *FIR* and *TIM*.

PHA Smallest increment of phase used in the interactive phase correction.